UNIVERSIDAD DE GUANAJUATO

DIVISIÓN DE CIENCIAS E INGENIERÍAS

Tensor Dark Matter

Thesis submitted for the degree of Doctor in Physics.

Haydee Hernández Arellano

Supervised by:

Dr. Mauro NAPSUCIALE

Dr. Simón RODRÍGUEZ

March 30, 2022

Contents

Abstract

In this work we propose an alternative explanation to the nature of dark matter which consists of an unconventional space-time structure of fields transforming in the $(1,0)\oplus(0,1)$ representation of the Homogeneous Lorentz Group (HLG), conventionally described using an equivalent antisymmetric tensor with two indices, thus we name it Tensor Dark Matter (TDM).

We review the spinor-like formalism for these fields and use it to describe free dark matter fields establishing the corresponding effective field theory for interactions with standard model fields. In this framework, we calculate the decay widths of Z^0 and Higgs bosons into TDM, compare the results with the invisible width limits for these bosons and find a relation between the mass of the TDM field and the values of the coupling constants. Then, we describe the calculation of the relic abundance and obtain bounds on the mass and the couplings of TDM from the observed value of the dark matter relic density. Considering these results, we test our hypothesis against experimental data. From the direct detection bounds set by XENON1T data we find that the spin-portal coupling is severely constrained. In regards to indirect detection limits, we find that the Gamma-Ray Excess that exists in the center of our Galaxy can be explained with a scalar coupling to the Higgs of $g_s \in [0.98, 1.01] \times 10^{-3}$ and $M \in [62.470, 62.505]\ GeV$. This sharp result is found to be consistent with other indirect detection bounds, such as annihilation into $\mu^+\mu^-$, $\tau^+\tau^-$, $\gamma\gamma$ and $\bar{b}b$. We show that including TDM annihilation into the antiproton production from cosmic rays improves the fit to the Antiproton-Proton ratio from the AMS-02 data.

Our prediction that these observables can be explained by a TDM field with $M \approx M_H/2$, along with the fact that the leading terms in the interaction Lagrangian are dimension-four, motivates the exploration of the possibility of dark matter interactions coming from a dark gauge structure. This is done by including a dark gauge group that involves a factor $U(1)_d$ subgroup that mixes kinetically with the $U(1)_Y$ of the standard model. We work out the consequences of this proposal.

Acknowledgements

I wish to express my deepest gratitude to the all the good people who were there at my side and whose continuous support made this work possible.

To my parents, Elena and Vicente, who are always supportive and caring.

To my sister, María, who was always there to listen to my crazy ideas.

To José Salvador and María Elena, who were an example of integrity in my life.

To Salvador for his constant advice and support.

To my friends who remained by my side despite the difficulties of our age.

To CONACYT for the financial support given to me via the National Scholarship Program, that made the completion of my doctoral studies possible.

And lastly to my advisors, Dr. Mauro and Dr. Simón, for their deeply appreciated teachings and invaluable academic and moral support throughout my career.

Chapter 1

Introduction

In humanity's search for the comprehension of the world around us, not frequently have we witnessed such successful endeavor as the development of particle physics. The Standard Model (SM) is the theory put together for the purpose of describing the phenomena regarding three of the four fundamental forces that we know exist in the universe, so called the electromagnetic, weak and strong forces. Such a theory beats the myth of the lone genius, since it is a team effort of hundreds of brilliant minds that worked from different perspectives and approaches, taking as basis the particle physics paradigm with a history spawning since the beginning of the 20th century with experiments regarding the atomic theory, and formally starting with the idea of a quantization of the electron field by Paul Dirac in the late 1920s. With the union between non-relativistic quantum mechanics and the special theory of relativity and electrodynamics, Dirac would lay the foundation of modern high-energy physics with a theory that emphasized elegance over practicality.

For Dirac, the beauty of a concept was more important than the consistency with an experiment, something that was not much of a problem at the moment since, as he wrote in 1927, "*hardly anything has been done up to the present on quantum electrodynamics*" [1]. In time, Dirac would be convinced of the contrary, that a theory no matter how elegant or beautiful, is only complete when it agrees with the experiment. Thankfully, not too long after, his theory began to reproduce results, when the observation of the positron by Carl Anderson in 1932 [2], gave clearance to the idea of antimatter predicted by Dirac, in what he called a *sea of particles with negative energy*. This was only the beginning for the important breakthrough presented by the particle physics paradigm.

Throughout the second half of the 20th century, great efforts and the collaboration of hundreds of scientist and institutions from all over the world culminated with the discovery of the Higgs boson in 2012, the last piece of the Standard Model puzzle and the set of fundamental particles that conform the known matter content of our universe

(see Fig. 1.1). This Quantum Field Theory encompasses the interactions of electromagnetic, weak and strong forces by the exchange of the corresponding spin-one gauge fields in what is known as a non-abelian gauge theory where the symmetry group is $SU(3)_C \times SU(2)_L \times U(1)_Y$, a theory which is theoretically self-consistent, that is, free of anomalies. With the experimentally found mass value of $M_H = 125\ GeV$ and the mass of the heaviest quark, $M_t = 175\ GeV$, the Standard Model is also recognized as a consistent perturbative scheme for the calculation of properties of systems at very high energies compared to the currently accessible by particle accelerators (the Large Hadron Collider, for example, has set the record for total collision energy of 13 TeV).

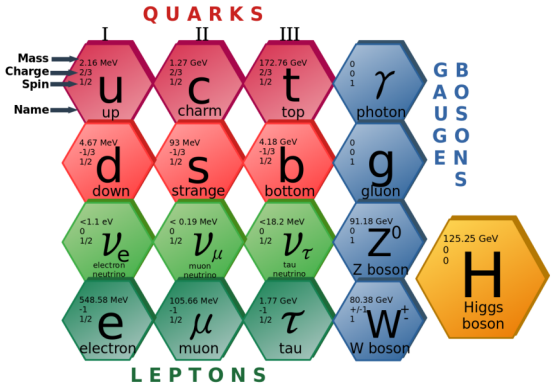

FIGURE 1.1: Elementary particles of the Standard Model (for a complete review of their properties see Ref. [3]). The first three columns, quarks and leptons, are called fermions and are divided in three generations (I, II, III). The first generation constitutes the ingredients of the ordinary matter we observe in our day-to-day life.

The SM is successful at predicting properties and phenomena for the interactions it was set up to describe, for example, the anomalous magnetic dipole moment of the electron predicted by quantum electrodynamics is the most accurately verified prediction in physics, agreeing with the experimental measurement to more than 10 significant figures. While also measured precisely, the same level of precision is not achieved for the muon [4], which exceeds the SM prediction by 4.2σ, and its one of the discrepancies that have yet to be deciphered. There are also many other unanswered questions that as particle physicists we aspire to address. For starters, **gravitational interactions** have yet to be included and we have not yet arrived to a full realization of quantum mechanics and general relativity as a consistent (quantum field) theory. There is also a visible excess of matter against antimatter, also known as **baryon asymmetry** [5], that we would like to attempt to explain. Additionally, the SM scheme works with the assumption that **neutrinos are massless**, but this is in fact not the case as seen from neutrino experiments. If we were to modify the theory to accommodate neutrino masses [6], there is still no elucidation as to their nature, whether it is a Majorana or a Dirac neutrino. Some attempts

to solve these obscure aspects of physics involve some extension or modification of the SM theory, which is often referred to as *physics beyond the standard model*.

Another fundamental problem that physicists face is the failure to account for as much as 95% of the energy content of our universe today. From the observation of the relic radiation from the Big Bang, what we know as the Cosmic Microwave Background (CMB) [7], and assuming the ΛCDM cosmological model as correct, we know that the conventional matter described by the Standard Model represents only 4.9% of the mass/energy density of the universe, while 26.0% is formed by what is known as *dark matter* and the remaining 68.9% corresponds to an unknown form of energy called dark energy that would be behind the accelerated expansion of the universe. The last two are not included or even elucidated by the successful theory mentioned above. The focus of this work is the first of these two crucial ingredients of the cosmos, dark matter. What is it and how do we know it exists?

First, let us understand the signs that indicate the presence of this mysterious phenomena.

1.1 Observational evidence of dark matter

Throughout history, the creation of knowledge involves two fundamental principles. One, that the Universe contains something that, until perceived, remains unknown to us, and two, that as new things are discovered, the development of new technology helps us reveal new phenomena that was previously undiscovered. In short, new discoveries foster the creation of technology which boosts further discoveries. This specially occurs when it comes to astronomy. For centuries, the wonder caused by the presence of the celestial bodies motivated the search and description of their composition and movement. Johannes Kepler, in the early 17th century, would formulate what is known today as the laws of planetary motion, where he explains the way in which the bodies of the solar system move through elliptical orbits. Isaac Newton would use these notions to formulate the first physical law of universal gravitation [8].

Over the years, several observations indicated a deviation from Newton's law of universal gravitation. When we attempt to solve such inconsistencies, one can choose to completely discard the theory or propose the existence of forces or bodies that act as causes of these deviations. For example, the existence of the planet Neptune was proposed precisely to account for deviations in planetary orbits, and was finally discovered in 1846 [9]. In a similar way, the existence of a planet between the Sun and Mercury was proposed in 1840, but after Einstein's theory of general relativity solved the problem, the existence of this planet was disproved. Astronomical discrepancies fall into one

of these two categories, where problems derived from observations that cannot be explained with known laws imply either the existence of an object or entity that we have not seen, or that the theory which predicts the non-observed result has to be reviewed.

In 1933, Fritz Zwicky, a Swiss-American astronomer, studied the redshifts of various galaxy clusters and noticed differences in the apparent velocities of eight galaxies in the Coma Cluster [10]. He then applied the virial theorem to estimate its mass. This theorem relates the averaged total kinetic energy of a stable discrete particle system with its potential energy, widely used in astronomy to quantify the mass and size of galaxies. Zwicky found that for a galaxy cluster of the size of the Coma Cluster, the velocity dispersion of its galaxies should be around 80 km/s, in contrast with the observed average velocity dispersion of 1000 km/s. He concluded that there was a presence of "*dunkle Materie*" (or dark matter) in much greater amounts than that of the luminous matter of the cluster. This is often quoted as the first observation (and usage of the term) of dark matter, but in fact such idea was formed as earlier as 1906, when Lord Kelvin attempted to estimate the amount of non-luminous matter in the Milky Way, where he stated that many stars within the galaxy might have been extinct or not bright enough to be observed, but still present as to affect the velocities of the stars. Henri Poincaré, in discussions with Lord Kelvin about this novel idea, explicitly called this phenomena "*matiere obscure*" [11].

Despite there being multiple accounts of discrepancies between observable matter and the apparent matter content from velocity distributions of galaxies after Zwicky's statement, the problem did not present an immediate concern in the field of astrophysics until the 1970s[12]. This is when the observations of the M31 rotation curve were published by Vera Rubin and Kent Ford [13], and the optical data presented became a clearer and explicit argument for the need to understand the discrepancy in rotation curves, which peaked at larger radii than predicted. More observations on this regard began to appear during this decade. Taking the Newtonian dynamics that describe the orbits of stellar objects, the rotational velocity of an object that orbits at a distance r from the center of a galaxy is $v(r) = \sqrt{GM(r)/r}$, where $M(r)$ is the mass enclosed within r. Thus, one expects that the velocity distribution scales as $1/\sqrt{r}$. However, the observations indicated that rotation curves became flat as one goes far from the center of the galaxy, as obtained by Rogstad and Shostak in 1972 [14] (see Fig. 1.2).

Soon, more similar observations would appear, and the argument emerged, that in order to have a rotation curve such as registered by the data, there had to be an object with the density profile of a halo within the galaxy that absorbed and emitted no light (see an example in Fig. 1.3). By looking that the mass-to-light ratio indicated by rotation curves of various galaxies and clusters, it was found that the masses of these objects was

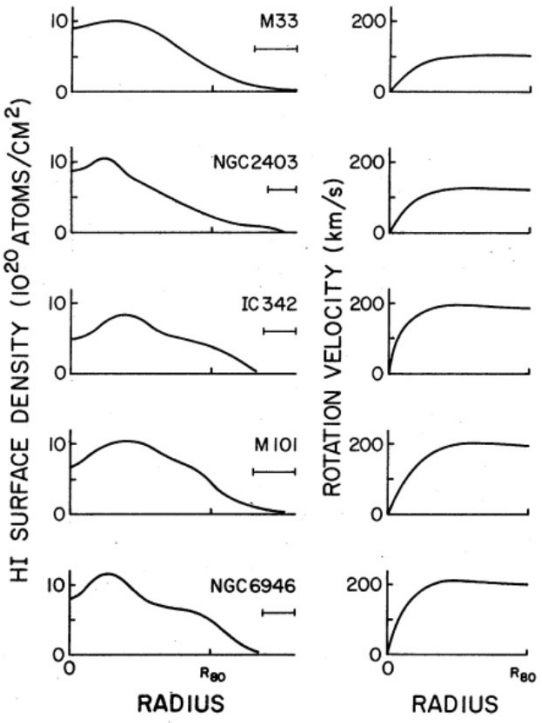

FIGURE 1.2: Rotation curves (right) for five galaxies as opposed to the hydrogen surface density profile (left) obtained by Rogstad and Shostak in 1972 [14]. R_{80} is the radius containing 80% of the observed hydrogen.

underestimated by a factor of about ten [15, 16]. This occurrence was the first convincing piece of evidence that a form of *matter* unobserved by current instruments exists.

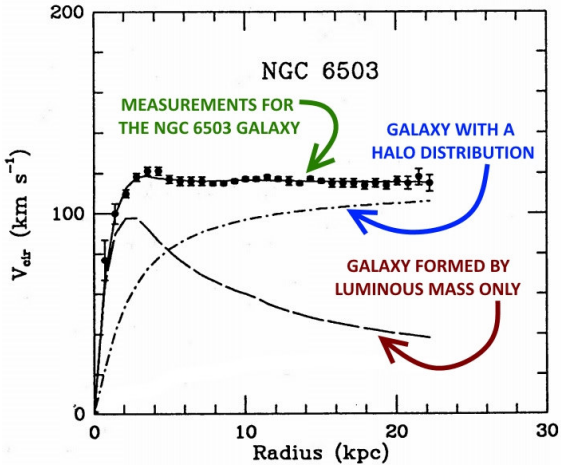

FIGURE 1.3: Rotation curve for the galaxy NGC6503 [17]. It is shown that the measurements indicate the presence of an object with a halo distribution in addition to the luminous mass profile of the galaxy.

Evidence for dark matter in galaxies and galaxy cluster spiked interest in astronomers

and astrophysicists who began to question the nature of this invisible material, considering first the possibility that said missing mass could consist of compact objects, much less luminous than ordinary stars, known as "MACHOs" (massive astrophysical compact halo objects)[12]. A proposal by Bohdan Paczynski envisioned a way to search for these compact objects within the dark halo of the Milky Way using the phenomena of gravitational microlensing [18]. Gravitational lensing is a phenomenon predicted by Einstein's theory of general relativity, in which light is deflected by gravity. In this case, monitoring the stars of a nearby galaxy, detecting variations in their brightness could indicate the presence of massive objects. For a dark halo to consist entirely of MACHOs, the microlensing optical depth, that is, the ratio of stars that would be magnified is one in two million. With this purpose, over a period of almost six years, the MACHO Collaboration reported the light curves of 40 million stars, where 14 to 17 possible microlensing events were identified, which was about the expected background rate [19]. Later, the EROS Collaboration added another seven years of data, only one microlensing event was identified, which placed an upper limit of 8% on the halo mass fraction from MACHOs [20, 21], which indicated that the missing mass in the Milky Way's halo could not be produced in its entirety by these compact objects.

An even stronger case against the MACHOs alternative in explaining the missing mass of the galaxies comes from the cosmic baryon density as a result from measurements of primordial light element abundances and the cosmic microwave background. The observation of the energy composition of the universe presents a compelling argument for the existence of this strange type of matter, which will be described in the following section.

1.2 Energy content of the universe

There is an epoch in the history of the universe, around 378,000 years after the Big Bang, where free electrons were bounded to protons forming hydrogen, known as the recombination period. This combination of electrons and protons generally occur in a high energy state, so the transition to the low energy state emits photons. The photons that are not captured by other hydrogen atoms are said to *decouple*, that is, are able to travel longer distances. This electromagnetic radiation can be detected today as radio waves in what is known as the cosmic microwave background (CMB). Observation of the CMB (CMB) points to an important idea, that the universe appears to be homogeneous and isotropic on large scales, pointing to the fact that all positions in the universe are essentially comparable (see Fig. 1.4). Around the 1940s, George Gamow, Ralph Alpher, and Robert Herman began to formulate what is now known as the Big-Bang model [22]. This model proposes that the early universe began as extremely dense and hot, and that with

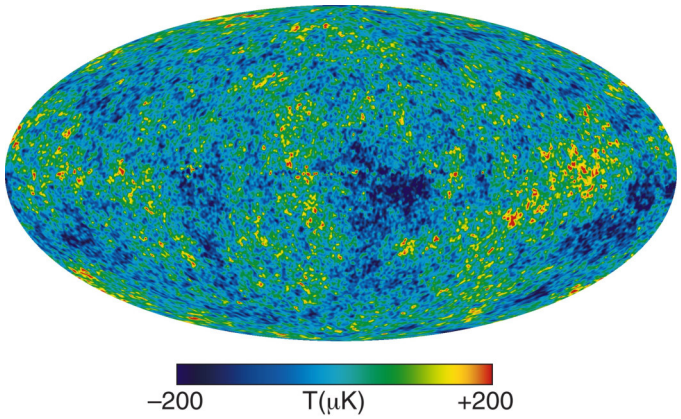

FIGURE 1.4: Internal Linear Combination Map (ILC), which is a linear combination of the WMAP (Wilkinson Microwave Anisotropy Probe) maps, at five different frequencies. This map shows the anisotropy of the CMB [23].

the passage of time it expanded and cooled, resulting in the presence of a "relic" radiation at the background of the universe, with a temperature of the order of a few Kelvin. The cosmic microwave background, and the observation of a temperature around 3 K, distinguish the Big Bang model as the most likely to describe the universe.

The geometry of the universe can be described by the curvature parameter k ($k = 1$ indicates a closed curvature, $k = 0$ is for a flat universe and $k = -1$ stands for an open curvature). In the late 1920s, after the derivation of the Friendman equations by including the metric of a homogeneous and isotropic universe into Einstein's field equations [24], it was discovered that the universe is expanding at a calculable rate [25, 26], that is, that the structures immerse in the universe are moving away from each other. This expansion can be measured using the parameter $R(t)$. The metric that describes this geometry is known as the Friedmann-Lemaître-Robertson-Walker (FLRW) metric, described by

$$ds^2 = g_{\mu\nu}dx^\mu dx^\nu = -dt^2 + R^2(t)\Big[\frac{dr^2}{1-kr^2} + r^2(d\theta^2 + sin^2\theta d\phi^2)\Big], \tag{1.1}$$

where we are considering $c = 1$. The equations of motion are derived from the Einstein equations,

$$\mathcal{R}_{\mu\nu} - \frac{1}{2}g_{\mu\nu}\mathcal{R} = 8\pi G_N T_{\mu\nu} + \Lambda g_{\mu\nu}, \tag{1.2}$$

where $g_{\mu\nu}$ is the metric in Eq. (1.1), $\mathcal{R}_{\mu\nu}$ is the Ricci tensor that depends on the metric and its derivatives, with $\mathcal{R} \equiv g^{\mu\nu}\mathcal{R}_{\mu\nu}$ being the Ricci scalar. G_N is the Newton constant and $T_{\mu\nu}$ is the energy-momentum tensor. $\mathcal{R}_{\mu\nu}$ and $T_{\mu\nu}$ are defined as follows for a perfect

fluid [3, 27],

$$\mathcal{R}_{\mu\nu} = \partial_\alpha \Gamma^\alpha_{\mu\nu} - \partial_\nu \Gamma^\alpha_{\mu\alpha} + \Gamma^\alpha_{\beta\alpha}\Gamma^\beta_{\mu\nu} - \Gamma^\alpha_{\beta\nu}\Gamma^\beta_{\mu\alpha}, \tag{1.3}$$
$$T_{\mu\nu} = -p g_{\mu\nu} + (p+\rho) u_\mu u_\nu,$$

where p stands for the isotropic pressure, ρ is the energy density, $u = (1,0,0,0)$ is the velocity of the isotropic fluid and $\Gamma^\sigma_{\lambda\delta}$ is called the Christoffel symbol, defined as [28],

$$\Gamma^\sigma_{\lambda\delta} = \frac{1}{2} g^{\sigma\eta}\Big(\frac{\partial g_{\eta\delta}}{\partial x^\sigma} + \frac{\partial g_{\sigma\eta}}{\partial x^\delta} - \frac{\partial g_{\sigma\delta}}{\partial x^\eta}\Big). \tag{1.4}$$

From the Einstein equations one can derive the Friedmann equation. For $\mu = \nu = 0$, the trace of R in Eq. (1.2) is

$$\Big(\frac{\dot{R}}{R}\Big)^2 \equiv H^2 = \frac{8\pi G_N \rho}{3} - \frac{k}{R^2} + \frac{\Lambda}{3}. \tag{1.5}$$

We define as critical density as that which renders $k = 0$ when $\Lambda = 0$,

$$\rho_c = \frac{3H^2}{8\pi G_N}. \tag{1.6}$$

The value of the critical density today is $\rho_{c,0} = \frac{3H_0^2}{8\pi G_N} = 1.05371 \times 10^{-5} h^2 GeV cm^{-3} = 2.77536 \times 10^{11} h^2 M_\odot Mpc^{-3}$ [3] where h is a dimensionless number that parametrizes H_0, which is called the Hubble constant, or the value of H today. It should not be mistaken for the Planck constant, which we set as $\hbar = h/2\pi = 1$ within this work. The parameter h is defined as

$$H_0 \equiv 100\, h\, km\, s^{-1}\, Mpc, \tag{1.7}$$

and its value was estimated $h = 0.677 \pm 0.004$ by recent Planck measurements of the CMB [7]. However, higher values ($h = 0.732 \pm 0.013$) have been derived from distance-ladder estimates [29].

We can rewrite Eq. (1.5) in terms of the critical density

$$H^2\Big(\frac{\rho}{\rho_c} + \frac{\rho_\Lambda}{\rho_c} - 1\Big) = \frac{k}{R^2}, \tag{1.8}$$

where $\rho_\Lambda = \frac{\Lambda}{3H^2}\rho_c$. The density parameter $\Omega_i = \rho_i/\rho_c$ is the energy density of a species "i" relative to the critical density. With this, the Friedmann equation can be written as

$$\sum_i \Omega_i + \Omega_\Lambda - 1 = \frac{k}{R^2 H^2}. \tag{1.9}$$

The parameters we just described track the history of the Universe, and the strongest probes we have to describe them come from the evolution of perturbations, that is, deviations from the homogeneity of the Universe. The density perturbation field which describes these density fluctiations is defined as

$$\theta(\boldsymbol{x}) \equiv \frac{\rho(\boldsymbol{x}) - \langle\rho\rangle}{\langle\rho\rangle}. \tag{1.10}$$

We can construct a Fourier-space representation of this function,

$$\theta(\boldsymbol{x}) = \int \frac{d^3k}{(2\pi)^{3/2}}\theta(\boldsymbol{k})e^{-i\boldsymbol{k}\cdot\boldsymbol{x}}. \tag{1.11}$$

One can employ periodic boundary conditions in a cube of large volume V to simplify the calculation due to an infinite Universe, and computing the variance in the field turns into a sum over modes of the power spectrum. Let us define

$$\langle\theta(\boldsymbol{k})\theta(\boldsymbol{k'})\rangle = |\theta(\boldsymbol{k})|^2\delta(\boldsymbol{k}-\boldsymbol{k'}) \equiv P(k)\delta(\boldsymbol{k}-\boldsymbol{k'}), \tag{1.12}$$

where we write $P(k)$ instead of $P(\boldsymbol{k})$ due to the isotropic nature of the fluctuations. We can see that, since $\theta(\boldsymbol{x})$ is dimensionless, $P(k)$ has the same dimension as k^{-3}. Additionally, it is easy to see that

$$\langle\theta(\boldsymbol{x})\theta(\boldsymbol{x})\rangle = \int \frac{\langle\theta(\boldsymbol{k})\theta(\boldsymbol{k'})\rangle}{(2\pi)^3}e^{-i(\boldsymbol{k}-\boldsymbol{k'})\cdot\boldsymbol{x}} = \int \frac{k^2dk}{2\pi^2}P(k) = \int d(lnk)\frac{k^3P(k)}{2\pi^2}. \tag{1.13}$$

From here, we define the *dimensionless power spectrum*, Δ^2 (or $\mathcal{P}$), as

$$\Delta^2(k) \equiv \frac{d\langle\theta^2\rangle}{dlnk} = \frac{k^3P(k)}{2\pi^2}. \tag{1.14}$$

This function contains the statistical description of the perturbations, and is the most powerful probe for the parameters of a cosmological model. Finding a fit to the dimensional power spectrum to the date gives us the values of the parameters that best describe the history of the Universe. If the density perturbations obey Gaussian statistics, the power spectum then provides all the properties of the perturbations [3].

It is observed that the CMB has a dipole anisotropy of the order of 10^{-3}, while higher-order multipole moments are much smaller (10^{-5}) and decaying rapidly for larger moments, which means fluctuations of temperature in the CMB are only important at large angular sclaes, and there are only tiny perturbations for small scales. This indicates that our Universe was very homogeneous at the beginning, and evolved first linearly and

then non-linearly to form the present structure. The fact that small-scale perturbations are small is a direct evidence that the matter of the Universe is formed primarily by non-baryonic (non-interacting with radiation) collisionless matter.

A useful and broadly accepted hypothesis is that the sole mechanism for generating these perturbations is the cosmic inflation, in which the density fluctuations are generated during a period of accelerated expansion of the early Universe by the amplification of quantum fluctuations [30]. For small perturbations, one can calculate their evolution through available numerical codes such as CAMB or CLASS [31, 32].

The Planck satellite offers important observations on CMB anisotropies which can be compared with the power spectrum obtained with the numerical codes to fix the parameters described above. The first parameter that can be obtained is Ω_γ, and is actually directly measured from the energy of the CMB. By determining its temperature to be $T = 2.7255 \pm 0.0006$ K from observations by the Far Infrared Absolute Spectrophotometer (FIRAS) of the CoBE satellite [33], the corresponding value is $\Omega_\gamma = 2.473 \times 10^{-5} h^{-2}$.

With the data from the primary CMB, and adding the Planck lensing measurements, while assuming that the dark energy is a cosmological constant, tields a 68% confidence constraint on Ω_{tot} [3],

$$\Omega_{tot} \equiv \sum_i \Omega_i + \Omega_\Lambda = 1.011 \pm 0.006. \tag{1.15}$$

And adding experimental data of distance measurements of the baryon acoustic oscillations (BAO), yields the value $\Omega_{tot} = 0.9993 \pm 0.0019$ [7]. We can then justify $k = 0$, which corresponds to a flat universe. This restriction allow us to relate the density parameters between each other. Ω_b describes the baryonic density, Ω_γ the photon density and Ω_ν the neutrino content. In the Cold Dark Matter (CDM) scheme, where we assume that interactions of dark matter (whose relative energy density is denoted as Ω_c) with the rest of the species is very small and that the species is non-relativistic, we can predict the structure formation in the early stages of the universe. With both the assumption of a cosmological constant, we refer to this scheme as ΛCDM.

With this assumption, a fit of the parameters Ω_b and Ω_c can be performed with data from the CMB, combined with measurements from gravitational lensing and baryon density from big-bang nucleosynthesis (BBN)[7]. The rest of the parameters are obtained from various experimental data such as distance measurements of the baryon acoustic oscillations (BAO) [3]. Finally, the energy content of the universe is described

by the following values

$$\begin{aligned} \Omega_\gamma h^2 &= 2.473 \times 10^{-5}, \\ \Omega_\nu h^2 &= (\sum m_\nu)/93.04eV \leq 0.0013, \\ \Omega_b h^2 &= 0.02242 \pm 0.00014, \\ \Omega_c h^2 &= 0.1193 \pm 0.0009, \\ \Omega_\Lambda &= 0.689 \pm 0.006, \end{aligned} \tag{1.16}$$

where $h = 0.677 \pm 0.004$. It is from these values that we state that the ordinary matter, that is, the elements described by the standard model, conforms only 4.9% of the energy in the universe, while dark matter constitutes 26.0%, and the remaining 68.9% is what is known as dark energy. In fact, although galaxy rotation curves were perhaps the first crucial observations in regards to dark matter, as we mentioned it in the previous section, in reality the CMB data is the strongest argument for the existance of DM and it gives a precise measurement of its abundance.

Now that we know for certain that there is a phenomenon that has yet to be explained, as we mentioned before, the next step to solve the mystery is to propose a solution. One possibility is to think of the problem of the missing mass in galaxies and clusters not as a sign of an additional species, but as a problem with the Newtonian gravitational theory. In this regard, the MOND (Modified Newtonian Dynamics) scheme is a proposal designed to account for the shapes of rotational curves of galaxies and other extragalactic phenomenology [34], and it has been proven successful at fitting these observables [35, 36] as well as the baryonic Tully-Fisher relation [37, 38], which empirically relates the luminosity and the emission line width of a galaxy. However, MOND cannot completely get rid of the need for dark matter in astrophysical systems such as galaxy clusters, which comes in contrast with the original idea of MOND solving the missing mass problem without dark matter. The MOND scheme also has difficulty explaining structure formation[39], as well as the observed anisotropies in the CMB[40].

We can also consider the solution to the dark matter problem to be a new particle derivated from an extension of the standard model. First, we must list the requirements that such particle must accomplish in order to be considered a good candidate for dark matter.

1.3 Candidates for dark matter

It is said that a proposal is considered a good dark matter candidate when it meets the following criteria.

- It must account for the relic density observed by the CMB (see Eq. (1.16)). For some time, standard model neutrinos were considered possible DM candidates, however it is easy to calculate the total relic density derived from these species and realize that it cannot account for the observed abundance, thus they were discarded [41].
- It must be "cold", that is, non-relativistic before the matter dominated era and can clump and form the cosmological structures we see today. Hot dark matter is found to be not sufficient to account for the dark matter content of the Universe [41], but it can be included in addition to a cold dark matter candidate. Alternatively, *warm dark matter* is also a possibility, in which this form of DM exhibits properties of both cold and hot DM. In these models, the non-vanishing velocity of the dark matter particle supresses the power spectrum on small scales, which is consistent with the observations [42–44].
- It must be effectively neutral, that is, it must interact very weakly with electromagnetic radiation to the point that it explains its *dark* nature. In standard model terms, it must effectively be a singlet of the $SU(3)_c \times SU(2)_L \times U(1)_Y$ group, and many stringent constraints exist in this regard [45].
- It must leave stellar evolution and Big Bang Nucleosynthesis predictions unchanged [46]. Additionally, another cosmological signature that puts strong constraints on galaxy formation models is the Tully-Fisher relation [47], which correlates the rotation velocity of disk galaxies with its baryonic mass, which can be used to test cosmological models such as ΛCDM [37, 48–50].
- It must be consistent with current experimental bounds. For instance, bounds on the DM-nucleon scattering cross section set by direct detection experiments such as XENON1T [51]. There are also bounds on dark matter annihilation into SM particles from indirect detection experiments, that involve the measurement of the surplus of gamma ray flux coming from satellite galaxies [52] and the center of the Milky Way [53]. Additionally, there are also limits for the dark matter production at high energy colliders [54, 55].

One of the currently proposed dark matter candidates proposed that must give solution to the mentioned issues are the **sterile neutrinos**. These are hypothetical particles similar to the SM neutrinos, but without weak interactions (aside from mixing) [56]. Light sterile neutrinos are ruled out from the CMB experiment (although they can be compatible if by some mechanism their presence in the early universe is supressed) [57, 58], so the stringent cosmological and astrophysical constraints on these candidates come mainly from the dark matter cosmological abundance and the decay products.

Dark matter candidates could also come from proposals that targeted other problems of the standard model, such as **axions**. These are particles introduced as an attempt to resolve the strong CP problem [59]. The solution involves the postulation of a global $U(1)_{PQ}$ quasi-symmetry [60], which after being broken spontaneously gives rise to a quasi-Nambu-Goldstone boson, which is the axion. Although the calculation of the axion relic density is uncertain and depends on assumptions of its production mechanism, there are acceptable ranges where axions are able to satisfy experimental constraints on dark matter, and thus remain a possible candidate [61].

Some dark matter candidates are chosen from popular extensions of the Standard Model. For instance, candidates from supersymmetry include neutralinos, sneutrinos, gravitinos and axinos. For a review of the theoretical, phenomenological and experimental aspects of some of these candidates, see Ref. [62].

In fact, supersymmetric extensions of the Standard Model predict particles with certain characteristics that can account for the dark matter relic density, and such coincidence is known as the *WIMP paradigm*. This paradigm, which has been by far the most studied and promising approach to dark matter in the last decades, arose from the observation that for typical weak-scale pair annihilation cross sections ($\sigma \sim G_F^2 T^2$, where G_F is the Fermi constant), for typical freeze-out temperatures ($T \sim M/20$) and electroweak-scale masses of the order of 100 $GeVs$, the thermal relic density is consistent with the observed cosmological density. This paradigm is understood only as a coincidence in terms of the values of the cross sections, and not unique to weak interactions. Usually, candidates of this regime fall into the structure of existing SM particles, such as fermion, scalar or vector fields. However, a recent study concluded that from experimental bounds and searches, WIMPs with these space time structures have not much room left in terms of mass-cross section range [63].

1.4 Our hypothesis: tensor dark matter

In this work we propose an alternative explanation to the nature of dark matter. We consider the possibility that dark matter fields have an unconventional space-time structure. The standard model is a gauge quantum field theory and basic principles (causality, cluster decomposition, etcetera) require that fields describing matter and energy transform in the irreducible representations (irreps) of the Homogeneous Lorentz Group (HLG).

The Lorentz group is defined as the set of transformations that leave the inner product of four-vectors invariant, that is, they preserve the quadratic form $t^2 - x^2 - y^2 - z^2$. Such

transformations include boosts, rotations and time and space translations. The Homogeneous Lorentz Group (HLG) is the group that includes these transformations but leaving out the space-time translations. This is not a connected group, as it is formed by four disjointed components: the isometry which contains time-reversal transformations, one for spatial reflections, another that includes both time-reversal and spatial reflections, and one that preserves the direction of time and spatial parity. The latter, $SO(3,1)$, which is the subset containing the identity, is also referred as the proper isochronous HLG.

The proper isochronous HLG transformations are isomorphic to $SU(2) \times SU(2)$, that is, its finite-dimensional irreps are characterized by two $SU(2)$ quantum numbers (a,b). The subsets of the HLG are mapped one into each other by discrete symmetries and the symmetries of a free particle include parity. Since the free particle description is the starting point for the usage of the gauge principle in the standard model, and parity maps the irreps $(a,b) \leftrightarrow (b,a)$, we actually need the free fields to transform in the representations $(a,b) \oplus (b,a)$, except in the case $a = b$ where the space (a,a) is also an irrep of parity. The standard model uses only a few of the irreps of the HLG: the $(1/2,0) \oplus (0,1/2)$ for quarks and leptons, the $(1/2,1/2)$ for gauge bosons and the $(0,0)$ for the Higgs boson. Proposals for physics beyond the standard model mentioned above use the very same representations (except for a few of them like supersymmetric theories which include spin $3/2$ particles in the Rarita-Schwinger formalism such as the gravitino [64, 65]), thus most of the existing candidates for dark matter have conventional space-time structures.

We explore here the possibility that dark matter particles are described by fields transforming in the $(1,0) \oplus (0,1)$ representation of the HLG. A field transforming in this representation is conventionally described using an equivalent antisymmetric tensor with two indices, thus we follow the conventional notation and name it **Tensor Dark Matter**.

This work is organized as follows: In Chapter 2, we review the spinor-like formalism for fields transforming in the $(1,0) \oplus (0,1)$ representation of the Homogeneous Lorentz Group, use it to describe free dark matter and construct the corresponding effective field theory for interactions with standard model fields in a hidden scenario.

This effective field theory gives rise to interactions between dark matter and standard model particles inducing transitions such as the decay of the Z^0 and the Higgs bosons into a dark matter particle-antiparticle pairs for light dark matter. In Chapter 3 we calculate the corresponding decay widths. The calculation of these transitions are straightforward and train us in the trace techniques for the matrices in the covariant basis. These transitions should contribute to the invisible widths of the Z^0 and H and we obtain the

first constraints on the mass and couplings of tensor dark matter from the measured invisible decay widths in this chapter.

With these results in mind, we go forward to the calculation of the most stringent criteria for a dark matter candidate: relic density. In Chapter 4, we describe in detail the calculation of the relic abundance and obtain bounds on the mass and the couplings of tensor dark matter from the observation mentioned in Eq. (1.16).

Once we make sure that tensor dark matter can account for the observed relic abundance, we further test our hypothesis against experimental data, such as the bounds set by direct detection experiments. The principle behind direct detection experiments is the notion that, if the galaxy contains dark matter particles, they have to pass through Earth, and we can search for possible signs of interactions between dark matter and standard model particles. The products of such interaction could appear as recoil energy of nuclei from, for example, dark matter-nucleon scattering. We give a thorough explanation of this type of dark matter probe in Chapter 5, where we compare the results of tensor dark matter-nucleon scattering with current bounds from the XENON1T experiment [51].

Another source of experimental bounds comes from what are known as indirect dark matter searches. Indirect detection is a technique that involves the observation of the products of dark matter annihilations (or decays). Typically, the products that we observe in this regard come in the form of radiation, of which telescopes and detectors obtain a flux that is proportional to the annihilation (or decay) rate of dark matter. Therefore, it is natural to assume that if we find an excess of radiation flux coming from the cosmos, either from the Center of the Galaxy or other astronomical sources, we can set limits on the annihilation or decay rate for our candidate. In this case, we work with three main sources. First, the gamma rays coming from the Galactic Center, of which we describe the flux and its calculation from the tensor dark matter approach in Chapter 6. In this chapter, we also look into gamma rays coming from a type of stellar object that is believed to have large amounts of dark matter, called dwarf spheroidal satellite galaxies. We go into the details of this signal and arrive to bounds to the mass and couplings of tensor dark matter.

An additional signal from indirect detection is the cosmic ray antiproton excess, which is a surplus of antimatter observed in our galaxy and that could be described with the products of dark matter annihilation. We explain this phenomena and propose tensor dark matter as a possible explanation in Chapter 7.

As we will see in the course of this work, the main conclusion from the phenomenological study of the proposal of a $(1,0) \oplus (0,1)$ space-time structure as a possible framework for a dark matter candidate is that several observables are successfully explained

with a tensor dark matter particle with a mass $M \approx M_H/2$, specifically within the $[62.470, 62.505]$ GeV window and with a scalar coupling to Higgs boson of the value of $g_s \in [0.98, 1.01] \times 10^{-3}$. These observables include bounds from Z and H bosons invisible decay widths, dark matter relic density, direct and indirect detection limits, including cosmic ray antiproton excess. This sharp prediction along with the fact that the leading terms in the interaction Lagrangian are dimension-four, motivated us to explore a more general construction. In this regard, we introduce the possibility of dark matter interactions coming from a dark gauge structure, a dark gauge group that includes a factor $U(1)_d$ subgroup that mixes kinetically with the $U(1)_Y$ of the standard model. We work out the consequences of this idea in Chapter 8.

Finally, the conclusions and perspectives concerning this work are presented in Chapter 9. Additionally, the Appendix includes the traceology of the covariant basis for fields transforming in the $(1,0) \oplus (0,1)$ representation, which is used for the calculations pertaining this proposition.

Chapter 2

Tensor Dark Matter

The Standard Model (SM) uses only a few representations of the HLG. The Higgs field transforms in the $(0,0)$ representation, the gauge fields in the $(1/2,1/2)$ representation, while the matter fields, quarks and leptons, use the $(1/2,0)\oplus(0,1/2)$ representation. Proposals for physics beyond the standard model consider higher spin representations involving gauge fields such as a spinor-vector in the $[(1/2,0)\oplus(0,1/2)]\otimes(1/2,1/2)$ representation, used in supersymmetry. However, elementary systems with high spin (or $j>1$) have been difficult to describe in the realm of quantum field theory (QFT). There are many problems in the construction of a QFT for high spin fields which in the widely used Rarita-Schwinger (RS) formalism can be traced to the constraints on the RS field necessary to describe single spin states. In the interacting theory these constraints are modified in such a way that the theory is inconsistent [66–72].

Aiming to construct a consistent QFT for interacting high spin fields, a covariant basis for the single spin $(j,0)\oplus(0,j)$ representation was worked out in Ref. [73], where the cases of $j=1/2,1$ and $3/2$ are explicitly derived. The $j=1/2$ case correctly reproduces the conventional basis for the Dirac representation. The $j=1$ case corresponds to a space-time structure that we will employ later in this work for the description of dark matter, which we will refer to as **Tensor Dark Matter**. We will describe the formalism for this representation in this chapter.

2.1 Representations of the Homogeneous Lorentz Group

A Lorentz transformation is a coordinate transformation between two inertial frames such that $x^\mu \to x'^\mu = \Lambda^\mu_\nu x^\nu + a^\mu$, with a^μ and arbitrary constant. Such transformation, by Einstein's principle of relativity, must satisfy the invariance of a spacetime interval, in other words

$$g_{\mu\nu}dx'^\mu dx'^\nu = g_{\mu\nu}dx^\mu dx^\nu. \tag{2.1}$$

Since a^μ is a constant, satisfying the invariance implies that

$$g_{\mu\nu}\Lambda^\mu_\alpha\Lambda^\nu_\beta = g_{\alpha\beta}. \tag{2.2}$$

Taking the determinant of Eq. 2.2, we arrive at the conclusion that $Det(\Lambda)^2 = 1$. The full set of transformations $\Lambda^\mu_\nu x^\nu + a^\mu$ forms a group generally known as the *inhomogeneous Lorentz group* or *Poincaré* group [74]. If we take only transformations with $a^\mu = 0$, we obtain a subgroup called *homogeneous Lorentz group*. From Eq. 2.2 we can also see that

$$\begin{aligned} g_{\mu\nu}\Lambda^\mu_0\Lambda^\nu_0 &= g_{00}(\Lambda^0_0)^2 + \sum_{\mu,\nu=1}^{3} g_{\mu\nu}\Lambda^\mu_0\Lambda^\nu_0 \\ &= -(\Lambda^0_0)^2 + \sum_{\nu=1}^{3}(\Lambda^\nu_0)^2 = g_{00} = -1, \end{aligned} \tag{2.3}$$

which implies that either $\Lambda^0_0 \leq 1$ or $\Lambda^0_0 \geq 1$. With this, it is easy to see that the Homogeneous Lorentz Group (HLG) is formed of four components: with $Det(\Lambda) = \pm 1$ and with $\Lambda^0_0 \leq 1$ or $\Lambda^0_0 \geq 1$. This means that the HLG is a disjoint group since, using the transformations of space inversion (P), time inversion (T) and space-time inversion (PT), we can chose the *proper orthochronous Lorentz group* $\mathcal{L}^\uparrow_+$, which is the one with $Det(\Lambda) = +1$ and $\Lambda^0_0 \geq 1$, and the other components would be discrete transformations of P, T or PT of this subgroup. Therefore, any Lorentz transformation can be written as the product of an element of the proper orthochronous Lorentz group with one of the aforementioned discrete transformations [74].

Any representation of the group is defined by the infinitesimal Lorentz transformations, of the form

$$\Lambda^\mu_\nu = \delta^\mu_\nu + \omega^\mu_\nu, \tag{2.4}$$

From Eq. 2.2, taking into account ω^μ_ν is an infinitesimal term, we find out that it must be antisymmetric, e.g. $\omega^\mu_\nu = -\omega^\nu_\mu$. The corresponding unitary operators are of the form [75]

$$U(1+\omega) = 1 + \frac{i}{2}\omega_{\alpha\beta}J^{\alpha\beta} + ... \qquad . \tag{2.5}$$

Since ω^μ_ν is an antisymmetric 4×4 tensor, we have $(4\times 3)/2 = 6$ independent parameters, that is, we have six operators $J^{\mu\nu}$ that describe the Lorentz transformation. We typically denote them as two Hermitian three-vectors $\boldsymbol{J}$, which generates rotations and $\boldsymbol{K}$, which generates boosts, which can be written as

$$J_i = \frac{1}{2}\epsilon_{ijk}J_{jk}, \qquad K_i = J_{i0} = J_{0i}. \tag{2.6}$$

From here, we find that these operators have the following properties

$$[J_i, J_j] = i\epsilon_{ijk}J_k, \tag{2.7}$$
$$[J_i, K_j] = i\epsilon_{ijk}K_k, \tag{2.8}$$
$$[K_i, K_j] = -i\epsilon_{ijk}J_k. \tag{2.9}$$

This does not form a subalgebra, but we can decouple these commutation relations by defining two generators

$$\boldsymbol{A} = \frac{1}{2}(\boldsymbol{J} + i\boldsymbol{K}), \qquad \boldsymbol{B} = \frac{1}{2}(\boldsymbol{J} - i\boldsymbol{K}), \tag{2.10}$$

which have the commutation relations

$$[A_i, A_j] = i\epsilon_{ijk}J_k, \tag{2.11}$$
$$[B_i, B_j] = i\epsilon_{ijk}K_k, \tag{2.12}$$
$$[A_i, B_j] = 0. \tag{2.13}$$

We can see these form two independent $SU(2)$ algebras with quantum numbers j_1 and j_2, each with $2j+1$ degrees of freedom. In conclusion, the HLG is *isomorphic* to $SU(2) \otimes SU(2)$, and its irreducible representations are described by two $SU(2)$ numbers. For example, $(0,0)$ is the trivial representation, which is used to describe scalar fields. We also have the Weyl representations, $(1/2,0)$ and $(0,1/2)$ which are the typical *Weyl* spinors or chiral spinors.

Let us work with the case $(1/2,0) \oplus (0,1/2)$, which is used to describe the Dirac fermions. For the $j = 1/2$ case, the generators $\boldsymbol{J}$ and $\boldsymbol{K}$ have the form [74]

$$\boldsymbol{J} = \begin{pmatrix} \boldsymbol{\tau} & 0 \\ 0 & \boldsymbol{\tau} \end{pmatrix}, \qquad \boldsymbol{K} = \begin{pmatrix} i\boldsymbol{\tau} & 0 \\ 0 & -i\boldsymbol{\tau} \end{pmatrix}, \tag{2.14}$$

where $\boldsymbol{\tau} = \frac{1}{2}\boldsymbol{\sigma}$, and $\boldsymbol{\sigma}$ are the Pauli matrices. The matrix form of a rotation and a boost in this case are

$$\mathcal{D}(\boldsymbol{\theta}) = e^{-i\boldsymbol{J}\cdot\boldsymbol{\theta}} = cos\frac{\theta}{2} - i(\boldsymbol{\sigma}\cdot\boldsymbol{n})sin\frac{\theta}{2}, \tag{2.15}$$
$$\mathcal{B}_{R/L}(\boldsymbol{\phi}) = e^{i\boldsymbol{J}\cdot\boldsymbol{\phi}} = cosh\frac{\phi}{2} \pm (\boldsymbol{\sigma}\cdot\boldsymbol{n})sinh\frac{\phi}{2}. \tag{2.16}$$

Here the tag R/L refers to the $(1/2, 0)$ representation (right, R) and for $(0, 1/2)$ (left, L). We introduce parity transformation Π such that the generators transform as

$$\Pi \boldsymbol{J} \Pi^{-1} = \boldsymbol{J}, \qquad \Pi \boldsymbol{K} \Pi^{-1} = -\boldsymbol{K}. \tag{2.17}$$

This means that the operators of the subalgebra, A and B transform as

$$\Pi \boldsymbol{A} \Pi^{-1} = \boldsymbol{B}, \qquad \Pi \boldsymbol{B} \Pi^{-1} = \boldsymbol{A}. \tag{2.18}$$

This implies that the parity transformation maps from (a, b) to (b, a). If we want our fields to be invariant under parity, we can only have two forms of representation: same quantum numbers (j, j) or a combination $(j, 0) \oplus (0, j)$. For the Dirac case, with $j = 1/2$, the transformations and the corresponding spinor are

$$\Lambda(\boldsymbol{\theta}, \boldsymbol{\phi}) = \begin{pmatrix} \Lambda_R(\boldsymbol{\theta}, \boldsymbol{\phi} & 0 \\ 0 & \Lambda_L(\boldsymbol{\theta}, \boldsymbol{\phi} \end{pmatrix}, \qquad \Psi(\boldsymbol{p}, \lambda) = \begin{pmatrix} \phi_R(\boldsymbol{p}, \lambda) \\ \phi_L(\boldsymbol{p}, \lambda) \end{pmatrix}, \tag{2.19}$$

where $\phi_{R/L}(\boldsymbol{p}, \lambda)$ are the corresponding states of $(1/2, 0)$ and $(0, 1/2)$, respectively. Parity is defined as

$$\Pi = \begin{pmatrix} 0 & 1 \\ 1 & 0 \end{pmatrix}, \tag{2.20}$$

and in the rest-frame, $\Psi(0)$ is an eigenstate under parity with eigenvalues $\pi = \pm 1$, satisfying the following rest-frame parity projection equation

$$\frac{1}{2}(1 \pm \Pi)\Psi(0) = \Psi(0). \tag{2.21}$$

If we perform a boost on both sides of the equation, we arrive at

$$\begin{pmatrix} -\pi & \frac{E+\boldsymbol{\sigma}\cdot\boldsymbol{p}}{m} \\ \frac{E-\boldsymbol{\sigma}\cdot\boldsymbol{p}}{m} & -\pi \end{pmatrix} \Psi(\boldsymbol{p}, \lambda) = 0. \tag{2.22}$$

It is easy to identify that after some work, we arrive at the well-known Dirac equation,

$$(\gamma^\mu \partial_\mu \mp m)\Psi(x) = 0, \tag{2.23}$$

where γ^μ are the Dirac (gamma) matrices.

One could in principle perform the same analysis for any $(j, 0) \oplus (0, j)$ representation,

however it results quite complicated for higher spins. Instead, it is more practical instead to work in a covariant formulation where we build a covariant basis for the operators acting on the $(j,0)\oplus(0,j)$ representation, which simplifies the work for higher spins. Such method is studied in Ref. [73], where the the explicit construction for $j=1/2$ and $3/2$ is worked out.

Let us display, as an example, the same $(1/2,0)\oplus(0,1/2)$ representation under this approach. First, we want to build a basis of covariant operators that act on the $(1/2,0)\oplus(0,1/2)$ space. We obtain the explicit form of the operators by performing the exterior product of the states in the $\{|j,m\rangle_R,|j,m\rangle_L\}$ basis, which provides a basis for the most general bilinear in the fields with HLG properties. The decomposition of the external product of states in this basis gives us the representation of the operators of the basis:

$$[(1/2,0)\oplus(0,1/2)]\otimes[(1/2,0)\oplus(0,1/2)]=(0,0)_2\oplus(1,0)\oplus(0,1)\oplus(1/2,1/2)_2. \tag{2.24}$$

From this, we identify that the covariant basis for this representation contains

- Two Lorentz scalar operators in the $(0,0)$ representation: the identity operator $\mathbf{1}$ and the chirality operator γ^5.
- Six operators transforming in the $(1,0)\oplus(0,1)$ representation, which are the group generators $\sigma_{\mu\nu}=\frac{i}{2}[\gamma_\mu,\gamma_\nu]$.
- Two traceless symmetric tensors transforming in the $(1/2,1/2)$ representation, identified as γ^μ and $\gamma^5\gamma^\mu$.

Steven Weinberg, in 1963 [75], studied the general case for any spin j and the generalized forms of the γ matrices and all the necessary ingredients to construct the Feynman rules of the $(j,0)\oplus(0,j)$ representation. There he noted that the general form of $2(2j+1)$-dimensional matrix notation of the equation of motion for the fields, after boosting the rest-frame parity equation, has the form

$$[\gamma^{\mu 1,\mu 2,\ldots,\mu 2j}\partial_{\mu 1}\partial_{\mu 2}\cdots\partial_{\mu 2j}+m^{2j}]\Psi(x)=0, \tag{2.25}$$

where in the $j=1/2$ case we arrive at the familiar Dirac equation.

With the complete covariant basis, one can easily find all the possible interaction terms for the fields in this representation, for any value of j. In this regard, we will use this method to find the corresponding basis for the $(1,0)\oplus(0,1)$ representation of the HLG in the following section.

2.2 Formalism of the $(1,0)\oplus(0,1)$ representation

Fields in this representation are conventionally described by an antisymmetric tensor with two indices and although we will use an equivalent six-component *"spinor"* $\psi(x)$, we call it the Tensor Dark Matter field.

It is important to note that, when one studies the various HLG representations, the $(1,0)\oplus(0,1)$ is associated to the antisymmetric Lorentz tensor of second rank that describes the electromagnetic field, $F^{\mu\nu}$. Indeed, one can take this approach and instead work in a tensorial formulation, as can be seen in Ref. [76]. However it turns out to be much easier to instead think of the field as a $2\times(2j+1)$ component spinor, and work in the same approach as the Dirac fields that were mentioned in the past section. One can, of course, choose to work this way or with the covariant representation of the fields and operators such as is convenient. For example, we employ the covariant form when calculating the traces of the products of the operators in the Appendix.

The QFT for a field transforming in the $(1,0)\oplus(0,1)$ representation including $U(1)$ gauge interactions was developed in Ref. [77]. We include here the necessary elements and refer the reader to that work for further details. The starting point is the construction of the parity-based covariant basis for the $(1,0)\oplus(0,1)$ representation space which is obtained as follows.

Any operator in the $(1,0)\oplus(0,1)$ representation space can be obtained from the external product of the basis of $(1,0)\oplus(0,1)$, thus operators transform in the product representation with the following Lorentz decomposition

$$[(1,0)\oplus(0,1)]\otimes[(1,0)\oplus(0,1)] = (0,0)_2\oplus(1,1)_2\oplus(1,0)\oplus(0,1)\oplus(2,0)\oplus(0,2). \tag{2.26}$$

From this relation we can see that the covariant basis is a set of 6×6 matrices containing:

- Two Lorentz scalar operators in the $(0,0)$ representation: the identity operator $\mathbf{1}$ and the chirality operator χ.
- Six operators transforming in the $(1,0)\oplus(0,1)$ representation, described by an antisymmetric tensor of rank 2 denoted by $M_{\mu\nu}$, which are the group generators.
- Two traceless symmetric tensors transforming in the $(1,1)$ representation, $S^{\mu\nu}$ and $\chi S^{\mu\nu}$.
- A four-index tensor with ten independent components transforming in the $(2,0)\oplus(0,2)$ representation, $C^{\alpha\beta\mu\nu}$.

Summarizing, the covariant basis for the $(1,0)\oplus(0,1)$ representation of the HLG is

$$\{\mathbf{1}, \chi, S^{\mu\nu}, \chi S^{\mu\nu}, M^{\mu\nu}, C^{\mu\nu\alpha\beta}\}. \tag{2.27}$$

The explicit construction of these operators goes as follows. First, the group generators $M^{\mu\nu}$ can be obtained from first principles from the representations of the rotations and boost generators for $(1,0)$ and $(0,1)$ as

$$M^{0i} = K_i \qquad M^{ij} = \epsilon_{ijk} J_k, \tag{2.28}$$

where $\boldsymbol{J}$ and $\boldsymbol{K}$ are obtained from a straightforward calculation of the $(1,0)\oplus(0,1)$ representation of the HLG as

$$\boldsymbol{J} = \begin{pmatrix} \boldsymbol{\tau} & 0 \\ 0 & \boldsymbol{\tau} \end{pmatrix} \qquad \boldsymbol{K} = \begin{pmatrix} i\boldsymbol{\tau} & 0 \\ 0 & -i\boldsymbol{\tau} \end{pmatrix}. \tag{2.29}$$

Here, $\boldsymbol{\tau}$ are 3×3 representation matrices of the generators of the rotation subgroup in the basis of well defined angular momentum $\{|1,m\rangle_R\}$ (for the "right" representation $(1,0)$) and $\{|1,m\rangle_L\}$ (for the "left" representation $(0,1)$).

Next, we can also construct the parity operator [1], which makes the switch between the chiral subspaces $(1,0)$ and $(0,1)$ and has the following representation,

$$\Pi = \begin{pmatrix} 0 & \mathbb{I}_{3\times 3} \\ \mathbb{I}_{3\times 3} & 0 \end{pmatrix}. \tag{2.30}$$

As it was studied in [73], this parity operator transforms in the $(1,1)$ representation of the HLG and is the time component ($\Pi = S^{00}$) of the traceless symmetric tensor $S^{\mu\nu}$. Therefore, we can write this tensor as

$$S^{\mu\nu} = \Pi(g^{\mu\nu} - i(g^{0\mu}M^{0\nu} + g^{0\nu}M^{0\mu}) - \{M^{0\mu}, M^{0\nu}\}). \tag{2.31}$$

It satisfies $S^{\mu}_{\ \mu} = 0$ which leaves only nine independent matrices. This is the conventional tensor used in the literature, where in the $j = 1/2$ case we would have a rank $2j = 1$ operator $S^{\mu} = \gamma^{\mu}$ and the chirality operator $\chi = \gamma^5$.

Next we have the chirality operator χ which takes the following form

$$\chi = \begin{pmatrix} \mathbb{I}_{3\times 3} & 0 \\ 0 & -\mathbb{I}_{3\times 3} \end{pmatrix}. \tag{2.32}$$

[1] Strictly speaking this is the parity operator in the rest frame, in other frames parity operation requires also to change $\boldsymbol{p} \to -\boldsymbol{p}$. In the following we will also call parity to this rest-frame parity operation for simplicity.

It is important to note that parity and chirality anticommute

$$\{\Pi, \chi\} = 0, \tag{2.33}$$

and this is a covariant relation i.e. in general,

$$\{S^{\mu\nu}, \chi\} = 0. \tag{2.34}$$

For these representantions, the Lorentz generators satisfy

$$\boldsymbol{K} = i\chi \boldsymbol{J}, \tag{2.35}$$

so, with the parity operator, we have the following relations

$$[\Pi, \boldsymbol{J}] = 0 \tag{2.36}$$

$$[\Pi, \boldsymbol{K}] = 2\Pi \boldsymbol{K}. \tag{2.37}$$

The tensor transforming in the $(2,0) \oplus (0,2)$ representation, $C^{\mu\nu\alpha\beta}$, is given by

$$C^{\mu\nu\alpha\beta} = 4\{M^{\mu\nu}, M^{\alpha\beta}\} + 2\{M^{\mu\alpha}, M^{\nu\beta}\} - 2\{M^{\mu\beta}, M^{\nu\alpha}\} - 8(g^{\mu\alpha}g^{\nu\beta} - g^{\mu\beta}g^{\nu\alpha}). \tag{2.38}$$

It satisfies the following symmetries,

$$C^{\mu\nu\alpha\beta} = C^{\alpha\beta\mu\nu} = -C^{\nu\mu\alpha\beta} = -C^{\mu\nu\beta\alpha}. \tag{2.39}$$

Additionally, it satisfies the Bianchi identity,

$$C^{\mu\nu\alpha\beta} + C^{\mu\alpha\beta\nu} + C^{\mu\beta\nu\alpha} = 0. \tag{2.40}$$

By contracting any pair of indices the tensor vanishes and these symmetries leave only ten independent components for $C^{\mu\nu\alpha\beta}$.

The operators in the covariant basis satisfy the following algebraic relations

$$[M^{\mu\nu}, M^{\alpha\beta}] = -i\left(g^{\mu\alpha}M^{\nu\beta} - g^{\nu\alpha}M^{\mu\beta} - g^{\mu\beta}M^{\nu\alpha} + g^{\nu\beta}M^{\mu\alpha}\right) \tag{2.41}$$

$$[M^{\mu\nu}, S^{\alpha\beta}] = -i\left(g^{\mu\alpha}S^{\nu\beta} - g^{\nu\alpha}S^{\mu\beta} + g^{\mu\beta}S^{\nu\alpha} - g^{\nu\beta}S^{\mu\alpha}\right), \tag{2.42}$$

$$\left\{M^{\mu\nu}, S^{\alpha\beta}\right\} = \varepsilon^{\mu\nu\sigma\beta}\chi S^{\alpha}{}_{\sigma} + \varepsilon^{\mu\nu\sigma\alpha}\chi S^{\beta}{}_{\sigma}, \tag{2.43}$$

$$[S^{\mu\nu}, S^{\alpha\beta}] = -i\left(g^{\mu\alpha}M^{\nu\beta} + g^{\nu\alpha}M^{\mu\beta} + g^{\nu\beta}M^{\mu\alpha} + g^{\mu\beta}M^{\nu\alpha}\right), \tag{2.44}$$

$$\left\{S^{\mu\nu}, S^{\alpha\beta}\right\} = \frac{4}{3}\left(g^{\mu\alpha}g^{\nu\beta} + g^{\nu\alpha}g^{\mu\beta} - \frac{1}{2}g^{\mu\nu}g^{\alpha\beta}\right) - \frac{1}{6}\left(C^{\mu\alpha\nu\beta} + C^{\mu\beta\nu\alpha}\right), \tag{2.45}$$

$$\{\chi, S^{\mu\nu}\} = [\chi, M^{\mu\nu}] = [\chi, C^{\mu\nu\alpha\beta}] = 0. \tag{2.46}$$

The calculation of cross sections below can be reduced to traces of products of matrices in the covariant basis. First, in the construction of the covariant basis the internal product $\langle A|B\rangle = Tr(AB)$ is used and from the orthogonality in the product space we get

$$\begin{aligned} &Tr(\chi) = Tr(S) = Tr(M) = Tr(\chi S) = Tr(C) = Tr(\chi M) = Tr(\chi C) \\ &= Tr(MS) = Tr(M\chi S) = Tr(MC) = Tr(S\chi S) = Tr(SC) = Tr(\chi SC) = 0. \end{aligned} \tag{2.47}$$

Secondly, the chirality operator satisfies $\chi^2 = 1$, anti-commutes with S and commutes with M and C tensors which can be used to obtain trace results in a simple way. It can be shown e.g. that the trace of an odd product of S matrices vanishes. For the purposes of this work, we will need the traces of the following matrices

$$\begin{aligned} &Tr(SMM) = Tr\left(\chi^2 SMM\right) = -Tr(\chi S\chi MM) \\ &= -Tr(\chi SMM\chi) = -Tr(SMM) \Rightarrow Tr(SMM) = 0. \end{aligned} \tag{2.48}$$

The trace of the product of $S^{\mu\nu}$ and $M^{\mu\nu}$ can be obtained making use of Eqs. (2.28) and (2.31),

$$\begin{aligned} Tr\left(M^{\mu\nu}M^{\alpha\beta}\right) &= 4(g^{\mu\alpha}g^{\nu\beta} - g^{\mu\beta}g^{\nu\alpha}) \equiv 4G^{\mu\nu\alpha\beta}, \\ Tr\left(S^{\mu\nu}S^{\alpha\beta}\right) &= 4\left(g^{\mu\alpha}g^{\nu\beta} + g^{\mu\beta}g^{\nu\alpha} - \frac{1}{2}g^{\mu\nu}g^{\alpha\beta}\right) \equiv 4T^{\mu\nu\alpha\beta}. \end{aligned} \tag{2.49}$$

The trace of products with more terms can be obtained using the algebraic relations above. As an example, we calculate explicitly,

$$\begin{aligned} Tr\left(S^{\mu\nu}S^{\alpha\beta}M^{\rho\sigma}\right) &= Tr\left(\left\{S^{\mu\nu},S^{\alpha\beta}\right\}M^{\rho\sigma}\right) - Tr\left(S^{\alpha\beta}S^{\mu\nu}M^{\rho\sigma}\right) \\ &= Tr\left(\left\{S^{\mu\nu},S^{\alpha\beta}\right\}M^{\rho\sigma}\right) - Tr\left(S^{\alpha\beta}\left[S^{\mu\nu},M^{\rho\sigma}\right]\right) - Tr\left(S^{\alpha\beta}M^{\rho\sigma}S^{\mu\nu}\right), \end{aligned}$$

Adding a term $Tr\left(S^{\alpha\beta}M^{\rho\sigma}S^{\mu\nu}\right)$ to both sides of the equation and multiplying by $\frac{1}{2}$, we have

$$\begin{aligned} Tr\left(S^{\mu\nu}S^{\alpha\beta}M^{\rho\sigma}\right) &= \frac{1}{2}\left(Tr\left(\left\{S^{\mu\nu},S^{\alpha\beta}\right\}M^{\rho\sigma}\right) - Tr\left(S^{\alpha\beta}\left[S^{\mu\nu},M^{\rho\sigma}\right]\right)\right) \\ &= -\frac{1}{2}Tr\left(S^{\alpha\beta}\left[S^{\mu\nu},M^{\rho\sigma}\right]\right) \\ &= \frac{-i}{2}Tr\left(S^{\alpha\beta}\left(g^{\rho\mu}S^{\sigma\nu} - g^{\sigma\mu}S^{\rho\nu} + g^{\rho\nu}S^{\sigma\mu} - g^{\sigma\nu}S^{\rho\mu}\right)\right) \\ &= -2i\left(g^{\rho\mu}T^{\alpha\beta\sigma\nu} - g^{\sigma\mu}T^{\alpha\beta\rho\nu} + g^{\rho\nu}T^{\alpha\beta\sigma\mu} - g^{\sigma\nu}T^{\alpha\beta\rho\mu}\right). \end{aligned} \tag{2.50}$$

The explicit form of other traces needed in our calculations in this work can be found in the Appendix.

From Eqs. (2.36) it is clear that parity under rotations is a Lorentz scalar, but not under boosts. From these relations it follows that performing a boost $B(p) = Exp(-i\boldsymbol{K}\cdot\boldsymbol{p})$ to the parity operator yields [73]

$$B(p)\Pi B^{-1}(p) = \frac{S^{\mu\nu}p_\mu p_\nu}{m^2} \equiv \frac{S(p)}{m^2}. \tag{2.51}$$

Performing the same boost to the rest-frame parity projection equation

$$\frac{1}{2}(1\pm\Pi)\psi(0) = \psi(0), \tag{2.52}$$

yields the following condition

$$(S^{\mu\nu}\partial_\mu\partial_\nu + m^2)\psi(x) = 0. \tag{2.53}$$

This is the equation that was proposed by S. Weinberg long ago [75], and has the main drawback that it contains unphysical solutions. Let us note that $(S^{\mu\nu}\partial_\mu\partial_\nu)^2 \equiv (S(\partial))^2 = \partial^4$. Then, multiplying Eq. (2.53) on the left by $S^{\mu\nu}\partial_\mu\partial_\nu - m^2$ gives

$$(\partial^4 - m^4)\psi(x) = 0, \tag{2.54}$$

which includes the tachyonic solutions, corresponding to the $p^2 = -m^2$ Poincarè orbit. To avoid this, we can use the simultaneous mass and parity projector

$$\frac{p^2}{m^2}\mathbb{P}_{\pm}(p) = \frac{1}{2m^2}(p^2 \pm S(p)). \tag{2.55}$$

Doing this projection to Eq. (2.52) permits to construct a consistent QFT for tensor dark matter. Performing a boost yields the new equation of motion

$$\left[\Sigma_{\mu\nu}\partial^{\mu}\partial^{\nu} - M^2\right]\psi(x) = 0, \tag{2.56}$$

where $\Sigma_{\mu\nu} = \frac{1}{2}(g_{\mu\nu} + S_{\mu\nu})$.

A suitable Lagrangian can be constructed for this equation of motion given by

$$\mathcal{L} = \partial^{\mu}\bar{\psi}(x)\Sigma_{\mu\nu}\partial^{\nu}\psi(x) - M^2\bar{\psi}(x)\psi(x), \tag{2.57}$$

where $\bar{\psi}(x) \equiv (\psi(x))^{\dagger}\Pi$.

The field $\psi(x)$ has a mass dimension one, so we could consider self-interactions that are naively renormalizable, adding to the Lagrangian terms such as $(\bar{\psi}\psi)^2$. Other terms are listed in Ref. [77]. We leave this discussion on hold, as for the purposes of this work we do not employ or calculate observables concerning self-interactions, however it is an important aspect of the theory that needs to be addressed in the future.

The field and its adjoint are written in the conventional Fourier series form as

$$\begin{aligned}\psi(x) &= \sum_{\lambda}\int \frac{d^3p}{\sqrt{(2\pi)^3 2E}}[a_{\lambda}(p)U(p,\lambda)e^{-ip.x} + b^{\dagger}_{\lambda}(p)V(p,\lambda)e^{ip.x}]\\ \bar{\psi}(x) &= \sum_{\lambda}\int \frac{d^3p}{\sqrt{(2\pi)^3 2E}}[a^{\dagger}_{\lambda}(p)\bar{U}(p,\lambda)e^{ip.x} + b_{\lambda}(p)\bar{V}(p,\lambda)e^{-ip.x}]\end{aligned} \tag{2.58}$$

where $U(p,\lambda)$ ($V(p,\lambda)$) is the particle (antiparticle) solutions to the equation of motion with polarization λ, with creation (annihilation) operators, $a_{\lambda}(p)$ ($a^{\dagger}_{\lambda}(p)$) and $b_{\lambda}(p)$ ($b^{\dagger}_{\lambda}(p)$), respectively. These operators satisfy the commutation relations

$$[a_{\lambda}(p), a^{\dagger}_{\gamma}(p')] = \delta_{\lambda\gamma}\delta_{pp'}, \qquad [b_{\lambda}(p), b^{\dagger}_{\gamma}(p')] = \delta_{\lambda\gamma}\delta_{pp'}. \tag{2.59}$$

The conjugated momenta ξ for the fields ψ are calculated by the usual procedure, given by

$$\begin{aligned}\bar{\xi}_d &= \frac{\partial \mathcal{L}}{\partial_0 \bar{\psi}_d} = \Sigma^{0\mu}_{da}(\partial_\mu \psi)_a \\ \xi_d &= \frac{\partial \mathcal{L}}{\partial_0 \psi_d} = (\partial_\mu \bar{\psi})_a \Sigma^{\mu 0}_{ad}.\end{aligned} \tag{2.60}$$

The details of the calculation can be found in Ref. [77], where the final result of the canonical quantization of the field gives the following commutators between the fields and their conjugated momenta, for equal time ($x^0_1 = x^0_2$)

$$[\xi_d(x_1), \psi_b(x_2)]_{x^0_{1,2}=0} = [\bar{\xi}_d(x_1), \bar{\psi}_b(x_2)]_{x^0_{1,2}=0} = -i\Big(\Sigma^{00} - \frac{(\boldsymbol{J}\cdot\nabla)^2}{2m^2} S^{00}\Big)_{bd} \delta(x_1 - x_2). \tag{2.61}$$

This is the expected result after a classical analysis performed in Ref. [77], where one finds that the theory only has second-class constraints which can be solved following the procedure outlined by Paul Dirac in his ancient *Lectures on Quantum Mechanics* [78]. Additionally, the total energy and total momentum of the field are

$$H = \frac{(2\pi)^3}{V} \Sigma_{p,\lambda} p_0 [a^\dagger_r(p) a_r(p) + b^\dagger_r(p) b_r(p)], \tag{2.62}$$

$$P_i = \frac{(2\pi)^3}{V} \Sigma_{p,\lambda} p_i [a^\dagger_r(p) a_r(p) + b^\dagger_r(p) b_r(p)]. \tag{2.63}$$

The charge associated to the $U(1)$ invariance turns out to be

$$Q = \frac{(2\pi)^3}{V} q \Sigma_{p,\lambda} (-a^\dagger_r(p) a_r(p) + b^\dagger_r(p) b_r(p)). \tag{2.64}$$

Contrary to the Dirac theory, for this representation the charge conjugation operator commutes with the rest frame parity operator, thus the particle and antiparticle have the same parity. These solutions satisfy the completeness relations

$$\sum_\lambda U(p,\lambda)\, \bar{U}(p,\lambda) = \frac{S(p) + M^2}{2M^2}, \qquad \sum_\lambda V(p,\lambda)\, \bar{V}(p,\lambda) = \frac{S(p) + M^2}{2M^2}, \tag{2.65}$$

where $S(p) \equiv S^{\mu\nu} p_\mu p_\nu$.

Following the usual procedure, we find the propagator by obtaining the Green's fuction ($\tilde{G}(p)$) of the wave equation in Eq. (2.56), so that

$$(\Sigma_{\mu\nu} \partial^\mu \partial^\nu - M^2) \tilde{G}(p) = \mathbb{I}. \tag{2.66}$$

The solution is

$$\tilde{G}(p) = \frac{\Delta(p)}{p^2 - M^2 + i\varepsilon}, \tag{2.67}$$

where

$$\Delta(p) = \frac{S(p) - p^2 + 2M^2}{2M^2}. \tag{2.68}$$

Thus, the propagator for particles in this representation is given by

$$i\pi(p) = i\frac{S(p) - p^2 + 2M^2}{2M^2(p^2 - M^2 + i\varepsilon)}. \tag{2.69}$$

A crucial result of this formalism is that the free field Lagrangian can be decomposed in terms of the chiral components. First, we use the chiral operator to construct chiral proyectors that will identify the fields that transform in the $(1,0)$ representation ("right") and $(0,1)$ ("left").

$$\begin{aligned} P_R &= \frac{1}{2}(1+\chi), \qquad & P_L &= \frac{1}{2}(1-\chi), \\ \psi_R &= P_R\psi, \qquad & \psi_L &= P_L\psi. \end{aligned} \tag{2.70}$$

As proyectors, P_R and P_L have the following properties

$$P_R + P_L = \mathbb{I}, \qquad P_R P_L = 0, \qquad P_{R,L}^2 = P_{R,L}. \tag{2.71}$$

The Lagrangian in Eq. (2.57) can then be decomposed in terms of the chiral fields as follows

$$\mathcal{L} = \frac{1}{2}\partial^\mu\overline{\psi_R}\partial_\mu\psi_L + \frac{1}{2}\partial^\mu\overline{\psi_R}S_{\mu\nu}\partial_\nu\psi_R - M^2\overline{\psi_R}\psi_L + R \leftrightarrow L. \tag{2.72}$$

In the massless case of Eq. (2.72), the kinetic term couples the left and right component, which means it is not invariant under chiral transformations. This implies that $(1,0)\oplus(0,1)$ fields cannot have chiral gauge interactions, however vector-gauge are allowed. In the case of interactions with the SM, these fields can either be SM singlets or only interact with $U(1)_Y$ or $SU(3)_C$ gauge fields; $SU(2)_L$ interactions are not allowed. This is the main motivation for us to consider this type of fields to describe dark matter.

2.3 Effective field theory of tensor dark matter

Let us consider the simplest possibility and describe tensor dark matter (TDM) particle as a field transforming in the $(1,0)\oplus(0,1)$ of the HLG. In order to contemplate the consequences of this choice, we must consider the interactions of TDM with the standard model fields.

The simplest possibility is for the TDM fields to transform as SM singlets, which means they do not have standard model charges. This is the most likely case because if the dark matter fields had $U(1)_Y$ or $SU(3)_C$ charges, effects of observables regarding this property would have already been measured by the numerous experiments available today. However, if there is more than one TDM field, it can have vector-like gauge interactions with its own dark gauge group. We will assume a $U(1)_D$ structure as the dark gauge group from now on. The purpose of including this dark gauge structure is to make it possible to distinguish TDM particles from its anti-particles by providing a dark charge, preventing their direct decay into SM particles.

We do not know how standard model and dark sectors couple at high energies, but we can understand the effects at low energy by doing an expansion in derivatives of the fields. The significance of each term will depend on the dimension of the associated operator, with the most relevant effects corresponding to the lowest dimension. Since the dark matter fields are standard model singlets, and in turn all standard model fields are dark sector singlets, for the interacting Lagrangian to be a complete scalar operator it must be composed of products of singlet dark and SM operators. The general form of the interaction between dark and SM fields can be written as follows

$$\mathcal{L}_{int} = \sum_n \frac{1}{\Lambda^{n-4}} \mathcal{O}_{SM} \mathcal{O}_{DM} \tag{2.73}$$

where Λ is an energy scale compensating the dimension n of the product of the SM singlet operators $\mathcal{O}_{SM}$, composed of SM fields and $\mathcal{O}_{DM}$, constructed with TDM fields.

From the standard model side, one of the singlet operators we can use is the $U(1)_Y$ stress tensor, $B_{\mu\nu} = cos\theta_W F_{\mu\nu} + sin\theta_W Z_{\mu\nu}$, where θ_W is the Weinberg angle, and $F_{\mu\nu}$ and $Z_{\mu\nu}$ is the electromagnetic and Z^0 stress tensors, respectively. This operator is of dimension 2 and under any $SU(N)$ transformation $\mathcal{U}(x)$, it transforms as

$$B^{\mu\nu} \to \mathcal{U}(x) B^{\mu\nu} \mathcal{U}^{-1}(x). \tag{2.74}$$

Because it is a $U(1)$ operator, it is invariant after such transformation, thus making it a singlet. Another singlet operator to include is $\phi^\dagger\phi$, where ϕ is the $SU(2)_L$ complex Higgs doublet. This dimension-2 product is the singlet of the $2 \otimes 2 = 3 \oplus 1$ decomposition of the $SU(2)_L$ group, and it is also a singlet under $SU(3)_c$ and $U(1)_Y$.

We can form other combinations for SM singlets, such as operators of the form $\bar{L}\mathcal{O}L$, where L is a left fermion and $\mathcal{O} = \{\mathbb{I}, \gamma^\mu, \gamma^5, \gamma^\mu\gamma^5, \sigma^{\mu\nu}\}$. However, these operators are dimension 3. This and every other combination will have a higher dimension.

In the case of the tensor dark matter fields, with a dark gauge group $U(1)_D$, the lowest dimension operators we can form that are singlets of the standard model and dark

gauge groups have the form $\bar{\psi}\mathcal{O}\psi$, where the operator is one of the 36 matrices of the TDM covariant basis, $\mathcal{O} = \{\mathbf{1}, \chi, S^{\mu\nu}, \chi S^{\mu\nu}, M^{\mu\nu}, C^{\mu\nu\alpha\beta}\}$. Such terms are of dimension 2, and taking into account their symmetry properties, we can construct a set of combinations to form the following interaction Lagrangian

$$\mathcal{L}_{int} = \bar{\psi}(g_s\mathbf{1} + ig_p\chi)\psi\tilde{\phi}\phi + g_t\bar{\psi}M_{\mu\nu}\psi B^{\mu\nu}, \tag{2.75}$$

where g_s, g_p and g_t are low energy coupling constants. We will refer to g_s (g_p) as the scalar (parity-violating) *Higgs portal* constant, and g_t as the *spin portal* constant. The spin portal term is an effective interaction that couples the dark matter field with the photon and the Z boson, however, notice that it does not involve the weak charges because the involved operators are singlets, but the coupling occurs through the higher multipoles (magnetic dipole and electric quadrupole moments) of the dark matter field. A $(1,0)\oplus(0,1)$ field has a magnetic moment that depends on its mass, $\mu \approx g_t/M$, and its electric quadrupole moment is proportional to $Q_E \approx g_t/M^2$ [76], therefore the spin portal interaction between TDM and SM particles will be suppressed at least as k/M, where k is the photon or Z^0 momentum. We also have dimension-4 self-interactions, which are described in [77]. However, as it was mentioned in the previous section, we do not calculate observables concerning self-interactions in this work, so we will set them aside, reiterating that this remains an important aspect of the theory that needs to be addressed in the future.

After spontaneous symmetry breaking and diagonalizing the gauge sector, we arrive at the following expression for the interaction Lagrangian

$$\mathcal{L}_{int} = \frac{1}{2}\bar{\psi}(g_s\mathbf{1} + ig_p\chi)\psi\,(H+v)^2 + g_t\cos\theta_W\bar{\psi}M_{\mu\nu}\psi F^{\mu\nu} - g_t\sin\theta_W\bar{\psi}M_{\mu\nu}\psi Z^{\mu\nu}, \tag{2.76}$$

where H is the Higgs field, v stands for the Higgs vacuum expectation value and $F^{\mu\nu}$, $Z^{\mu\nu}$ are the electromagnetic and Z boson stress tensors. The Lagrangian in Eq. (2.76) gives a set of Feynman rules that are shown in Fig. 2.1. These rules induce transitions between the tensor dark matter particles and standard model particles.

We can calculate some of these processes and compare our results with existing experimental measurements in order to set constraints on the constants that characterize the tensor dark matter effective field theory described above. This proposal was published in Ref. [79], and the results of following three chapters can be found there. Additionally, the continuation of the work followed with the publication of Ref. [80], where we present some of the final results of Chapter 4 and the results of Chapter 6.

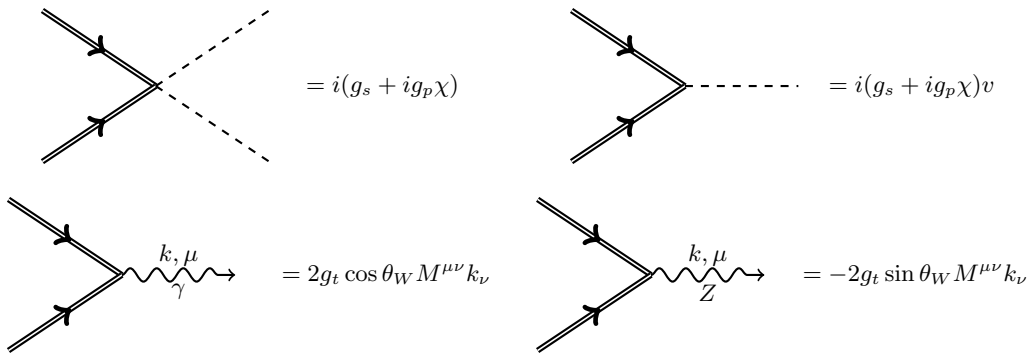

FIGURE 2.1: Feynman rules from the leading terms in the effective theory.

Chapter 3

Constraints from Z and H invisible widths

The Lagrangian in Eq. (2.76) indicates the possibility of annihilation of tensor dark matter into standard model particles such as $\bar{D}D \to \bar{f}f$, $\gamma\gamma$, W^+W^-, Z^0Z^0, HH, $Z^0\gamma$, $H\gamma$, Z^0H, under appropriate kinematical conditions. The decays $Z^0 \to \bar{D}D$ and $H \to \bar{D}D$ are kinematically allowed for light dark matter ($M < M_Z/2$ and $M < M_H/2$, respectively), which could contribute to the invisible Z^0 and H decay widths, respectively.

The invariant amplitude for the $Z^0(k,\epsilon) \to D(p_1)\bar{D}(p_2)$ decay is calculated as follows

$$-i\mathcal{M} = 2g_t S_W \bar{U}(p_1,\lambda_1) M^{\mu\nu} k_\nu V(p_2,\lambda_2))\epsilon_\mu(k), \tag{3.1}$$

where $S_W = \sin\theta_W$. The averaged squared amplitude, using the completeness relation in Eq. (2.65), is obtained as follows

$$\begin{aligned}\sum_{\lambda,\lambda_1,\lambda_2} |\mathcal{M}_{Z\to\bar{D}D}|^2 =& |\bar{\mathcal{M}}_Z|^2 = \frac{1}{3}(2g_t S_W)^2\Big(-g^{\mu\alpha} + \frac{k^\mu k^\alpha}{M_Z^2}\Big) \\ &\times Tr\Big[\Big(\frac{S(p_2)+M^2}{2M^2}\Big) M_{\mu\nu}(p_1+p_2)^\nu \Big(\frac{S(p_1)+M^2}{2M^2}\Big) M_{\alpha\beta}(p_1+p_2)^\beta\Big] \\ =& \frac{4}{3} g_t^2 S_W^2 Tr\left[\frac{S(p_1)+M^2}{2M^2} M^{\mu\nu} \frac{S(p_2)+M^2}{2M^2} M^{\alpha\beta}\right] k_\nu k_\beta (-g_{\mu\alpha} + \frac{k_\mu k_\alpha}{M_Z^2}).\end{aligned} \tag{3.2}$$

Using the results of the traceology of matrices in the $(1,0)\oplus(0,1)$ space (see the appendix), yields the following decay width

$$\Gamma(Z^0 \to \bar{D}D) = \frac{g_t^2 S_W^2}{24\pi M^4}(M_Z^2 - 4M^2)^{3/2}(M_Z^2 + 2M^2). \tag{3.3}$$

The invisible width of the Z^0 boson, that is, the width of the decay into undetected modes is $\Gamma^{inv}_{exp}(Z) = 499.0 \pm 1.5\ MeV$, reported by the Particle Data Group [3]. This value includes the decay to $\nu\bar{\nu}$, which can be calculated as follows

$$\Gamma(Z^0 \to \bar{\nu}\nu) \equiv \sum_i \Gamma(Z^0 \to \bar{\nu}_i \nu_i) = \sum_{i,\alpha} U^2_{i\alpha} \frac{M_Z^2}{24\pi v^2}\sqrt{M_Z^2 - 4m^2_{\nu_i}} = \frac{M_Z^3}{8\pi v^2} = \frac{\sqrt{2}G_F M_Z^3}{8\pi}, \tag{3.4}$$

where we have neglected the neutrino masses and used the unitarity of the Pontecorvo-Maki-Nakagawa-Sakata (PMNS) matrix (or neutrino mixing matrix) elements. The Particle Data Group value for the Z boson mass is $M_Z = 91.1876 \pm 0.0021\ GeV$ and the most precise measurement of the Fermi constant (reported by the $\mu - Lan$ collaboration) is $G_F = 1.1663788(6) \times 10^{-5}\ GeV^{-2}$ [81]. Using these values, we obtain

$$\Gamma(Z^0 \to \bar{\nu}\nu) = 497.64 \pm 0.03\ MeV. \tag{3.5}$$

We subtract this quantity from the reported value for the invisible width to get the constraint $\Gamma(Z \to \bar{D}D) < \Gamma^{inv}_Z \equiv \Gamma^{inv}_{exp}(Z) - \Gamma(Z \to \bar{\nu}\nu) = 1.4 \pm 1.5\ MeV$. The Z boson decay width into TDM depends on the coupling g_t and the dark matter mass M, thus we can constrain these parameters to the region shown in Fig. 3.1. Explicitly, the upper limit for the value of g_t is written as

$$g_t \leq \Big[\frac{(1.4)24\pi M^4}{S_W^2}\Big((M_Z^2 - 4M^2)^{3/2}(M_Z^2 + 2M^2)\Big)^{-1}\Big]^{1/2} \tag{3.6}$$

In a similar way, the decay $H \to \bar{D}D$ yields the following invariant amplitude

$$i\mathcal{M}_{H\to D\bar{D}} = iv\overline{\mathcal{V}}(p_2)(g_s\mathbb{I} + ig_p\chi)\mathcal{U}(p_1). \tag{3.7}$$

Then, the average squared amplitude is

$$\sum_{\lambda,\lambda_1,\lambda_2} |\mathcal{M}_{H\to\bar{D}D}|^2 = \frac{1}{3}v^2 Tr\Big[\Big(\frac{S(p_2) + M^2}{2M^2}\Big)(g_S\mathbb{I} + ig_P\chi)\Big(\frac{S(p_1) + M^2}{2M^2}\Big)(g_S\mathbb{I} + ig_P\chi)\Big] \tag{3.8}$$

$$= \frac{v^2}{6M^4}\Big(g_S^2(6M^4 - 4M^2M_H^2 + M_H^4) + g_P^2M_H^2(M_H^2 - 4M^2)\Big).$$

Which gives the following decay width,

$$\Gamma(H \to \bar{D}D) = \frac{v^2}{32\pi M_H^2 M^4}\sqrt{M_H^2 - 4M^2}\left[g_s^2\left(M_H^2\left(M_H^2 - 4M^2\right) + 6M^4\right) + g_p^2M_H^2\left(M_H^2 - 4M^2\right)\right]. \tag{3.9}$$

The Higgs decay width into TDM depends on the mass M and the coupling constants g_s and g_p. The invisible Higgs width has a reported value of $\Gamma_H^{inv} = 1.14 \pm 0.04\ MeV$ [82, 83], for which the contribution of the $\nu\bar{\nu}$ channel is negligible. Fig. 3.1 shows the constraints on g_s, g_p arising from the contribution of the Higgs decay into TDM to the invisible Higgs decay width. The solid lines are the central values and the shadowed regions correspond to one sigma regions. We can see from a broad review of the results that the coupling of the spin portal g_t can be larger than the Higgs portal constants g_s or g_p, by at least one order of magnitude. As a first approximation, for illustrative purposes, if we assume that $g_s \approx g_p$, the constraint is given by

$$g_s \approx g_p \leq \left[\frac{(1.14)16\pi M_H^2 M^4}{v^2}\left(\sqrt{M_H^2 - 4M^2}(3M^4 - 4M^2M_H^2 + M_H^4)\right)^{-1}\right]^{1/2}. \quad (3.10)$$

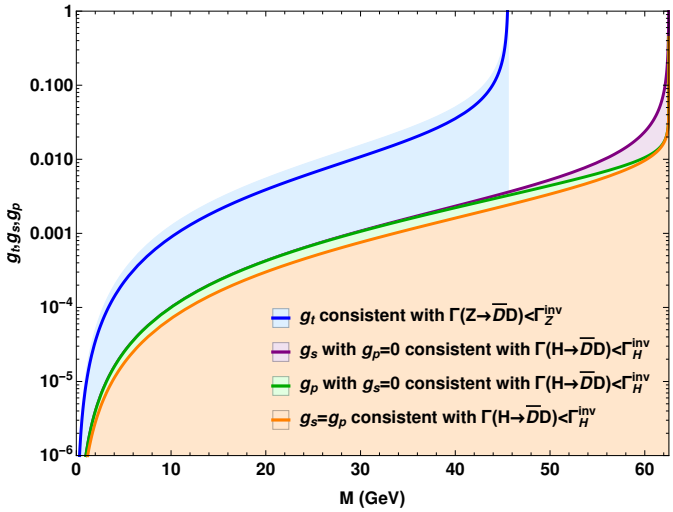

FIGURE 3.1: Parameter space for g_t, g_s and g_p consistent $\Gamma(Z \to \bar{D}D) < \Gamma_Z^{inv} = 1.4 \pm 1.5\ MeV$ and $\Gamma(H \to \bar{D}D) < \Gamma_H^{inv} = 1.14 \pm 0.04\ MeV$ for $M < M_Z/2$. Solid lines correspond to the central values of the invisible decay widths, and the shadowed region stands for the 1σ value.

Chapter 4

Tensor Dark Matter Relic Density

The early universe was hot, dense and radiation-dominated, a condition in which the rate of interactions between the particles was much larger than the rate of the expansion of the universe, and this energy exchange between the particles caused them to have a common average temperature, something that is known as thermal equilibrium.

As the universe expands, the average temperature decreases and the interactions between particles do not occur fast enough, which makes the different species *cool down* and the conditions for thermal equilibrium are no longer achieved. It is said that the species *decouple* when their rate of interaction is not large enough to compete with the expansion rate of the universe. This is a crucial step in the formation of new elements. For example, the formation of hydrogen due to the recombination of electrons and protons that have decoupled. The information of when and how this step occurs is given by the evolution of the comoving number density of the species. The species that decoupled continue travelling through the universe, its rate of interactions getting lower as the universe expands and cools down further, and the density of said species that remains today is called *relic density*.

As we have mentioned in Chapter 1, the dark matter relic density is measured from the data of the CMB and is one of the most stringent properties that dark matter candidates need to account for. In this sense, we want to calculate the relic density for Tensor Dark Matter to then compare it with the measured value. To obtain it, we must solve the *Boltzmann equation* for this species.

4.1 Boltzmann equation

The Boltzmann equation relates the time evolution of the number density with a function that is related to the interaction rate of the species. We can write this equation in operator form,

$$\boldsymbol{L}[f] = \boldsymbol{C}[f], \tag{4.1}$$

where f is the distribution function of the species, $\boldsymbol{L}$ is called the Liouville operator and $\boldsymbol{C}$ is the collision operator, which is related to the interaction rate. We will proceed to describe each operator.

The Liouville operator is the time derivative that includes the phase space evolution, which can be written in covariant form as

$$\boldsymbol{L} = p^{\alpha}\frac{\partial}{\partial x^{\alpha}} - \Gamma^{\alpha}_{\beta\gamma}p^{\beta}p^{\gamma}\frac{\partial}{\partial p^{\alpha}}, \tag{4.2}$$

where p is the momentum and $\Gamma^{\alpha}_{\beta\gamma}$ is the second kind Christoffel symbol, and the metric used to describe our universe, which is isotropic, homogeneous and expanding, is the Friedmann-Lemaître-Robertson-Walker (FLRW) metric (we refer to Chapter 1 for the expressions of $\Gamma^{\alpha}_{\beta\gamma}$ and the metric).

Employing the FLRW metric, the Liouville operator acting on $f(E,t)$ is

$$\boldsymbol{L}[f(E,t)] = E\frac{\partial}{\partial t}f(E,t) - \frac{\dot{R}}{R}|\vec{p}|^2\frac{\partial}{\partial E}f(E,t). \tag{4.3}$$

Integrating the Eq. (4.1) over the phase space, and dividing by the energy of the system E, we obtain

$$g\int\frac{d^3p}{E(2\pi)^3}\boldsymbol{L}[f(E,t)] = g\int\frac{d^3p}{E(2\pi)^3}\boldsymbol{C}[f(E,t)]$$

$$g\int\frac{d^3p}{(2\pi)^3}\Big[\frac{\partial}{\partial t}f(E,t) - \frac{\dot{R}}{ER}|\vec{p}|^2\frac{\partial}{\partial E}f(E,t)\Big] = g\int\frac{d^3p}{E(2\pi)^3}\boldsymbol{C}[f(E,t)]. \tag{4.4}$$

Working on the left side of Eq. (4.4), using the fact that the number density in terms of the distribution function $f(E,t)$ is

$$n(t) = g\int\frac{d^3p}{(2\pi)^3}f(E,t), \tag{4.5}$$

we get

$$
\begin{aligned}
g\int\frac{d^3p}{(2\pi)^3}\Big[\frac{\partial}{\partial t}f(E,t)-\frac{\dot{R}}{ER}|\vec{p}|^2\frac{\partial}{\partial E}f(E,t)\Big] & \\
&= g\Big[\frac{\partial}{\partial t}\int\frac{d^3p}{(2\pi)^3}f(E,t)-\frac{\dot{R}}{R}\int\frac{d^3p}{E(2\pi)^3}|\vec{p}|^2\frac{\partial}{\partial E}f(E,t)\Big] \\
&= \frac{\partial}{\partial t}n(t)-g\frac{\dot{R}}{R}\int\frac{dEd\Omega_p}{(2\pi)^3}(E^2-m^2)^{3/2}\frac{\partial}{\partial E}f(E,t) \\
&= \frac{\partial}{\partial t}n(t)+3\frac{\dot{R}}{R}g\int\frac{EdEd\Omega_p}{(2\pi)^3}(E^2-m^2)^{1/2}f(E,t) \\
&= \frac{\partial}{\partial t}n(t)+3\frac{\dot{R}}{R}g\int\frac{d^3p}{(2\pi)^3}f(E,t) \\
&= \dot{n}(t)+3\frac{\dot{R}}{R}n(t) \\
&= R^{-3}\frac{d(R^3n)}{dt}.
\end{aligned}
$$

Therefore, Eq. (4.1) can be written as

$$
R^{-3}\frac{d(R^3n)}{dt}=g\int\frac{d^3p}{E(2\pi)^3}\boldsymbol{C}[f(E,t)]. \tag{4.6}
$$

We can assume that the only process that is involved in the evolution of the abundance of a species is the annihilation with its antiparticle, and the inverse process, which can be expressed as $1+2\longleftrightarrow 3+4$, where we are interested in the production and annihilation of the species 1 and 2. The right side of Eq. (4.4) can be written as

$$
\begin{aligned}
g\int\frac{d^3p}{E(2\pi)^3}\boldsymbol{C}[f(E,t)] &= -\int d\Pi_1 d\Pi_2 d\Pi_3 d\Pi_4(2\pi)^4\delta^4(P_1+P_2-P_3-P_4) \\
&\times\Big[|M|^2_{1+2\to3+4}f_1f_2(1\pm f_3)(1\pm f_4)-|M|^2_{3+4\to1+2}f_3f_4(1\pm f_1)(1\pm f_2)\Big],
\end{aligned} \tag{4.7}
$$

where the $\pm$ sign corresponds to a boson/fermion, respectively, and $d\Pi_i=\frac{d^3p}{2E_i(2\pi)^3}$. P_i, f_i stand for the momentum and distribution function of particle "i", and $|M|^2$ is the invariant amplitude of the process. We can consider that the process is time reversal invariant, in a way that

$$
|M|^2_{1+2\to3+4}=|M|^2_{3+4\to1+2}=|M|^2. \tag{4.8}
$$

Rewriting Eq. (4.7), we have

$$g\int\frac{d^3p}{E(2\pi)^3}\boldsymbol{C}[f(E,t)] = -\int d\Pi_1 d\Pi_2 d\Pi_3 d\Pi_4 (2\pi)^4\delta^4(P_1+P_2-P_3-P_4)$$
$$\times|M|^2\Big[f_1f_2(1\pm f_3)(1\pm f_4) - f_3f_4(1\pm f_1)(1\pm f_2)\Big]. \tag{4.9}$$

In absence of Bose-Einstein condensation or Fermi degeneracy, the term $(1\pm f_i)\simeq 1$. Thus, we write,

$$g\int\frac{d^3p}{E(2\pi)^3}\boldsymbol{C}[f(E,t)] = -\int d\Pi_1 d\Pi_2 d\Pi_3 d\Pi_4 (2\pi)^4\delta^4(P_1+P_2-P_3-P_4)$$
$$\times|M|^2\Big[f_1f_2 - f_3f_4\Big]. \tag{4.10}$$

It is a good approximation to consider thermal equilibrium for the product species (3 and 4) [30], so we can write f_3 and f_4 as Maxwell-Boltzmann distributions. The delta in Eq. (4.10) indicates energy conservation, i.e. $E_1+E_2=E_3+E_4$, thus

$$f_3f_4 = (e^{(\mu_3-E_3)/T})(e^{(\mu_4-E_4)/T}) \xrightarrow{\delta} (e^{-(E_1+E_2)/T})(e^{(\mu_3+\mu_4)/T}). \tag{4.11}$$

The number density in equilibrium for any species is written as

$$n_i^{(0)} \equiv g_i\int\frac{d^3p}{(2\pi)^3}e^{-E_i/T}. \tag{4.12}$$

We can then rewrite the term $f_1f_2-f_3f_4$ in Eq. (4.10) as follows

$$f_1f_2 - f_3f_4 \xrightarrow{\delta} e^{-(E_1+E_2)/T}\Big[\frac{n_1n_2}{n_1^{(0)}n_2^{(0)}} - \frac{n_3n_4}{n_3^{(0)}n_4^{(0)}}\Big]. \tag{4.13}$$

We can replace this term in the right side of Eq. (4.10), which yields

$$\Big[\frac{n_1n_2}{n_1^{(0)}n_2^{(0)}} - \frac{n_3n_4}{n_3^{(0)}n_4^{(0)}}\Big]\int d\Pi_1 d\Pi_2 d\Pi_3 d\Pi_4 (2\pi)^4\delta^4(P_1+P_2-P_3-P_4)e^{-(E_1+E_2)/T}|M|^2. \tag{4.14}$$

Recall that the cross section has a similar form to the one above. It is written as

$$\sigma = \frac{1}{Flux}\int d\Pi_3\int d\Pi_4(2\pi)^4\delta^4(p_1+p_2-p_3-p_4)|M|^2, \tag{4.15}$$

where the flux is defined as follows

$$Flux \equiv \frac{n_1 n_2}{E_1 E_2}\sqrt{(P_1\cdot P_2)^2 - M^4} = 4\sqrt{(P_1\cdot P_2)^2 - M^4} = 2\sqrt{s(s-4M^2)}. \tag{4.16}$$

The relative velocity is defined as [84]

$$v_{rel} = \frac{\sqrt{(P_1\cdot P_2)^2 - M^4}}{(p_1\cdot p_2)} = \frac{\sqrt{|\boldsymbol{v_1}-\boldsymbol{v_2}|^2 - |\boldsymbol{v_1}\times\boldsymbol{v_2}|^2}}{1-\boldsymbol{v_1}\cdot\boldsymbol{v_2}}. \tag{4.17}$$

We can write this velocity in terms of the flux,

$$v_{rel} = \frac{\sqrt{(p_1\cdot p_2)^2 - M^4}}{(p_1\cdot p_2)} = \frac{\sqrt{s(s-4M^2)}}{s-2M^2} = \frac{Flux}{2(s-2M^2)}. \tag{4.18}$$

In the non-relativistic limit, $1-\boldsymbol{v_1}\cdot\boldsymbol{v_2}\approx 1$ and $p_1\cdot p_2 \approx E_1E_2$. This way, $v_{rel}\approx v_r = |\vec{v}_1-\vec{v}_2|$, thus we can rewrite the flux in terms of the velocity

$$Flux \equiv \frac{n_1 n_2}{E_1 E_2}\sqrt{(P_1\cdot P_2)^2 - M^4} = 4\sqrt{(P_1\cdot P_2)^2 - M^4} = 4E_1E_2v_r \tag{4.19}$$

At the time of decoupling, the dark matter is non-relativistic [27]. This is consistent with data on dark matter relic density extracted from precision measurements of the cosmic background radiation [3, 85]. Since we are interested in the decoupling of dark matter, we can work in this limit to write

$$\begin{aligned}\sigma v &= \frac{1}{2(s-2M^2)}\int d\Pi_3\int d\Pi_4 (2\pi)^4\delta^4(p_1+p_2-p_3-p_4)|M|^2 \\ &\approx \frac{1}{4E_1E_2}\int d\Pi_3\int d\Pi_4 (2\pi)^4\delta^4(p_1+p_2-p_3-p_4)|M|^2.\end{aligned} \tag{4.20}$$

Additionally, we can perform the average of σv over the initial states, which yields

$$\langle\sigma v\rangle = \frac{1}{n_1^{(0)}n_2^{(0)}}\int\frac{g_1d^3p_1}{(2\pi)^2}f(E_1)\int\frac{g_2d^3p_2}{(2\pi)^2}f(E_2)\sigma v. \tag{4.21}$$

Replacing Eq. (4.20) in Eq. (4.21), we obtain

$$\langle\sigma v\rangle = \frac{g_1g_2}{n_1^{(0)}n_2^{(0)}}\int d\Pi_1 d\Pi_2 d\Pi_3 d\Pi_4 (2\pi)^4\delta^4(P_1+P_2-P_3-P_4)e^{-(E_1+E_2)/T}|M|^2, \tag{4.22}$$

which evidently is the right side of Eq. (4.10).

Using the expression in Eq. (4.22) in Eq. (4.6), we have

$$R^{-3}\frac{d(R^3 n)}{dt} = -(n_1^{(0)} n_2^{(0)})\langle\sigma v\rangle\left[\frac{n_1 n_2}{n_1^{(0)} n_2^{(0)}} - \frac{n_3 n_4}{n_3^{(0)} n_4^{(0)}}\right] \tag{4.23}$$

The temperature is inversely proportional to the scale factor, $T \propto R^{-1}$, so if we define a new quantity

$$Y \equiv \frac{n}{T^3}, \tag{4.24}$$

and we consider that particle and antiparticle are found in the same proportion, that is, $n_1 = n_2$, Eq. (4.23) becomes an equation of Y. Since we are assuming that the species 3 and 4 are in equilibrium, i.e. $n_3 = n_4 = n_{EQ}$, we can write Eq. (4.23) as

$$\frac{dY}{dt} = -T^3\langle\sigma v\rangle\left[Y^2 - Y_{EQ}^2\right], \tag{4.25}$$

where $Y_{EQ} = T^{-3}n^{(0)}$, and $n^{(0)}$ is the number density of the species in thermal equilibrium. It is convenient to use the variable $x = M/T$, which defines an approximate scale of the temperature. Progressively, the universe cools down and the value of x increases. We can then express the time derivative as

$$\frac{dY}{dt} = -\frac{dY}{dx}\frac{dx}{dt} = xH\frac{dY}{dx} = \frac{H(M)}{x}\frac{dY}{dx}, \tag{4.26}$$

where $H(M)$ comes from the definition of the Hubble parameter H,

$$H = \sqrt{\frac{8\pi G_N \rho}{3}} = \sqrt{\frac{8\pi^3 G_N g_*}{90}}T^2 = \sqrt{\frac{8\pi^3 G_N g_*}{90}}M^2 x^{-2} = H(M)x^{-2}. \tag{4.27}$$

Here, $G_N = 6.70861 \times 10^{-39} GeV^{-2}$ [3] is Newton's gravitational constant [3], and $g_* = g_*(T)$ stands for the relativistic effective degrees of freedom, which are dependent on the contents of the universe and the temperature,

$$g_* = \sum_{i=bosons, m_i \ll T} g_i\left(\frac{T_i}{T}\right)^4 + \frac{7}{8}\sum_{i=fermions, m_i \ll T} g_i\left(\frac{T_i}{T}\right)^4. \tag{4.28}$$

Finally, we can write Eq. (4.25) as

$$\frac{dY}{dx} = -\frac{\lambda(x)}{x^2}(Y^2 - Y_{eq}^2), \tag{4.29}$$

where we define $\lambda(x)$ as

$$\lambda(x) \equiv \frac{M^3\langle\sigma v_r\rangle}{H(M)}. \tag{4.30}$$

This is a complicated equation but we can solve it numerically, by matching the solution $Y(x)$ with $Y_{eq}(x)$ at high temperatures (i.e. $x << 1$) as the initial condition. In order to solve it, we need to calculate $\langle \sigma v_r \rangle$. It is a good approximation to perform a non-relativistic expansion of $\langle \sigma v_r \rangle$ keeping only the leading terms in the expansion in powers of $v_r << 1$. This expansion requires the calculation of the flux for dark matter particles in the thermal bath, which can be written as [86, 87]

$$F = 4\sqrt{(p_1 \cdot p_2)^2 - M^4} = 2(s - M^2)v_r, \tag{4.31}$$

where the Mandelstam variable $s = (p_1 + p_2)^2$ is related to v_r as

$$s = 2M^2 \left(1 + \frac{1}{\sqrt{1 - v_r^2}}\right) = 4M^2 + M^2 v_r^2 + ... \tag{4.32}$$

The cross section σ is a function of s, which means we can expand this function in terms of v_r as

$$\sigma v_r = a + b v_r^2. \tag{4.33}$$

We can perform the thermal average, which yields

$$\langle \sigma v_r \rangle = a + \frac{6b}{x}. \tag{4.34}$$

With this approximation in mind, in the next section we will calculate the coefficients a and b of the annihilation cross-section of Tensor Dark Matter. Once we find these coefficients for all involved channels, we can then use it to calculate the dark matter relic density.

4.2 Annihilation of tensor dark matter into a fermion-antifermion pair.

As a first case, for non-relativistic and light tensor dark matter, the channels that are kinematically allowed are $\bar{D}D \to \bar{f}f$ for fermions with $m_f < M$ and $\bar{D}D \to \gamma\gamma$.

The contributions to the process $D(p_1)\bar{D}(p_2) \to f(p_3)\bar{f}(p_4)$ are shown in Fig. 4.1.

FIGURE 4.1: Feynman diagrams for $\bar{D}D \to \bar{f}f$.

The corresponding amplitudes for each contribution, derived from the rules shown in Fig. 2.1, are given by

$$\begin{aligned}
-i\mathcal{M}_H &= i\frac{m_f}{s-M_H^2}\bar{u}\left(p_3\right)v\left(p_4\right)\bar{V}\left(p_2\right)\left(g_s I + ig_p\chi\right)U\left(p_1\right), \\
-i\mathcal{M}_\gamma &= -\frac{4Q_f g_t M_W S_W C_W}{vs}\bar{u}\left(p_3\right)\gamma^\mu v\left(p_4\right)\bar{V}\left(p_2\right)M_{\mu\beta}\left(p_1+p_2\right)^\beta U\left(p_1\right), \\
-i\mathcal{M}_Z &= \frac{g_t M_Z S_W}{v(s-M_Z^2)}\bar{u}\left(p_3\right)\gamma^\mu\left(A_f+B_f\gamma_5\right)v\left(p_4\right)\bar{V}\left(p_2\right)M_{\mu\beta}\left(p_1+p_2\right)\beta U\left(p_1\right).
\end{aligned} \tag{4.35}$$

Here, $C_W = \cos\theta_W$, Q_f is the fermion charge in units of the proton charge e, and A_f, B_f are factors related to the corresponding fermion weak isospin T_3^f, defined as

$$A_f = 2T_3^f - 4Q_f S_W^2, \qquad B_f = -2T_3^f. \tag{4.36}$$

For illustration purposes, the average squared amplitude for the Higgs portal contribution is

$$\begin{aligned}
|M_H|^2 = \frac{1}{9}\sum_\lambda M_H M_H^\dagger = \frac{m_f^2}{9(s-m_H^2)^2} tr[(\not{q}_2 - m_f)(\not{q}_1 + m_f)]\times \\
Tr[(\frac{S(p_2)+M^2}{2M^2})(g_s\mathbb{I}+ig_P\chi)(\frac{S(p_1)+M^2}{2M^2})(g_s\mathbb{I}+ig_P\chi)].
\end{aligned} \tag{4.37}$$

We can calculate this quantity making use of the traceology that can be found in the Appendix, and similarly for the rest of the contributions. For the complete process, the calculation yields the following average squared amplitude in terms of the Mandelstam

variables

$$
\begin{aligned}
|\overline{\mathcal{M}_{\bar{f}f}}|^2 = &-\frac{g_t^2 M_Z^2 S_W^2}{9M^4 v^2 (s-M_Z^2)^2}[4M^2(A_f^2+B_f^2)m_f^4(4M^2-s)+4m_f^2.(4M^2-s)(A_f^2M^2(2M^2+s-t-u).\\
&+B_f^2(2M^4-M^2(s+t+u)-s^2))+.(A_f^2+B_f^2)(16M^8-4M^6(s+4(t+u)).\\
&+4M^4(t+u)(s+t+u)+M^2(4s^3-2s(t^2+u^2))+s^2((t-u)^2-s^2))]\\
&+\frac{8A_f C_W Q_f g_t^2 M_W M_Z S_W^2}{9M^4 s v^2 (s-M_Z^2)}[4M^2m_f^2(4M^2-s)(2M^2+s-t-u)+4m_f^4(4M^4-M^2s)+16M^8.\\
&.-4M^6(s+4(t+u))+4M^4(t+u)(s+t+u)+M^2(4s^3-2s(t^2+u^2))+s^2((t-u)^2-s^2)]\\
&+\frac{4A_f m_f^2 g_s g_t M_Z S_W}{9M^4 v(s-M_H^2)(s-M_Z^2)}s(2M^2-s)(t-u)-\frac{16C_W m_f^2 Q_f g_s g_t M_W S_W}{9M^4 v(s-m_H^2)}(2M^2-s)(t-u)\\
&-\frac{16C_W^2 Q_f^2 g_t^2 M_W^2 S_W^2}{9M^4 s^2 v^2}[4M^2m_f^2(4M^2-s)(2M^2+s-t-u)+4m_f^4(4M^4-M^2s).\\
&.+16M^8-4M^6(s+4(t+u))+4M^4(t+u)(s+t+u)+M^2(4s^3-2s(t^2+u^2))+s^2((t-u)^2-s^2)]\\
&+\frac{m_f^2}{9M^4(s-M_H^2)^2}(s-4m_f^2)[g_p^2 s(s-4M^2)+g_s^2(6M^4-4M^2s+s^2)]. \qquad (4.38)
\end{aligned}
$$

We obtain the cross section for $\bar{D}D \to \bar{f}f$ by integrating the final state phase space of the average squared amplitude. It is easy to identify the individual contributions from the Higgs and Z bosons and γ exchange, as well as the $Z^0-\gamma$ interference:

$$
\begin{aligned}
\sigma_{\bar{f}f}(s) = &\frac{1}{72\pi M^4\sqrt{s}}\frac{\sqrt{s-4m_f^2}}{F}\left[\frac{m_f^2\left(s-4m_f^2\right)\left(g_p^2 s\left(s-4M^2\right)+g_s^2\left(6M^4-4M^2s+s^2\right)\right)}{\left(s-M_H^2\right)^2}\right.\\
&+\frac{2g_t^2 M_Z^2 S_W^2 s\left(s-4M^2\right)\left(2M^2+s\right)\left(2\left(A_f^2-2B_f^2\right)m_f^2+s\left(A_f^2+B_f^2\right)\right)}{3v^2\left(s-M_Z^2\right)^2}\\
&+\frac{32C_W^2 Q_f^2 g_t^2 M_W^2 S_W^2\left(s-4M^2\right)\left(2M^2+s\right)\left(2m_f^2+s\right)}{3v^2 s}\\
&\left.-\frac{16A_f C_W Q_f g_t^2 M_W M_Z S_W^2\left(s-4M^2\right)\left(2M^2+s\right)\left(2m_f^2+s\right)}{3v^2\left(s-M_Z^2\right)}\right]. \qquad (4.39)
\end{aligned}
$$

The $H-Z$ and $H-\gamma$ interferences vanish after solving the integration of phase space.

4.3 Tensor dark matter annihilation into two photons

This process is induced by the dark matter exchange in the t and u channels, shown in Fig. 4.2. The corresponding amplitudes are given by

$$-i\mathcal{M}_t = i\frac{2g_t^2 C_W^2}{M^2}\bar{V}(p_2,\lambda_2)M_{\alpha\beta}\frac{S(p_1-p_3)-t+2M^2}{t-M^2}M_{\mu\nu}U(p_1,\lambda_1)p_4^\alpha\eta^\beta(p_4)p_3^\mu\epsilon^\nu(p_3), \tag{4.40}$$

$$-i\mathcal{M}_u = i\frac{2g_t^2 C_W^2}{M^2}\bar{V}(p_2,\lambda_2)M_{\mu\nu}\frac{S(p_1-p_4)-u+2M^2}{u-M^2}M_{\alpha\beta}U(p_1,\lambda_1)p_4^\alpha\eta^\beta(p_4)p_3^\mu\epsilon^\nu(p_3). \tag{4.41}$$

The average squared amplitude is given by

$$\overline{|\mathcal{M}_{\gamma\gamma}|^2} = \left(\frac{2g_t^2 C_W^2}{3M^2}\right)^2 Tr\left[\frac{S(p_2)+M^2}{2M^2}T_{\alpha\beta\mu\nu}\frac{S(p_1)+M^2}{2M^2}\bar{T}_{\sigma\ \rho}^{\ \beta\ \nu}\right]p_3^\mu p_3^\rho p_4^\alpha p_4^\sigma, \tag{4.42}$$

where

$$T_{\alpha\beta\mu\nu} = M_{\alpha\beta}\frac{S(p_1-p_3)-t+2M^2}{t-M^2}M_{\mu\nu} + M_{\mu\nu}\frac{S(p_1-p_4)-u+2M^2}{u-M^2}M_{\alpha\beta}, \tag{4.43}$$

$$\bar{T}_{\alpha\beta\mu\nu} = M_{\mu\nu}\frac{S(p_1-p_3)-t+2M^2}{t-M^2}M_{\alpha\beta} + M_{\alpha\beta}\frac{S(p_1-p_4)-u+2M^2}{u-M^2}M_{\mu\nu}. \tag{4.44}$$

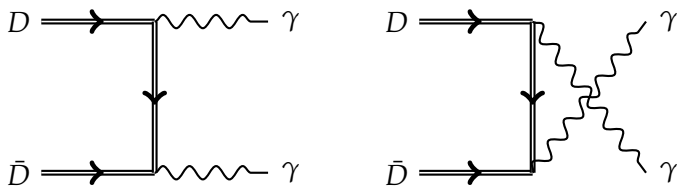

FIGURE 4.2: Feynman diagrams for $\bar{D}D \to \gamma\gamma$.

Performing the calculation using the traceology relations in the appendix yields

$$\begin{aligned}\overline{|\mathcal{M}_{\gamma\gamma}|^2} = \frac{2C_W^4 g_t^4}{9M^8\left(t-M^2\right)^2\left(u-M^2\right)^2}\Big[&6\left(tu\right)^4 + 2\left(tu\right)^3\left(-13M^4+11M^2s+2s^2\right)\\ &+\left(tu\right)^2\left(42M^8-76M^6s+33M^4s^2+4M^2s^3+2s^4\right)\\ &+2M^2tu\left(-15M^{10}+43M^8s-44M^6s^2+17M^4s^3-6M^2s^4+2s^5\right)\\ &+M^4\left(8M^{12}-32M^{10}s+51M^8s^2-40M^6s^3+25M^4s^4-12M^2s^5+2s^6\right)\Big],\end{aligned} \tag{4.45}$$

which results in the following cross section

$$\sigma_{\gamma\gamma}(s) = \frac{1}{F\sqrt{1-\frac{4M^2}{s}}}\frac{C_W^4 g_t^4}{540\pi M^8}\left[120M^4\left(4M^4-3M^2s-2s^2\right)\tanh^{-1}\sqrt{1-\frac{4M^2}{s}}\right.$$
$$\left.+s\sqrt{1-\frac{4M^2}{s}}\left(-10M^6+228M^4s-99M^2s^2+43s^3\right)\right]. \tag{4.46}$$

4.4 Tensor dark matter relic density

4.4.1 Non-relativistic expansion

Performing and expansion of the $\bar{D}D \to \bar{f}f$ and $\bar{D}D \to \gamma\gamma$ cross sections in terms of v_r, as mentioned in Section 4.1, we get

$$\sigma v_r \equiv \sigma_{\gamma\gamma} v_r + \sum_f \sigma_{\bar{f}f} v_r = a + b v_r^2, \tag{4.47}$$

where the sum runs over all the fermion states that are kinematically allowed, i.e. for $m_f < M$. As seen in the previous sections, the coefficients a and b turn out to be

$$a = \frac{29C_W^4 g_t^4}{18\pi M^2} + \sum_f \frac{N_f g_s^2 m_f^2\left(M^2-m_f^2\right)^{\frac{3}{2}}}{12\pi M^3\left(M_H^2-4M^2\right)^2},$$
$$b = \frac{365C_W^4 g_t^4}{216\pi M^2} + \sum_f \frac{N_f\sqrt{M^2-m_f^2}}{864\pi M^5}\left(\frac{96M^4 g_t^2 M_Z^2 S_W^2\left(\left(A_f^2-2B_f^2\right)m_f^2+2M^2\left(A_f^2+B_f^2\right)\right)}{v^2\left(M_Z^2-4M^2\right)^2}\right. \tag{4.48}$$
$$+\frac{192A_f M^2 C_W Q_f g_t^2 M_W M_Z S_W^2\left(m_f^2+2M^2\right)}{v^2\left(M_Z^2-4M^2\right)}+\frac{96C_W^2 Q_f^2 g_t^2 M_W^2 S_W^2\left(m_f^2+2M^2\right)}{v^2}$$
$$-\frac{6M^2m_f^2\left(8g_p^2\left(4M^2-M_H^2\right)\left(M^2-m_f^2\right)+g_s^2\left(-8m_f^2\left(M^2-M_H^2\right)-11M^2M_H^2+20M^4\right)\right)}{\left(M_H^2-4M^2\right)^3}$$
$$\left.-\frac{9M^2m_f^2g_s^2\left(4M^2-5m_f^2\right)}{\left(M_H^2-4M^2\right)^2}\right),$$

with $N_f = 3$ for quarks to account for each color and $N_f = 1$ for leptons.

The Higgs and spin portal contributions to $\langle\sigma v_r\rangle = a + \frac{6b}{x}$ are shown in Fig. 4.3 where we show the Higgs and spin portal, as a function of the couplings for $M = 10$ and 45 GeV and $x = 20$.

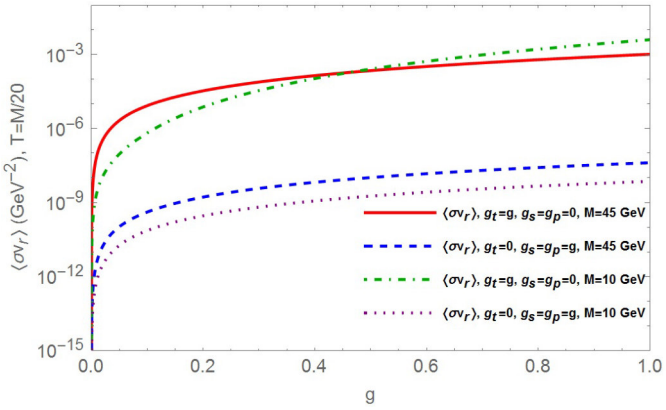

FIGURE 4.3: Individual contributions of the spin portal ($g_t = g$, $g_s = g_p = 0$) and the Higgs portal ($g_t = 0$, $g_s = g_p = g$) to $\langle\sigma v_r\rangle$. Similar results are obtained in the second case when varying independently g_s or g_p.

Using Eqs. (4.34) and (4.48), we can solve the Boltzman equation (4.29) numerically for different values of g_t, g_s and g_p. The solutions are shown in Fig. 4.4. We can see that, at some value $x = x_f$, the solution $Y(x)$ departs from the equilibrium solution $Y_{eq}(x)$, which is when it is said that dark matter decouples from the cosmic plasma in the non-relativistic regime, i.e. $x >> 1$.

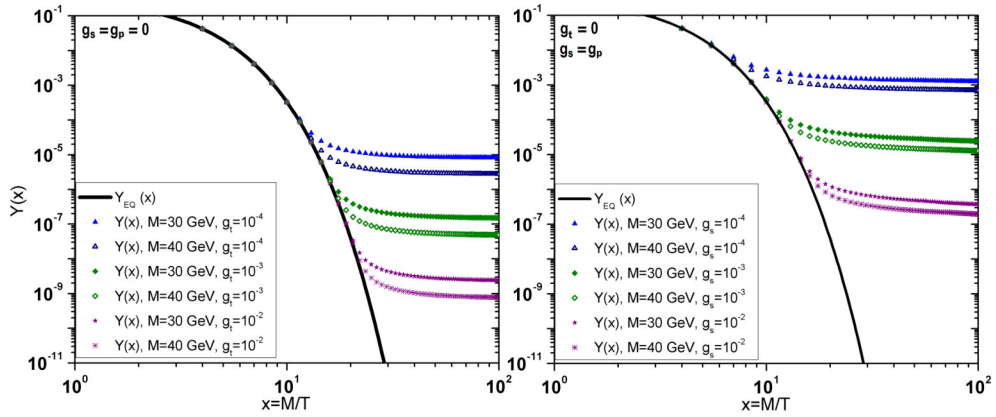

FIGURE 4.4: Solution of the Boltzman equation for the spin portal (left) and Higgs portal (right). Similar results are obtained in the later case when varying independently g_s and g_p. The solid line corresponds to $Y_{eq}(x)$.

The dark matter relic density is given by

$$\Omega_{DM} = \rho_{DM}/\rho_c = M(2 * Y(T_0))T_0^3/\rho_c, \tag{4.49}$$

where $\rho_c = \frac{3H^2}{8\pi G_N} = 1.05371(5) \times 10^{-5} h^2\ GeV/cm^3 = 8.09619(38) \times 10^{-47} h^2\ GeV^4$ is the critical density, where h is the renormalized Hubble parameter such that $H \equiv 100\ h\ km\ s^{-1}\ Mpc$, and $T_0 = 2.7255(6)\ K = 2.34865(52) \times 10^{-13}\ GeV$ is the temperature of the cosmic background at the present [3].

In order to obtain the dark matter relic density we need to solve the Boltzmann equation (4.29) and evaluate $Y(x_0 = M/T_0)$. This can be done using the numerical solution and evaluating for specific values of the couplings and M, scanning the parameter space consistent with the measured relic density. This can be complicated due to the form of $\langle \sigma v_r \rangle$, and it is more illustrative to follow a semi-analytic procedure, taking into account the freeze out mechanism. For $x > x_f$, we have that $Y(x) >> Y_{eq}(x)$ and we can find an approximate solution by neglecting $Y_{eq}(x)$ in the right hand side of Eq.(4.29). Integrating from T_f to T_0, we get

$$\frac{1}{Y(x_0)} = \frac{1}{Y(x_f)} + \sqrt{\frac{90}{8\pi^3 G_N}} M \int_{x_f}^{x_0} \frac{\langle \sigma v_r \rangle}{\sqrt{g_*(x)} x^2} dx. \tag{4.50}$$

We can neglect the term $Y(x_f)^{-1}$ in Eq. (4.50) which is very small compared with the second term in the left hand side of Eq. (4.50), to obtain the relic density

$$\Omega_{DM} h^2 = \frac{2T_0^3 h^2}{\rho_c} \sqrt{\frac{8\pi^3 G_N}{90}} \left(\int_{x_f}^{x_0} \frac{\langle \sigma v_r \rangle}{\sqrt{g_*(x)} x^2} dx \right)^{-1} = 4.337 \times 10^{-11}\ GeV^{-2} \left(\int_{x_f}^{x_0} \frac{\langle \sigma v_r \rangle}{\sqrt{g_*(x)} x^2} dx \right)^{-1}. \tag{4.51}$$

Notice that the relic density depends on the couplings (g_t, g_s, g_p) and M. We may use the complete function $g_*(x)$ but our results are quite similar if we use the average over the range of energies considered, $\bar{g}_* = 33$.

We only need the value of x_f. For that we need to understand when *freeze out* happens. Rearranging Eq. (4.29) in the following form

$$\frac{x}{Y_{eq}(x)} \frac{dY}{dx} = -\frac{\lambda(x) Y_{eq}(x)}{x} \left[\left(\frac{Y(x)}{Y_{eq}(x)} \right)^2 - 1 \right], \tag{4.52}$$

we can see that the factor $\frac{\lambda(x) Y_{eq}(x)}{x}$ decreases as x increases. Eventually, the value of this factor is small enough that $Y(x)$ becomes a constant. We can consider that this change happens when said factor $\frac{\lambda(x) Y_{eq}(x)}{x} \approx 1$, in other words, when

$$n_{eq}(x_f) \langle \sigma v_r \rangle (x_f) = H(x_f). \tag{4.53}$$

Using the non-relativistic form for $n_{eq}(x)$ and Eq. (4.34) leads to

$$\left(a + \frac{6b}{x_f}\right)\sqrt{x_f}e^{-x_f} = \frac{(2\pi)^3}{3M}\sqrt{\frac{G_N g^*(x_f)}{90}}. \tag{4.54}$$

The value of x_f depends on the coupling constants and M, which means that we can obtain a set of values of g and M that, after numerically solving the dark matter relic density, are consistent with the observed value $\Omega^{exp}_{DM}h^2 = 0.1193 \pm 0.0009$ [3]. We checked that these solutions are consistent with the approximations used, i.e., that decoupling occurs when dark matter is non-relativistic. In the case of the spin portal contribution, the values of x_f lie in the range $23.8 < x_f < 27.9$, thus $x_f >> 1$ is consistent with the non-relativistic approach. The set of values $g_t(M)$ obtained is shown in Fig. 4.5. We also directly calculated $Y(x)$ from the numeric general solution of the Boltzman equation for the set of values $g_t(M)$, using $Y(x) = Y_{eq}(x)$ for $x << x_f$ as initial condition, finding that $1/Y(x_f)$ is small compared to $1/Y(x_0)$ in Eq. (4.50). A similar procedure is used for the two couplings of the Higgs portal.

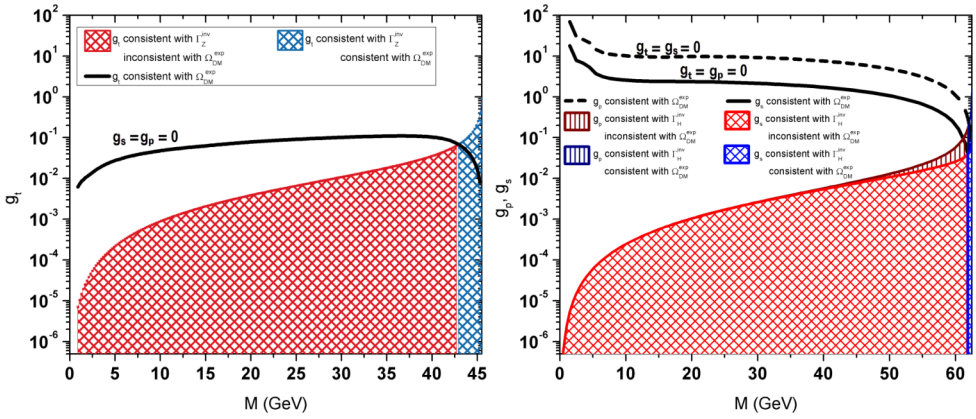

FIGURE 4.5: Values of the couplings consistent with the measured dark matter relic density, $\Omega^{exp}_{DM}h^2 = 0.1193 \pm 0.0009$ (solid line), as a function of M. The shadowed region in the left panel corresponds to the values consistent with the Z^0 invisible width, $\Gamma(Z^0 \to \bar{D}D) < \Gamma^{inv}_Z = 1.4 \pm 1.5\ MeV$, for the spin portal. These constraints exclude masses below 43 GeV for the spin portal. In the right panel, the shadowed region are the values consistent with the constraint $\Gamma(H \to \bar{D}D) < \Gamma^{inv}_H = 1.14 \pm 0.04\ MeV$ for the Higgs portal, where masses below 62 GeV are excluded.

For the Higgs portal, we obtained results for $g_p = 0$ varying g_s and $g_s = 0$ varying g_p, and similar results are obtained varying both couplings simultaneously. We conclude from Fig. 4.5 that, for the spin portal, consistency of the measured relic density with the constraints from data on the Z^0 invisible width (see Section 3), requires that the TDM

mass $M \geq 43\ GeV$. In a similar way, for the Higgs portal, consistency between the relic density and H^0 invisible width constraints requires a TDM mass $M \geq 62\ GeV$.

4.4.2 Complete calculation

Although the non-relativistic expansion of the cross-section used previously is a good approximation for the calculation of relic density, this procedure can fail in the presence of resonances [88]. The extent of this discrepancy depends on the mass and width of the resonance. As we will see in the following chapters, for the purposes of our work it is important to take a deep look into the region containing the Higgs resonance. As such, we need to perform the complete calculation of relic density for the mass range around this point, that is, in the vicinity of $M \approx M_H/2$.

In this case, we are interested in the case of $g_t = 0, g_p = 0$, since the resonance is present in the terms of the cross section with g_s. We can also perform a similar analysis with the Z^0 resonance, but as we will discover in subsequent chapters, the value of g_t turns out to be heavily limited by direct detection experiments, so we will skip this calculation in this work.

The complete calculation of the dark matter relic density involves the full thermal average cross-section $\langle \sigma v_r \rangle(x)$ for the annihilation of TDM into SM states. For $M \approx M_H/2$, dark matter annihilates only into $\bar{f}f$, $\gamma\gamma$ and $Z^0\gamma$. The annihilation of TDM into the last two final states vanishes when $g_t = 0$ at tree level, however in the presence of the $M \approx M_H/2$, the additional one-loop transitions offer sizable contributions (see diagram in Fig. 4.6). The $H\gamma\gamma$ and $H\gamma Z$ three-point functions have been previously studied in the literature (see Refs. [89–91]). In this case, we need to take into account the following effective interactions

$$\mathcal{L}_{eff} = H[G_{\gamma\gamma}F^{\mu\nu}F_{\mu\nu} + G_{Z\gamma}F^{\mu\nu}Z_{\mu\nu}], \tag{4.55}$$

where $G_{\gamma\gamma}, G_{Z\gamma}$ are the respective form factors. We can normalize these factors from a phenomenological approach, by doing $G_{\gamma\gamma} = \frac{g_{\gamma\gamma}}{M_H}$, $G_{Z\gamma} = \frac{g_{Z\gamma}}{M_H}$. We use the measured branching rations $BR[H \to \gamma\gamma] = 2.27 \times 10^{-3}$, $BR[H \to Z\gamma] = 1.53 \times 10^{-3}$ [92], to obtain the couplings $g_{\gamma\gamma} = 1.91 \times 10^{-3}$, $g_{Z\gamma} = 3.30 \times 10^{-3}$, which correspond to the on-shell momentum form factors. This approximation is justified since we are working in the resonant case.

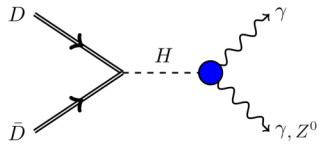

FIGURE 4.6: One loop contributions induced by the scalar Higgs portal to tensor dark matter annihilation into $\gamma\gamma$ and $Z^0\gamma$.

The $\bar{D}D \to \gamma\gamma, Z^0\gamma$ process via the scalar Higgs portal produces the following cross-sections:

$$(\sigma v_r)_{\gamma\gamma} = \frac{g_{\gamma\gamma}^2 g_s^2 v^2 s^2 (6M^4 - 4M^2 s + s^2)}{288\pi M^4 M_H^2 (s - 2M^2)[(s - M_H^2)^2 + M_H^2 \Gamma_H^2]}, \tag{4.56}$$

$$(\sigma v_r)_{Z\gamma} = \frac{g_{Z\gamma}^2 g_s^2 v^2 (s - M_Z^2)^3 (6M^4 - 4M^2 s + s^2)}{144\pi M^4 M_H^2 (s - 2M^2) s[(s - M_H^2)^2 + M_H^2 \Gamma_H^2]}. \tag{4.57}$$

We include these in addition to the $\bar{D}D \to \bar{f}f$ transition discussed previously to calculate the complete thermal average cross-section numerically. Our results are shown in Fig. 4.7, where we can see that even for values of M far from the resonance there are clear differences. Near the resonance, the deviation from the non-relativistic expansion goes far enough that it extends to the non-relativistic regime ($x >> 1$), so it is clear that we need to use the complete calculation in order to obtain the relic density.

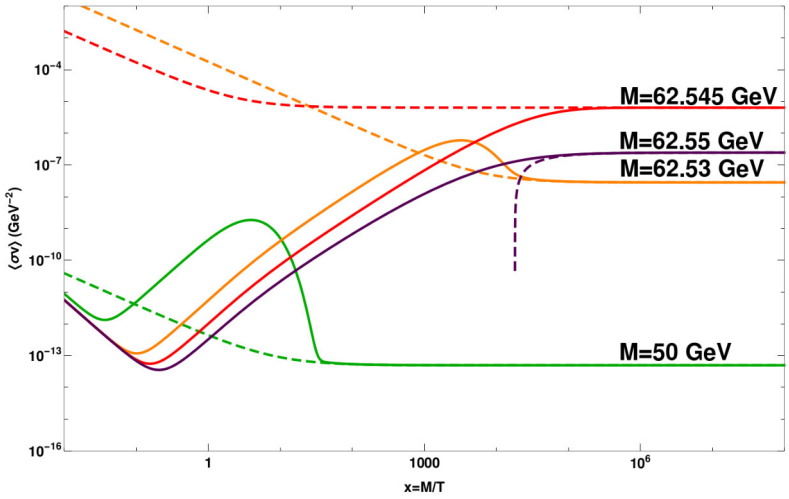

FIGURE 4.7: Thermal average cross-section (solid) and comparison with the non-relativistic expansion (dashed), for different values of the TDM mass.

The complete function $\langle \sigma v_r \rangle(x)$ was used to solve the freezing condition and the Boltzmann equation in a similar way to what was performed in the previous section, where

we use the program Wolfram Mathematica to find the freezing temperature x_f from the condition in Eq. 4.54 and solve the integral in Eq. 4.51 numerically. The freezing temperature obtained is around $x_f \approx 25$, similar to the non-relativistic expansion calculation. The obtained values of the coupling g_s and the dark matter mass M that are consistent with the measured relic density are plotted in Fig. 4.8. We then compare these values with the constraint from the invisible width of the Higgs boson found in Chapter 3, and the results are shown in Fig. 4.9. In this case, the lower limit is reduced when using the full calculation of the relic density, excluding masses below 58.9 GeV for the scalar Higgs portal.

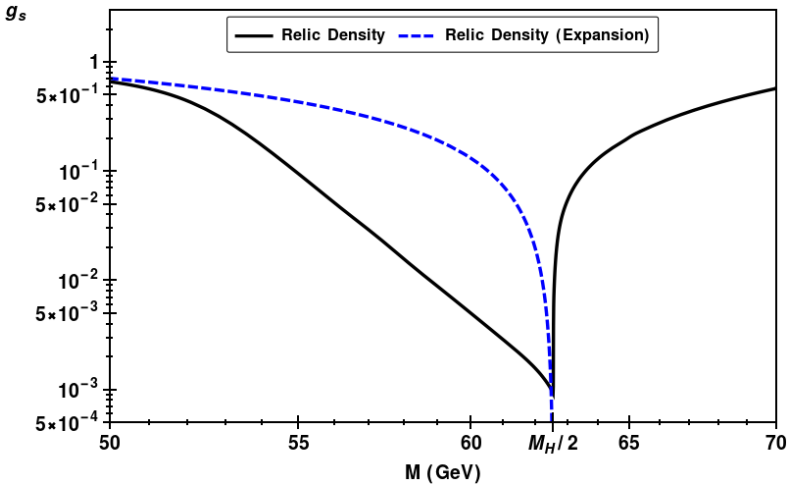

FIGURE 4.8: Values of the coupling g_s and TDM mass M consistent with the measured relic density near the Higgs resonance obtained without the v_r^2 expansion (continuous line). The dashed line corresponds to the conventional calculation via the non-relativistic expansion of the cross-section.

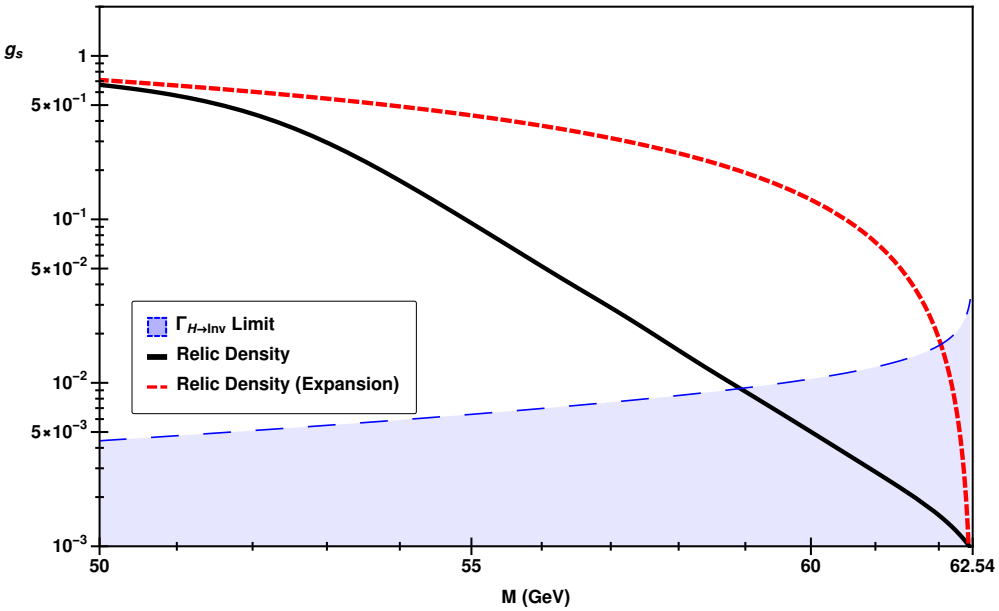

FIGURE 4.9: Values of the scalar Higgs portal coupling g_s consistent with the measured dark matter relic density, $\Omega_{DM}^{exp}h^2 = 0.1193 \pm 0.0009$, using the non-relativistic expansion (dashed red line) and the complete calculation of $\langle \sigma v_r \rangle$ (solid black line), as a function of M. The shadowed region represents the values of g_s consistent with the constraint $\Gamma(H \to \bar{D}D) < \Gamma_H^{inv} = 1.14 \pm 0.04\ MeV$ for the Higgs portal. Masses below 58.9 GeV are excluded considering the full consistency with relic density and the invisible width limit.

Chapter 5

Direct Detection Limits for Tensor Dark Matter

Let us part from the idea that the galaxy may contain a dark matter halo. We can then assume that, in the case of WIMPs, the flux of these particles arriving on Earth, assuming they have a velocity around $\sim 300km/s$ and with a standard density $\rho_{DM} = 0.3GeVcm^{-3}$, is of the order of $\phi \approx \rho_{DM} \times \langle v \rangle / M \sim 10^5 (100\text{GeV}/M_{DM}) cm^{-2}s^{-1}$ [93]. This is potentially a large enough flux that, even if the interactions with SM particles are feable (e.g. smaller in order than the weak scale $\langle \sigma v \rangle \sim 10^{-26} cm^{-3}s^{-1}$), the scattering off nuclei found in its way may produce a measurable signal [94]. The elastic scattering of nuclei will cause nuclear recoils, which then can be measured by low background detectors. This is the basic principle behind dark matter *direct detection* experiments. A great number of experiments have been put forth during the past few years using different techniques for the detection of the corresponding nuclei recoil kinetic energy T (for a recent review see [95]).

In this chapter we will discuss the calculation of the signal typically measured in direct detection experiments, the dark matter-nucleon scattering cross section, which we will calculate for Tensor Dark Matter and then compare our results with one of the most stringent direct detection limits, set by the XENON1T experiment [51].

5.1 General formalism for direct detection of dark matter

In order to discuss the signal given by direct detection experiments, we must understand and measure the rate of interactions (counts per day per kilogram in the nuclear kinetic energy recoil range dT) of a DM particle. First assume that the target nucleus of mass M_N moves with a velocity v relative to the DM particle of mass M. The nucleus interacts within a given time dt with any particle inside a volume $dV = \sigma v dt$, where σ is the DM-nucleus cross section. Then, the number of DM particles that the nucleus can

interact with is

$$dN = n_{DM} f(v) \sigma v dt = \frac{\rho}{M} f(v) \sigma v dt, \tag{5.1}$$

where $n_{DM} = \rho/M$ is the DM number density, with ρ being the local mass density of the DM particle, and $f(v)$ is the local velocity distribution of dark matter on Earth.

The local mass density of dark matter (that is, the average over a volume of a few hundred parsecs around the Sun) carries great weight when it comes to the dynamical information of the Galaxy, and is relevant in direct and indirect detection experiments. There are different methods to determine the magnitude of the local mass density from observations (see Ref. [96]), and depending of them and the stellar objects of study, the value falls in the range of $\rho \in [0.2, 1.5] GeV/cm^3$. The specific form of *rho*, however, also called density profile, is another point of study in cosmology, and there are many proposals based on observations. We get into this topic and mention some of these profiles in Chapter 6. For now, in the case of direct detection, we do not have to consider a specific mass density for the purposes of comparison with XENON1T data, as we will see later on.

While we are not yet able to measure local velocity distribution of dark matter particles directly, we can assume that this distribution follows the Maxwellian distribution:

$$f(v) = \frac{1}{k} e^{-\frac{(v-v_E)^2}{v_0^2}}, \tag{5.2}$$

with k being a normalization constant, v_E is the Earth velocity around the sun and v_0 stands for the average DM velocity in the galactic halo, which is typically taken as $v_0 = 220\,\text{km/s}$, although methods involving the measurement of the Sun's velocity with respect to an object at rest with the Galactic center and methods that measure the local radial force allow for this velocity to be within $v_0 = (218 - 246)\,\text{km/s}$ [3]. The rate of interactions is then the rate of DM particles that interact with the nuclei times the number of nuclei per kilogram of material, $\frac{N_0}{A}$, and integrated over the velocity space,

$$dR = \frac{N_0}{A} \int \frac{dN}{dt} d^3v = \frac{N_0}{A} \int \frac{\rho}{M} f(v) \sigma v d^3v. \tag{5.3}$$

Thus, the differential interaction rate is

$$\frac{dR}{dT} = \frac{\rho}{M M_A} \int |\mathbf{v}| f(\mathbf{v}) \frac{d\sigma}{dT}(T, \mathbf{v}) d^3\mathbf{v}, \tag{5.4}$$

where T is the nuclei recoil energy and $\frac{d\sigma}{dT}(T, \mathbf{v})$ describes the dark matter-nucleus differential cross section. We must integrate from $v_{min}(T)$, the minimal velocity of an incoming dark matter required to produce a nuclear recoil of energy T, to $v_{esc} = 557\ km/sec$,

which is the escape velocity of a dark matter particle in our galaxy (the maximum velocity that a dark matter particle is allowed to have to continue being bound by the galactic halo).

This is measured in the laboratory reference system (LAB), and we will now calculate all relevant quatities in this frame of reference. The differential cross section for the dark matter-nuclei interaction, $D(p_1)N_A(p_2) \to D(p_3)N_A(p_4)$, is

$$\frac{d\sigma}{dT}(T, v) = \frac{|\overline{\mathcal{M}}(s,t,u)|^2}{32\pi M_A p_1^2}, \tag{5.5}$$

where $p_1 = (E_1, \boldsymbol{p_1}) = (E_1, M\boldsymbol{v})$, $p_2 = (M_A, 0)$, $p_3 = (E_3, \boldsymbol{p_3})$, $p_4 = (M_A + T, \boldsymbol{p_A})$, and the Mandelstam variables are written as

$$s = (E_1 + M_A)^2 - \mathbf{p}_1^2 = (M + M_A)^2 + MM_A\mathbf{v}^2 + \mathcal{O}(\mathbf{v}^4), \tag{5.6}$$

$$t = T^2 - |\mathbf{p}_A|^2 = -2M_A T, \tag{5.7}$$

$$u = 2M^2 + 2M_A^2 - s - t = (M - M_A)^2 + 2M_A T - MM_A\mathbf{v}^2 + \mathcal{O}(\mathbf{v}^4). \tag{5.8}$$

We can see that the averaged squared amplitude, $|\overline{\mathcal{M}}(s,t,u)|^2$, only depends on the nuclear recoil energy and the incoming dark matter velocity. For the incoming momentum p_1, the nuclear recoil energy is given by

$$T = \frac{2M_A M^2\mathbf{v}^2\cos^2\theta}{(E_1 + M_A)^2 - M^2\mathbf{v}^2\cos^2\theta} = \frac{2M_A M^2\mathbf{v}^2\cos^2\theta}{(M + M_A)^2} + \mathcal{O}(\mathbf{v}^4), \tag{5.9}$$

where θ is the angle of the nuclear recoil measured with respect to the direction of the incoming dark matter particle. When the DM particle transfers the maximum momentum to the nucleus ($\theta = 0$), we obtain the minimal velocity required to produce an energy recoil T, and it is given by

$$v_{min}^2(T) = \frac{(M + M_A)^2}{2M_A M^2} T = \frac{M_A}{2\mu_A^2} T, \tag{5.10}$$

where $\mu_A = M_A M/(M + M_A)$ is the DM-nucleus reduced mass.

In order to calculate the invariant amplitude $\mathcal{M}$, we must proceed from the effective field theory approach of the dark matter-nucleus interactions. We begin with the fundamental interactions of DM with standard model particles and from there, an effective theory for the DM-nucleons interaction can be built. After this, we can construct an effective theory for interactions with nuclei. It is important to note that for low momentum transfer processes, the finite size of the nucleus must be taken into account. We can

write the amplitude as follows

$$\mathcal{M} = \mathcal{M}_0 F(q^2), \tag{5.11}$$

where $\mathcal{M}_0$ is the invariant amplitude calculated with the effective theory at the nuclear level and $F(q^2)$ is the nucleus form factor. The differential cross section using this terminology yields

$$\frac{d\sigma}{dT}(T, \mathbf{v}) = \frac{|\bar{\mathcal{M}}_0(s,t,u)|^2}{32\pi M_A M^2 \mathbf{v}^2} F^2(T). \tag{5.12}$$

This is the differential cross section in terms of the nuclear recoil energy T. Our purpose is to use this to compare with experimental results, however, since the scattering takes place at low momentum transfer (low T in the LAB frame), it is usual to see the results reported in terms of the total $D - N_A$ cross section at zero momentum transfer. In the XENON1T experiment, the detector is sensitive to $T \in [3, 50]\ KeV$. Additionally, dark matter particles on Earth have a velocity in the range of $|\mathbf{v}| \in [0, v_{esc}]$ with $v_{esc}/c = 1.85 \times 10^{-3}$, and have an average velocity $v_0/c = 0.73 \times 10^{-3}$.

Interactions between standard model and dark matter particles can be assumed to appear in two forms: exchanging a massive particle (in our case, H and Z^0), or via a massless mediator (like the photon). In the massive mediator case, in the effective theory, the leading term is a four-point interaction that has an effective coupling suppressed by the mass of the exchanged particle. Therefore, the average squared amplitude $|\bar{\mathcal{M}}_0(s,t,u)|^2 \equiv g(T, \mathbf{v}^2)$ is a regular function of T that we can expand as

$$g(T, \mathbf{v}^2) = g_0(\mathbf{v}^2) + g_1(\mathbf{v}^2) T + ... \tag{5.13}$$

Since the process takes place at low T, we can keep only the leading term in the expansion, taking the following form

$$\frac{d\sigma}{dT}(T, \mathbf{v}) \approx \frac{g_0(\mathbf{v}^2)}{32\pi M_A M^2 \mathbf{v}^2} F^2(0). \tag{5.14}$$

This is the differential cross section at zero momentum transfer. We can relate this expression with the total cross section if we integrate on T from 0 to the maximum nuclear recoil $T_{max} = 2\mu_A^2 \mathbf{v}^2 / M_A$. We obtain

$$\sigma(\mathbf{v}) \approx \frac{g_0(\mathbf{v}^2)}{32\pi M_A M^2 \mathbf{v}^2} \frac{2\mu_A^2 \mathbf{v}^2}{M_A} F^2(0) \approx \frac{\mu_A^2 g_0(v^2)}{16\pi M_A^2 M^2} F^2(0) \equiv \sigma_{SI} F_{SI}^2(0), \tag{5.15}$$

where we have expanded $g_0(\mathbf{v}^2)$ around $\mathbf{v}^2 \simeq 0$ and kept the leading terms. We choose the notation σ_{SI} since at this stage we are only considering point interactions of dark

matter with the nucleus, which is spin-independent (SI). We can generalize this expression to consider spin-dependent interactions, which arise from the couplings from the dark matter field to the quark axial current. In the case of supersymmetric models, for example, the neutralino-nucleon scattering occurs via the exchange of a Z boson or a squark [97]. In our case, we will see later on that the spin-independent interactions are dominant, so we will focus on them from now on. We can write the actual differential cross section in Eq. (5.12) to leading order in T (in the dynamics) as

$$\frac{d\sigma}{dT}(T,\mathbf{v}) = \frac{M_A}{2\mu_A^2\mathbf{v}^2}\sigma_{SI}F_{SI}^2(T), \tag{5.16}$$

where σ_{SI} is the $D-N_A$ total cross section at zero momentum transfer. In the general case, if spin-dependent contributions are more prominent, there would be an additional term with $\sigma_{SD}F_{SD}^2(T)$.

The XENON1T experiment has one of the most stringent limits on direct detection of dark matter at the WIMP mass scale ($\sim 100GeV$). Its most recent data [51] assumes isospin conserving dark matter-nucleus interactions and report the following observable [98]

$$\sigma_p = \frac{\mu_p^2}{A^2\mu_A^2}\sigma_{SI}, \tag{5.17}$$

where μ_p stands for the dark matter-proton reduced mass. In our case, tensor dark matter-nucleus interactions are mediated by H, Z^0 and γ and are not isospin conserving. When massive particles, such as H and Z, are exchanged they produce four-point dark matter-nucleus interactions for small momentum transfer and its treatment is the same as it was stated above, but when we have exchange of photons, the propagator has a pole at $q^2 = 0$, so we have to modify relations given previously to properly obtain the observable reported by XENON1T, which does not correspond with the zero-momentum dark matter-proton cross section when interactions are isospin conserving. The $D-N_A$ differential cross section in Eq. (5.12) can be written as

$$\frac{d\sigma}{dT}(T,\mathbf{v}) = \frac{\xi}{\mathbf{v}^2}g(T,\mathbf{v}^2)F_{SI}^2(T), \tag{5.18}$$

where $\xi = (32\pi M_A M^2)^{-1}$. The function $g(T,\mathbf{v}^2)$ is no longer a regular function of T due to the poles of the exchanged massless particle. It is not possible to perform an expansion around $T=0$, however we can use the fact that experiments start detecting nuclear recoil at a given $T = T_{min}$. Doing an expansion around this value we get

$$\begin{aligned}\frac{d\sigma}{dT}(T,\mathbf{v}) &= \frac{\xi}{\mathbf{v}^2}\left[g(T_{min},\mathbf{v}^2) + g'(T_{min},\mathbf{v}^2)(T-T_{min})\right]\left[F^2(T_{min}) + (F^2)'(T_{min})(T-T_{min})\right] \\ &= \frac{\xi}{\mathbf{v}^2}g(T_{min},\mathbf{v}^2)F_{SI}^2(T_{min}) + \mathcal{O}(T-T_{min}).\end{aligned} \tag{5.19}$$

Integrating now from T_{min} to $T_{max} = 2\mu_A^2\mathbf{v}^2/M_A$ and keeping only the leading term gives

$$\sigma_A = \frac{\xi}{\mathbf{v}^2} g(T_{min}, \mathbf{v}^2) F_{SI}^2(T_{min})(T_{max} - T_{min}). \tag{5.20}$$

This is the total dark matter-nucleus cross section at the fixed momentum transfer $q^2 = -2M_A T_{min}$. Rewriting the differential cross section in terms of this quantity has the same form as Eq.(5.16), but with

$$\sigma_{SI} = \frac{\sigma_A}{F_{SI}^2(T_{min})} \frac{T_{max}}{T_{max} - T_{min}} = \frac{\mu_A^2}{16\pi M_A^2 M^2} g(T_{min}, \mathbf{v}^2). \tag{5.21}$$

We will later show that for TDM, the average squared amplitude takes the following form

$$g(T, \mathbf{v}^2) = a_0 + \left(\frac{b_0}{T} + c_0\right)\mathbf{v}^2 + \mathcal{O}(T, \mathbf{v}^4). \tag{5.22}$$

The observable σ_p reported by XENON1T is, then,

$$\sigma_p = \frac{1}{16\pi A^4 (M + M_p)^2}\left[a_0 + \left(\frac{b_0}{T_{min}} + c_0\right)\mathbf{v}^2 + \mathcal{O}(T, \mathbf{v}^4)\right]. \tag{5.23}$$

For small values of $\mathbf{v}^2$, the leading contribution would be given by a_0, but the contribution from the photon coupling ($\mathcal{O}(\mathbf{v}^2)$) is $b_0\mathbf{v}^2/T$, which is enhanced by small values of T and could also give sizable contributions. The term with c_0 is, however, neglectable. Up to only the sizable contributing terms, we have

$$\sigma_p = \frac{1}{16\pi A^4 (M + M_p)^2}\left[a_0 + \frac{b_0\mathbf{v}^2}{T_{min}}\right]. \tag{5.24}$$

5.2 Nucleon scattering from tensor dark matter

The tensor dark matter - nucleon differential cross section involves the effective interactions of H, γ and Z^0 with nuclei, which require the calculation of the nucleon interactions from effective theory. At the nucleon level, the corresponding effective Lagrangian is given by [99]

$$\mathcal{L}_{eff}^N = \sum_{N=p,n}\left(g_{HNN} H\bar{N}N - e\bar{N}Q_N\gamma^\mu N A_\mu - \frac{M_Z}{2v}\bar{N}\gamma^\mu(A_N + B_N\gamma^5)NZ_\mu\right), \tag{5.25}$$

where $Q_p = 1$, $Q_n = 0$ and

$$g_{HNN} = -\left(7\sum_{u,d,s} f_{Tq}^{(N)} + 2\right)\frac{m_N}{9v}, \tag{5.26}$$

$$A_p = 2A_u + A_d = 1 - 4\sin^2\theta_W, \tag{5.27}$$
$$A_n = A_u + 2A_d = -1, \tag{5.28}$$

and

$$B_N = -\Delta_u^{(N)} + \Delta_d^{(N)} + \Delta_s^{(N)}, \tag{5.29}$$
$$B_p = -\Delta_u^{(p)} + \Delta_d^{(p)} + \Delta_s^{(p)}, \tag{5.30}$$
$$B_n = -\Delta_d^{(p)} + \Delta_u^{(p)} + \Delta_s^{(p)}. \tag{5.31}$$

The specific parameters for each quark are given in Table 5.1 .

	$f_{Tq}^{(p)}$	$f_{Tq}^{(n)}$	$\Delta_q^{(p)}$
u	0.023	0.019	0.77
d	0.034	0.041	-0.40
s	0.140	0.140	-0.12

TABLE 5.1: Values for the coefficients $f_{Tq}^{(p)}$, $f_{Tq}^{(n)}$ and $\Delta_q^{(p)}$ extracted from Ref. [100].

At nuclear level, the Lagrangian takes a similar form,

$$\mathcal{L}_{eff}^{A} = g_{HN_AN_A} H\bar{N}_A N_A - Ze\bar{N}_A\gamma^\mu N_A A_\mu - \frac{M_Z}{2v}\bar{N}_A\gamma^\mu(A_A + B_A\gamma^5)N_A Z_\mu, \tag{5.32}$$

with

$$\begin{aligned} g_{HN_AN_A} &= Zg_{Hpp} + (A-Z)g_{Hnn}, \\ A_A &= ZA_p + (A-Z)A_n, \\ B_A &= ZB_p + (A-Z)B_n, \end{aligned} \tag{5.33}$$

where Z is the atomic number and A stands for the total number of nucleons inside the nucleus.

The invariant amplitude for $D(p_1)N_A(p_2) \to D(p_3)N_A(p_4)$ is the exchange of H, γ and Z^0 in the t channel. The contributions are given by

$$-i\mathcal{M}_H = i\frac{g_{DN_AH}}{t-m_H^2}\overline{U}(p_3)\left(g_s I + ig_p\chi\right)U(p_1)\,\bar{N}_A(p_4)\,N_A(p_2), \tag{5.34}$$

$$-i\mathcal{M}_\gamma = -\frac{g_{DN_A\gamma}}{t}\overline{U}(p_3)\,M_{\alpha\beta}(p_1-p_3)^\beta\,U(p_1)\,\bar{N}_A(p_4)\,\gamma^\alpha N_A(p_2), \tag{5.35}$$

$$-i\mathcal{M}_Z = \frac{g_{DN_AZ}}{t-M_Z^2}\overline{U}(p_3)\,M_{\alpha\beta}(p_1-p_3)^\beta\,U(p_1)\,\bar{N}_A(p_4)\,\gamma^\alpha\left(A_A+B_A\gamma_5\right)N_A(p_2), \tag{5.36}$$

where

$$g_{DN_AH} = -vg_{HN_AN_A}, \tag{5.37}$$

$$g_{DN_A\gamma} = 2Zeg_t\cos\theta_W, \tag{5.38}$$

$$g_{DN_AZ} = \frac{M_Z g_t \sin\theta_W}{v}. \tag{5.39}$$

The spin-independent contributions come mainly from the Higgs and photon interactions with TDM and the weak vector current in the Z^0 exchange. For the spin-dependent case, the leading contributions come from the axial current. A covariant calculation of the squared amplitude gives

$$\begin{aligned}
\left|\bar{\mathcal{M}}\right|^2 = {} & \frac{g_{DN_AH}^2}{6M^4\left(t-m_H^2\right)^2}\left(4M_A^2-t\right)\left(\left(g_p^2+g_s^2\right)t\left(t-4M^2\right)+6g_s^2M^4\right) \\
& + \frac{g_{DN_A\gamma}^2}{3M^4t}\Big[-2M_A^4\left(M^2-t\right)+M_A^2\left(4M^4+4M^2(s+t)-2t(2s+t)\right)-2M^6 \\
& + 2M^4(2s+3t)-M^2\left(2s^2+6st+t^2\right)+2st(s+t)\Big] \\
& + \frac{g_{DN_AZ}^2}{3M^4\left(t-M_Z^2\right)^2}\Big[\left(A_A^2+B_A^2\right)\left(2M_A^4\left(t-M^2\right)-2M^6+2M^4(2s+3t)\right. \\
& - M^2\left(2s^2+6st+t^2\right)+2st(s+t)\big) \\
& \left. + M_A^2\left(A_A^2\left(4M^4+4M^2(s+t)-2t(2s+t)\right)-4B_A^2\left(3M^4-M^2s+st\right)\right)\Big]t \\
& - \left(\frac{g_{DN_AH}g_{DN_A\gamma}}{t-m_H^2}\right)\left(\frac{2g_sM_A}{3M^4}\right)\left(2M^2-t\right)(s-u) \\
& + \frac{g_{DN_AH}g_{DN_AZ}}{\left(t-m_H^2\right)\left(t-M_Z^2\right)}\left(\frac{2A_Ag_sM_A}{3M^4}\right)\left(2M^2-t\right)(s-u)\,t \\
& - \frac{2A_A}{3M^4}\frac{g_{DN_A\gamma}g_{DN_AZ}}{\left(t-M_Z^2\right)}\Big[-2M_A^4\left(M^2-t\right)+M_A^2\left(4M^4+4M^2(s+t)-2t(2s+t)\right)-2M^6 \\
& + 2M^4(2s+3t)-M^2\left(2s^2+6st+t^2\right)+2st(s+t)\Big].
\end{aligned} \tag{5.40}$$

Expanding the average squared amplitude and keeping the leading terms in $\mathbf{v}^2$ and T we get

$$\left|\bar{\mathcal{M}}\right|^2 = \frac{4g_s^2 g_{DN_A H}^2 M_A^2}{m_H^4} + \frac{2g_{DN_A\gamma}^2}{3M^2}\left(M^2 - 2MM_A + 3M_A^2\right) + \frac{16 g_s g_{DN_A\gamma} g_{DN_A H} M_A^2}{3M m_H^2} + \left(\frac{4g_{DN_A\gamma}^2 M_A}{3T} - \frac{16 A_A g_{DN_A\gamma} g_{DN_A Z} M_A^2}{3M_Z^2} + \frac{8 g_s g_{DN_A\gamma} g_{DN_A H} M_A^2}{3M m_H^2} - \frac{2g_{DN_A\gamma}^2 M_A}{3M^2}\left(M - 4M_A\right)\right)\mathbf{v}^2. \tag{5.41}$$

We can see that the leading contributions come from the spin-independent interactions. The spin-dependent contributions, those from the axial current, appear with the coefficient

$$\frac{4M_A^2 g_{DN_A Z}^2}{3A^2 M M_Z^4} T(MM_A + 4\mathcal{O}(\mathbf{v}^4)). \tag{5.42}$$

Since it is proportional to $T\,\mathbf{v}^4$ this contribution is heavily suppressed. Additionally, the g_p coupling does not contribute as highly as g_t or g_s to the TDM-nucleon cross section. This comes from the fact that the coupling to the Z^0 is done through the higher multipoles of the tensor dark matter field and not from weak charges (since they are standard model singlets). The coefficients in Eq. (5.22) are identified as

$$a_0 = \frac{4g_s^2 g_{DN_A H}^2 M_A^2}{m_H^4} + \frac{2g_{DN_A\gamma}^2}{3M^2}\left(M^2 - 2MM_A + 3M_A^2\right) + \frac{16 g_s g_{DN_A\gamma} g_{DN_A H} M_A^2}{3M m_H^2}, \tag{5.43}$$

$$b_0 = \frac{4g_{DN_A\gamma}^2 M_A}{3}, \tag{5.44}$$

$$c_0 = -\frac{16 A_A g_{DN_A\gamma} g_{DN_A Z} M_A^2}{3M_Z^2} + \frac{8 g_s g_{DN_A\gamma} g_{DN_A H} M_A^2}{3M m_H^2} - \frac{2g_{DN_A\gamma}^2 M_A}{3M^2}\left(M - 4M_A\right). \tag{5.45}$$

We plot σ_p as a function of the TDM mass M for different values of the couplings g_t and g_s, as shown in Fig. 5.1. Here, we are considering $A = 131$, $Z = 54$ and $T_{min} = 3\ KeV$, appropriate for XENON1T experiment and compare with the recently published XENON1T results [51]. The leading spin portal contributions ($g_s = 0$) are due to the photon exchange and dominated by the photon pole. We can see that, in comparison to the Higgs portal coupling, the spin portal coupling is quite restricted by the XENON1T data ($g_t \approx 10^{-4}$) for tensor dark matter with a mass of the order of a few hundreds GeV. We can correlate the values of g_s and M that are consistent with this limit and compare the result with the relic density bounds obtained in Chapter 4. We show the comparison in Fig. 5.2, where we can see that full consistency for these two observables is obtained for $M \in [60.056, 62.554]\ GeV$.

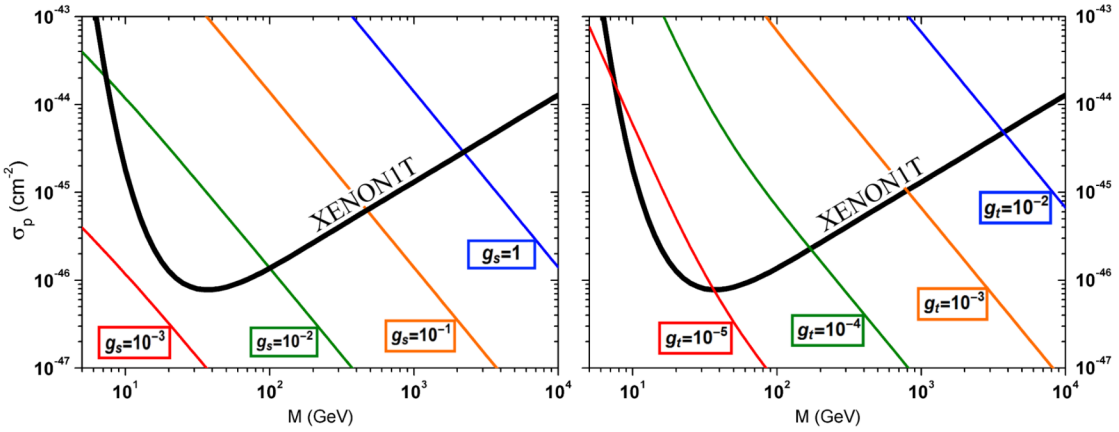

FIGURE 5.1: Observable σ_p as a function of the dark matter mass M for the Higgs ($g_t = 0$, left panel) and spin ($g_s = 0$, right panel) portals, compared with the XENON1T upper bounds [51].

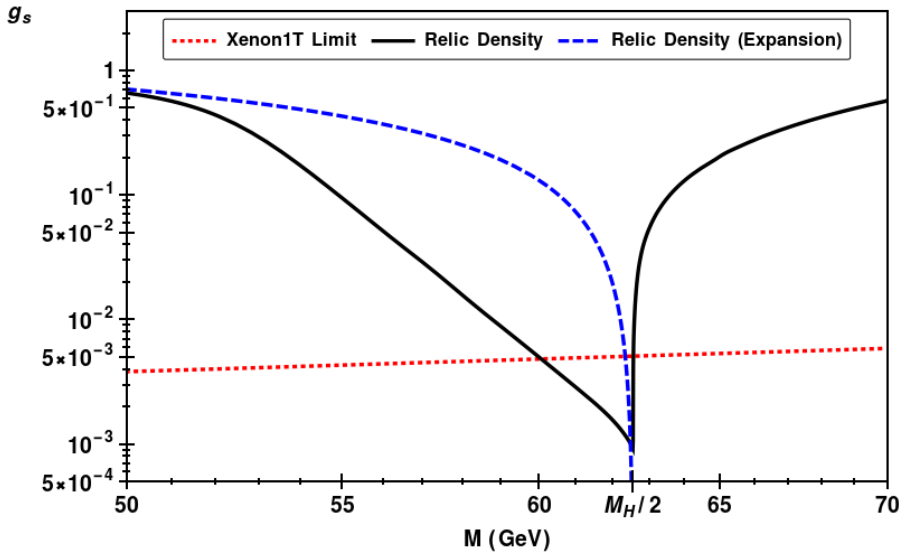

FIGURE 5.2: Values of g_s and M that are consistent with the Xenon1T direct detection limits (dotted red line), consistent with relic density using the non-relativistic expansion of $\langle \sigma v \rangle$ (dashed blue line), and consistent with the complete calculation of the relic density (solid black line). Full consistency for these two observables is obtained for $M \in [60.056, 62.554]\ GeV$.

Chapter 6

Indirect Detection Limits for Tensor Dark Matter

A big convenience presented by dark matter indirect searches is that we are taking advantage of interactions that are already potentially happening all around the cosmos, with data that we can collect with the numerous probes and telescopes already present and available. These searches involve looking for Standard Model particles produced by decay or annihilation of dark matter, or secondary effects from these processes. Because they happen at cosmological scales, it is possible to probe higher energies, weaker particle couplings and longer decay lengths. Not to mention that, primarily, all the evidence for dark matter comes from astrophysics and cosmological observations. With this in mind, indirect detection experiments are a promising tool for dark matter discovery and, as will be presented in this chapter, bounds for dark matter models.

The principle of indirect dark matter searches is to observe the products of DM annihilations (or decays). If some of those products are SM particles, most of them will decay on short timescales and, at the end of those decay chains, there could be stable particles that we can detect. We can try to scan the sky in search for any excess of these particles, e.g. electrons, positrons, protons, antiprotons, photons, neutrinos. In this chapter we will look at the bounds projected by the photon flux coming from two particular sources: the galactic center and a group of galaxies considered to have a large amount of dark matter content, know as dwarf spheroidal satellite galaxies (or dSphs). In this work, we also look into antiproton signals as indirect detection of tensor dark matter, but we dedicate a separate chapter for this purpose.

6.1 Gamma Rays from the Galactic Center

Among the particles that we can detect, the most sought out for are the gamma rays, coming from the Sun, the center of our galaxy, other galaxies and even from extragalactic sources. Since these are neutral to astrophysical magnetic fields, they propagate in straight lines directly from the source provided they are not absorbed in the way. Dark matter annihilation produces gamma rays directly, or by hadronization of the final states.

There has been reports from several groups that an excess over the expected gamma ray flux from known sources in the Milky Way galactic center exists in the observations provided by the Fermi Large Area Telescope (FermiLAT) data, at around 3 GeV [101–111]. There are, however, large uncertainties involved in the interpretation of FermiLAT data, which have been previously analyzed by the FermiLAT collaboration [112]. The conclusion is that a gamma-ray excess (GRE) in a region around 3 GeV indeed exists, but the signal may exist within a broad band of possible values for the differential flux as a function of the photon energy. This excess could be explained by little known astrophysical sources [101, 113–117], however the annihilation of dark matter into final states containing photons remains as an attractive possibility [107, 118–127].

In general, a detector has a two-dimensional view of the sky and observations involve the number of photons arriving within a certain solid angle in a certain time. Let A be the area on the detector, measuring a signal coming from a volume dV at the coordinates (r, θ, ϕ), with Earth at $r = 0$. Since we are working with tensor dark matter, we will consider products from annihilation. Suppose that $\frac{dN_i^\gamma}{dE}$ is the photon spectrum from an annihilation channel i, and assuming that the energy of the photons does not change through its way to the detector (by redshifting, absorption, etc.), then the spectrum of gamma rays received at Earth per volume per time is [128]

$$\frac{dN_\gamma}{d\omega dt dV} = \left(\frac{1}{2}\right) \sum_i \left(\frac{dN_i^\gamma}{d\omega}\right) \frac{A}{8\pi r^2} \langle \sigma v_r \rangle_i n(\vec{r})^2, \tag{6.1}$$

where $\langle \sigma v_r \rangle_i$ stands for the non-radiative cross section for the i-channel and ω is the energy of the photon. The first factor $\frac{1}{2}$ is included for non-self-conjugated dark matter, which is the case of TDM. $n(\vec{r}) = \rho(\vec{r})/M$ is the DM number density. We can integrate over the line of sight, s, that relates to r (distance from the Galactic Center) by the following expression

$$r(s, \theta) = (r_\odot^2 + s^2 - 2 r_\odot s \, cos\theta)^{1/2}, \tag{6.2}$$

where $r_\odot = 8.33$ kpc [129] is the distance between the Sun and the Galactic Center and θ is the angle between the direction of the line of sight and the line connecting the Earth

to the Galactic Center. Integrating Eq. (6.1) over s, we get

$$\frac{dN_\gamma}{d\omega dt d\Omega} = \left(\frac{A}{16\pi}\right) \sum_i \left(\frac{dN_i^\gamma}{d\omega}\right) \frac{\langle \sigma v_r \rangle_i}{M^2} \int_0^\infty \rho(r(s,\theta))^2 ds. \tag{6.3}$$

If the source is localized, we can integrate over the solid angle subtended by the object to obtain

$$\frac{dN_\gamma}{d\omega dt} = \left(\frac{A}{16\pi}\right) \sum_i \left(\frac{dN_i^\gamma}{d\omega}\right) \frac{\langle \sigma v_r \rangle_i}{M^2} \int_0^\infty \rho(r(s,\theta))^2 ds d\Omega. \tag{6.4}$$

The photon spectrum $\frac{dN_i^\gamma}{dE}$ can also be written as

$$\frac{dN_i^\gamma}{d\omega} \equiv \frac{B_i}{\langle \sigma v_r \rangle_i} \frac{d\langle \sigma v_r \rangle_\gamma^i}{d\omega}, \tag{6.5}$$

where B_i is the number of photons produced by the process in channel i. It is conventionally assumed that this non-radiative cross section contains the details on the annihilation of dark matter entering the radiative process, and it is considered that the spectrum includes the information of the photon production from standard model i-states which can be calculated and is well-known. In this construction, model independent fits to data can be done with $\langle \sigma v_r \rangle_i$ and M as free parameters. In summary, since the flux is defined as the number of photons received per area per interval of time, the differential photon flux is given by

$$\frac{d\Phi}{d\omega} = \left(\sum_i \frac{B_i}{16\pi M^2} \frac{d\langle \sigma v_r \rangle_i^\gamma}{d\omega} \right) \int_{\Delta\Omega} \int_{l.o.s} \rho^2(r(s,\theta)) ds d\Omega. \tag{6.6}$$

The term in the parentheses in Eq.(6.6) contains all the information regarding the dark matter interactions that pertain the model, whereas the integral contains the details of the dark matter content of the area of interest for the observation window defined by the solid angle $\Delta\Omega$, also known as *J-factor*

$$J(\Delta\Omega) = \int_{\Delta\Omega} \int_{l.o.s} \rho^2(r(s,\theta)) ds d\Omega. \tag{6.7}$$

The dark matter distribution in the Milky Way, described by the density $\rho(r)$, has not yet been determined, so multiple propositions have been made in order to describe the cosmological observations. There are different functions that are usually employed, the most traditional being the Navarro-Frenk-White (NFW) profile [130], with a functional form motivated by cosmological N-body simulations. Among other frequently used functions are the Einasto profile [131], considered a better fit to recent numerical simulations [132, 133], and proposals motivated by galactic rotation curve observations such

as the Burkert [134] and Isothermal [135] profiles, which in turn are inconsistent with numerical simulations[136]. In addition, the NFW profile can be considered a specific case of a general family of profile models in a function that introduces an additional parameter γ [137], referred to as generalized NFW profile. It is important to note that here we are not accounting for galactic substructures in DM halos, which have been demostrated to contain great amounts of subhalos by high-resolution N-body simulations [138]. The substructure problem is an active field of research, and by not adding this into our calculations we are making strong assumptions. However, for the purposes of simplifying the calculation, we take the dark matter profiles mentioned as good approximation. The profiles mentioned above can be written as

$$\begin{aligned}
\text{NFW} : \rho_{NFW} &= \rho_s \frac{r_s}{r}\left(1+\frac{r}{r_s}\right)^{-2} \\
\text{Einasto} : \rho_{Ein} &= \rho_s Exp\Big\{-\frac{2}{\alpha}\Big[\Big(\frac{r}{r_s}\Big)^{\alpha}-1\Big]\Big\} \\
\text{Burkert} : \rho_{Bur} &= \frac{\rho_s}{(1+r/r_s)(1+(r/r_s)^2)} \\
\text{Isothermal} : \rho_{Iso} &= \frac{\rho_s}{1+(r/r_s)^2} \\
\text{Generalized NFW} : \rho_{gNFW} &= \rho_s \frac{r_s^3}{r^{\gamma}(r+r_s)^{3-\gamma}},
\end{aligned} \tag{6.8}$$

where α and γ are free parameters, the scale radius $r_s = 20kpc$ and ρ_s is determined in such a way that the dark matter density at the location of the Sun ($r = r_{\odot}$) is $\rho_{\odot} = 0.4\ \text{GeV}/cm^3 = 1.0536 \times 10^{-2} M_{\odot}(pc)^{-3}$. Our choice for r_s and $\rho_{\odot}$ are made to coincide with the studies by the FermiLAT collaboration [112] for the purposes of comparison, but they can vary for different conventions. For example, direct detection experiments use $\rho_{\odot} = 0.3\ \text{GeV}/cm^3 = 7.9020 \times 10^{-3} M_{\odot}(pc)^{-3}$.

We opt to use the generalized Navarro-Frenk-White (gNFW) dark matter profile with $\gamma = 1.25$ for the slope of the inner part of the profile, and the corresponding scale density to fit the value of $\rho_{\odot}$ is $\rho_s = 0.225\ GeV/cm^3 = 5.9265 \times 10^{-3} M_{\odot}(pc)^{-3}$. We chose this value of γ in order to properly compare with the analysis done in Ref. [112], where this specific value is used. The region of interest is a disk around the Galactic Center with an aperture $|l| < 10$ and $2 < |b| < 10$ for one quadrant, where l and b are the longitude and latitude in the galactic coordinate system, respectively. This means we are observing a 20×20 aperture from the center of the Galaxy with a 2 mask right in the center, which is the region studied in Ref. [112]. The purpose of this mask is to avoid the bright sources around a small region of the center of the galaxy. The aperture of the region of interest is related to the angle θ by $cos\theta = cosb\ cosl$. For these parameters, the J-factor in Eq. (6.7) yields $J_0 = 7.118 \times 10^5 GeV^4/cm^2 seg = 6.097 \times 10^{22} GeV^2 cm^{-5}$. This is the value we will

use to calculate the photon flux in the galactic center.

The prompt gamma-ray flux produced in the Galactic Center by the annihilation of dark matter into $\bar{q}q, \bar{c}c, \bar{b}b, e^+e^-, \mu^+\mu^-, \tau^+\tau^-, W^+W^-, ZZ, hh, gg$ was fitted to the FermiLAT data in Ref. [124]. Here, $\bar{q}q$ refers to the sum of the contributions of light quarks (u, d and s). In Ref. [124], the dark matter mass (M) and the cross section are treated as free parameters. Their conclusion was that the gamma-ray excess can be explained by these processes, except for the e^+e^- channel, for a dark matter mass in the range $5 - 174\ GeV$, depending on the specific channel, for a corresponding cross section of the order of the thermal cross section $\langle \sigma v_r \rangle \approx 10^{-26} cm^3/seg$. Annihilation of dark matter into fermionic states, $\bar{D}D \to \bar{f}f$ with $f = \mu, \tau, q, c, b$, turned out to yield a good fit to the GRE data for masses in the $9 - 61\ GeV$ range.

There is also another possibility that the GRE can be explained by production of gamma rays as secondary product from Inverse Compton Scattering (ICS). Here, electron and muon pairs produced in dark matter annihilation propagate over the Galactic Center and scatter photons coming from the Cosmic Microwave Background and from starlight [123]. For the electron channel, e^+e^-, a large cross section $\langle \sigma v_r \rangle_e$ is needed to account for the GRE, but it turns out to be severely constrained by the positron fraction data from the AMS Collaboration [139, 140]. However, as it was found in Ref. [124], the muon channel can yield sizable contributions that can explain the GRE in addition to the prompt photon production for a mass around $M \approx 61\ GeV$, for cross section values of the order of the thermal cross section. Tau pairs decay too quickly for this effect to happen.

Tensor Dark Matter can annihilate directly into $\gamma\gamma$, γZ and γH, producing sharp line spectra. However, in order to explain the GRE observed by FermiLAT [112], we need to account for the broad form of the spectrum. In the following, we will present and calculate the contributions of TDM annihilation to the photon flux in the Galactic Center, including contributions from prompt photons and secondary emission from Inverse Compton Scattering.

6.1.1 Prompt photon production from Tensor Dark Matter annihilation into fermions

First we will consider TDM annihilation into final states that contain at least one photon. These can occur in three forms: initial state radiation, internal bremsstrahlung (or internal radiation) and final state radiation. The simplest case are transitions of two-body processes, $\bar{D}D \to \gamma R$ with $R = \gamma, Z^0$ whose amplitudes are $\mathcal{O}(g_t^2)$, or with $R = H$ which is $\mathcal{O}(g_t g_s, g_t g_p)$. Additionally, considering non-perturbative QCD corrections in

general R in these processes can convert to quarkonium states resonances $\bar{Q}Q[^{2S+1}L_J]$ producing also γ-quarkonium final two body states.

The photons produced by these processes have energy spectra centered at $\omega = M(1 - \frac{M_R^2}{4M^2})$, with a width related to the width of the resonance of R. If we then consider the decay of R into two particles, these contributions become a three-body final state process that produces a continuous photon spectrum when R is off-shell. We refer to this as initial state radiation.

For three-body processes, it is also possible that the TDM annihilates into a pair of particle-antiparticle with the subsequent emission of a photon, this is final state radiation.

In addition, we can have a process where the exchanged particle R decays into another particle emitting a photon, with a subsequent decay into a particle-antiparticle pair, which we call internal radiation or internal bremsstrahlung. The diagrams for the processes mentioned are shown in Fig. 6.1.

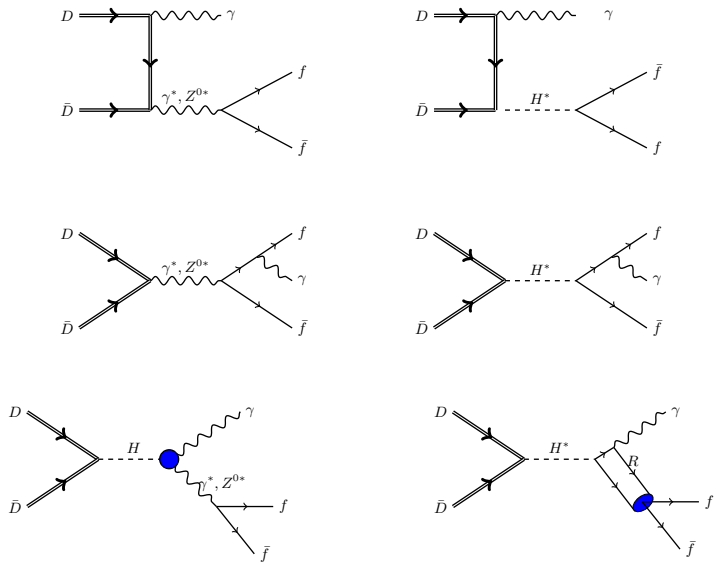

FIGURE 6.1: Annihilation of TDM into final states containing one photon. The first two correspond to initial state radiation, followed by two diagrams for the final state radiation, and finally the last two are for the internal radiation or internal bremsstrahlung.

Initial state radiation

Initial state radiation is induced at tree level by the first two diagrams in Fig. 6.1. Initial state radiation can produce spectra with shape similar to the GRE, provided there are resonant effects involved in the process. In this case the resonant effects translates into

wider peaks in the photon spectrum (see Ref. [141] for these effects in colliders at low energies). The first diagram in Fig. 6.1 (γ and Z exchange) provides contributions of order $\mathcal{O}(v_r^2)$, so the initial state radiation is dominated by Higgs exchange, the second diagram. The amplitude for this process (see the corresponding diagram in Fig. 6.2), can be written as

$$\mathcal{M}(p_1, p_2\,; k, p_3, p_4) = \mathcal{M}_\gamma[\bar{D}(p_1)D(p_2) \to \gamma(k)H^*(q)]\frac{i}{q^2 - M_H^2 + iM_H\Gamma_H}\mathcal{M}_H[H^*(q) \to \bar{f}(p_3)f(p_4)], \tag{6.9}$$

where $q = p_3 + p_4$. The cross section is calculated as follows

$$d\sigma = \frac{(2\pi)^4|\mathcal{M}|^2}{4\sqrt{(p_1\cdot p_2)^2 - M^4}}\delta^4(p_1 + p_2 - k - p_3 - p_4)\frac{d^3k}{(2\pi)^3 2\omega}\frac{d^3p_3}{(2\pi)^3 2E_3}\frac{d^3p_4}{(2\pi)^3 2E_4} \tag{6.10}$$

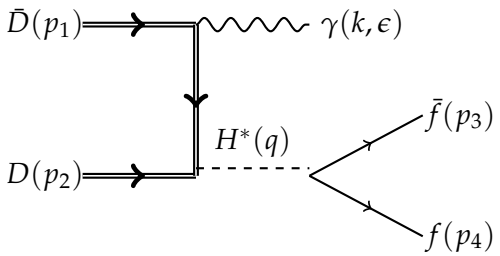

FIGURE 6.2: Diagram for the initial state radiation with a Higgs boson exchange for TDM annihilation.

.

Integrating out p_4 using $\frac{d^3p_4}{2E_4} = d^4p_4\delta(p_4^2 - m_4^2)\Theta(E_4)$, we obtain

$$d\sigma = \frac{1}{(2\pi)^5}\frac{|\mathcal{M}|^2}{4\sqrt{(p_1\cdot p_2)^2 - M^4}}\delta\Big((p_1 + p_2 - k - p_3)^2 - m_4^2\Big)\frac{d^3k}{2\omega}\frac{d^3p_3}{2E_3}. \tag{6.11}$$

In the Center of Mass System (CMS), we have $p_1 + p_2 = (\sqrt{s}, 0)$. The term inside the delta is

$$\begin{aligned}(p_1 + p_2 - k - p_3)^2 - m_4^2 &= s + m_3^2 - 2\sqrt{s}\omega + 2k\cdot p_3 - 2\sqrt{s}E_3 - m_4^2 \\ &= s - 2\sqrt{s}(E_3 + \omega) + 2E_3\omega(1 - \beta cos\theta),\end{aligned} \tag{6.12}$$

where we consider $m_3 = m_4 = m_f$ and $k\cdot p_3 = E_3\omega - E_3\omega\beta cos\theta$. The delta term can then be written as

$$\delta\Big((p_1 + p_2 - k - p_3)^2 - m_4^2\Big) = \frac{1}{2\omega|p_3|}\delta\Big(cos\theta - \frac{s + 2E_3\omega - 2\sqrt{s}(E_3 + \omega)}{2\omega|p_3|}\Big). \tag{6.13}$$

Integrating $cos\theta$ and ϕ_γ using $\frac{d^3p_3}{2E_3}\frac{d^3k}{2\omega} = \frac{1}{4}\omega|p_3|d\omega dE_3 d(cos\theta_\gamma)d\phi_\gamma d(cos\theta)d\phi_f$, we have

$$d\sigma = \frac{1}{(2\pi)^4}\frac{|\mathcal{M}|^2}{32\sqrt{(p_1\cdot p_2)^2 - M^4}}d\omega dE_3 d\phi_f d(cos\theta_\gamma). \tag{6.14}$$

Recall that $4\sqrt{(p_1\cdot p_2)^2 - M^4} = 2(s-2M^2)v$. Thus,

$$\frac{d\sigma v}{d\omega(cos\theta_\gamma)} = \frac{1}{(2\pi)^4}\frac{|\mathcal{M}|^2}{16(s-2M^2)}dE_3 d\phi_f. \tag{6.15}$$

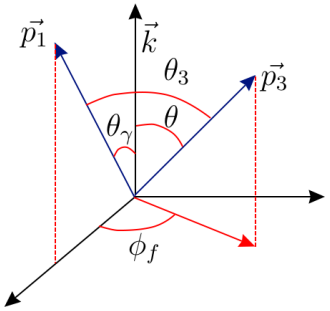

FIGURE 6.3: Scheme of the coordinates for the $\bar{D}(p_1)D(p_2) \to \gamma(k)H^*(q)$ process.

We denote θ_3, θ_γ and θ as the angles between $\vec{p_1}\angle\vec{p_3}$, $\vec{k}\angle\vec{p_1}$ and $\vec{k}\angle\vec{p_3}$, respectively. ϕ_f is the angle formed between the proyection of $\vec{p_1}$ and the proyection of $\vec{p_3}$ on the normal plane of $\vec{k}$. From geometry we know that

$$cos\theta_3 = cos\theta cos\theta_\gamma + sin\theta sin\theta_\gamma cos\phi_f. \tag{6.16}$$

And from the delta function in Eq. 6.13,

$$cos\theta = \frac{s + 2E_3\omega - 2\sqrt{s}(E_3+\omega)}{2\omega\sqrt{E_3^2 - m_f^2}}. \tag{6.17}$$

Additionally, we have the following products

$$\begin{aligned}
&p_1\cdot p_1 = p_2\cdot p_2 = M^2\,; \quad k\cdot k = 0\,; && p_3\cdot p_3 = p_4\cdot p_4 = m_f^2\\
&p_1\cdot p_2 = \frac{1}{2}(s-2M^2)\,; && k\cdot p_1 = \frac{\sqrt{s}}{2}\omega(1-\beta cos\theta_\gamma)\\
&p_1\cdot p_3 = \frac{\sqrt{s}}{2}(E_3 - \beta\sqrt{E_3^2-m_f^2}cos\theta_3)\,; && k\cdot p_2 = \frac{\sqrt{s}}{2}\omega(1+\beta cos\theta_\gamma)\\
&p_2\cdot p_3 = \frac{\sqrt{s}}{2}(E_3 + \beta\sqrt{E_3^2-m_f^2}cos\theta_3)\,; && k\cdot p_3 = \omega(E_3 - \sqrt{E_3^2-m_f^2}cos\theta).
\end{aligned} \tag{6.18}$$

To integrate over ϕ_f, we need the explicit form of $|\mathcal{M}|^2$. However, to integrate over E_3 we need to find the minimum and maximum value allowed kinematically by Eq. 6.17. Working in the CMS of $p_1 + p_2$, we have the constraint $\vec{k} + \vec{p_3} + \vec{p_4} = 0$. Then, the minimum value of $q^2 = (p_3 + p_4)^2$ is $4m_f^2$, which is obtained when $p_3 \cdot p_4 = m_f^2$, which means $\vec{p_3} = \vec{p_4} = -\frac{1}{2}\vec{k}$. Thus, the minimum happens when $cos\theta = -1$. Similarly q^2 will be at its maximum value when $\vec{p_3} = -\vec{p_4}$, that is to say, when $cos\theta = 0$. We then find the maximum and minimum values of E_3 by solving the constraint in Eq. 6.17 with $\theta = 0, \pi$, which means solving the following

$$s - 2\sqrt{s}\omega - 2(\sqrt{s} - \omega)E_3 = \pm 2\omega\sqrt{E_3^2 - m_f^2}. \tag{6.19}$$

By squaring both sides of the equation, we can find the minimum (E_3^-) and maximum (E_3^+) values of E_3.

$$E_3^{\pm} = \frac{1}{2}(\sqrt{s} - \omega) \pm \frac{\omega}{2}\sqrt{1 - \frac{4m_f^2}{s - 2\sqrt{s}\omega}}. \tag{6.20}$$

In the non-relativistic limit, $s \approx 4M^2$, and

$$E_3^{\pm} = M - \frac{\omega}{2} \pm \frac{\omega}{2}\sqrt{1 - \frac{m_f^2}{M(M - \omega)}}. \tag{6.21}$$

Except for the top quark, we have that $M^2 >> m_f^2$, thus

$$M - \omega \lesssim E_3 \lesssim M. \tag{6.22}$$

Therefore, under these considerations, the allowed values for ω are $\omega < M$. The squared amplitude for this process, in the non-relativistic limit ($\beta \to 0$), in terms of the coupling constants g_t, g_p and g_s is

$$\begin{aligned}
|M|^2 = &-\frac{4\cos^2\theta_W g_t^2 m_f^2}{9M^8}(-c_\theta\omega\sqrt{E_3^2 - m_f^2} + E_3(\omega - \sqrt{s}) + 2m_f^2) \\
&\times \Big(g_p^2(-24M^6 + 2M^4(s - 8\sqrt{s}\omega) + M^2 s(4\sqrt{s}\omega + s - 15\omega^2) + 6s^2\omega^2) \\
&+ g_s^2(-8M^6 + 2M^4(s - 4\sqrt{s}\omega) + M^2 s(4\sqrt{s}\omega + s - 23\omega^2) + 6s^2\omega^2)\Big) \\
&/\Big(4E_3^2((c_\theta^2 + 1)\omega^2 - 2\sqrt{s}\omega + 2) - 4c_\theta^2 m_f^2\omega^2 + M_H^2(\Gamma_H^2 - 4c_\theta\omega\sqrt{E_3^2 - m_f^2} - 4E_3\sqrt{s} + 4E_3\omega) \\
&+ 8c_\theta E_3\omega\sqrt{E_3^2 - m_f^2}(\sqrt{s} - \omega) + M_H^4\Big),
\end{aligned}$$

where $c\theta = cos\theta$, $c_\gamma = cos\theta_\gamma$ and $c_W = cos\theta_W$. We use this expression to calculate

$\frac{d\sigma v}{d\omega dcos\theta_\gamma}$ using Eq. 6.15, including the factor N_c to account for color number, in the non-relativistic limit, when $s \approx 4M^2$ and $\beta \approx 0$,

$$\frac{d\sigma v_{isr}}{d\omega dc_\gamma} = \frac{N_c cos^2\theta_W g_t^2 m_f^2 \omega}{9(2\pi)^3 M^6}(M^2 - M\omega - m_f^2)\sqrt{1+\frac{m_f^2}{M(\omega - M)}}\frac{9g_p^2\omega^2 + g_s^2(\omega+2M)^2}{\left(4M(M-\omega) - M_H^2\right)^2 + \Gamma_H^2 M_H^2}.$$

The differential cross section, integrating over θ_γ, is

$$\frac{d\langle\sigma v_r\rangle_{isr}}{d\omega} = \sum_f \frac{N_c \cos^2\theta_W g_t^2 m_f^2 \omega(M-\omega)\left(1-\frac{m_f^2}{M(M-\omega)}\right)^{3/2}}{72\pi^3 M^5} \times \frac{9g_p^2\omega^2 + g_s^2(2M+\omega)^2}{\left(4M(M-\omega) - M_H^2\right)^2 + \Gamma_H^2 M_H^2}, \tag{6.23}$$

where the sum runs over all kinematically allowed SM fermions. As expected, for $M > M_H/2$ the photon spectrum has a bump at energies corresponding to di-fermion invariant mass close to the Higgs resonance. The location of this bump depends on the dark matter mass. For $M = 64\ GeV$ it coincides with the GRE bump at $3\ GeV$. However, this is a contribution of the order $\mathcal{O}(g_t^2 g_s^2)$. Recall that in the previous section, we found that the coupling g_t is severely constrained to $g_t \leq 2\times 10^{-4}$ by the XENON1T results on direct detection for a TDM mass of the order of 100 GeV, which makes the initial state radiation very small compared with the GRE data.

Final state radiation

Prompt photons can be also emitted by the final fermions in the reaction $\bar{D}D \to \bar{f}f\gamma$. These contributions are given by the next two diagrams in Fig. 6.1. The γ and Z exchange and the Higgs exchange with pseudoscalar coupling g_p are $\mathcal{O}(v_r^2)$, so the leading contributions are given by the diagrams with the Higgs exchange and scalar coupling. The cross section is obtained in a similar way as before, with the appropriate changes in the invariant amplitude, which is

$$-i\mathcal{M}_{H-f} = \frac{Q_f m_f}{s - M_H^2 + i\Gamma_H M_H}\bar{u}(p_3)\, i\left[\frac{\gamma^\mu(\not{p}_3 + \not{k} + m_f)}{(p_3+k)^2 - m_f^2} - \frac{(\not{p}_4 + \not{k} - m_f)\gamma^\mu}{(p_4+k)^2 - m_f^2}\right]\varepsilon_\mu(k)\, v(p_4) \times \bar{V}(p_2)\left(g_s + ig_p\chi\right)U(p_1). \tag{6.24}$$

Following a similar procedure, we obtain the following differential averaged cross section

$$\frac{d\langle\sigma v_r\rangle_{fsr}}{d\omega} = \sum_f \frac{N_c \alpha Q_f^2 g_s^2 m_f^2}{6\pi^2 M^4 \omega \left(\left(4M^2 - M_H^2\right)^2 + \Gamma_H^2 M_H^2\right)}$$
$$\left[\left[2M^3(M-\omega) + M^2\left(\omega^2 - 3m_f^2\right) + 2Mm_f^2\omega + m_f^4\right] ArcTanh\sqrt{1 - \frac{m_f^2}{M(M-\omega)}}\right.$$
$$\left. - M(M^2 - m_f^2)(M-\omega)\sqrt{1 - \frac{m_f^2}{M(M-\omega)}}\right]. \tag{6.25}$$

The corresponding differential photon flux as a function of the dark matter mass is shown in Fig.6.4 . These contributions are also resonant, and these effects occur at

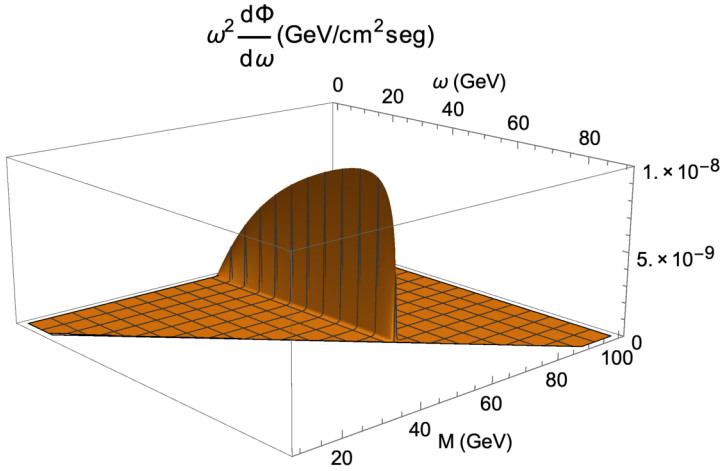

FIGURE 6.4: Differential photon flux for final state radiation as a function of ω, M for $g_s = 5 \times 10^{-3}$.

$$s = (p_1 + p_2)^2 = 4M^2\left(1 + \frac{v_r^2}{4} + \mathcal{O}(v_r^4)\right)^2 = M_H^2. \tag{6.26}$$

We can see from the plot in Fig. 6.4 that the results for $\omega^2 d\Phi/d\omega$ of the order of the GRE are obtained only for Higgs exchange in the resonance region. Since dark matter is non-relativistic, this requires $M \approx M_H/2$.

Photons emitted directly by the fermion produced in TDM annihilation is only one of many processes that yield prompt photons. For $f = \mu, \tau, q, c, b$ there are additional prompt photons produced by the decay products in the case of leptons or by the jet of particles produced in the hadronization of quarks. These effects modify our results in Eq. (6.25) substantially for all fermions except for $f = e, \mu$, which do not have hadronic

decays and receive only modifications from suppressed higher order electroweak radiative corrections.

With the tabulated spectrum defined as provided by DARKSUSY [100] and PPC4DMID [142], we can calculate the complete prompt photon flux for $f = e, \mu, \tau, q, c, b$ including radiative corrections [143]. We verified the consistency of results using both packages and use the spectrum given by the direct photon emission by electrons and muons in Eq.(6.25) to cross-check results. A comparison between this and our results is shown in Fig. 6.5. Indeed, the spectrum suffers a substantial change for $f = \tau, q, c, b$, while for e and μ, there are no significant changes.

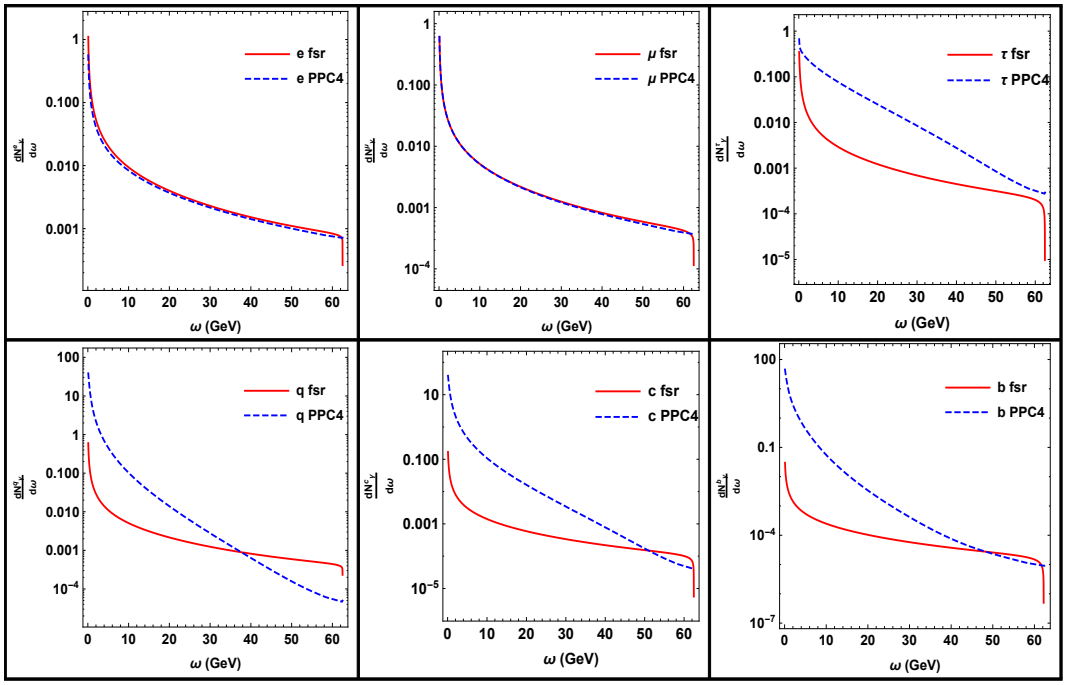

FIGURE 6.5: Comparison of the tree level result in Eq. (6.25) for $\frac{dN_\gamma^f}{d\omega}$ versus the results using PPC4DMID tabulated spectrum, for leptons and quarks, as a function of ω for $M = 62.5\ GeV$.

Internal Bremsstrahlung

The internal state radiation is given by the last two diagrams of Fig. 6.1. The first of these diagrams involve the $H \to \gamma\gamma$ and $H \to Z\gamma$ transitions which takes place at one-loop level in the standard model, which were discussed in Chapter 4 (see Eq. (4.55), for

example). For the sequential decay with γ and Z^0 intermediate states we obtain

$$\frac{\langle d\sigma v_r\rangle_{Z^*}}{d\omega} = \sum_f \frac{N_c g_{Z\gamma}^2 g_s^2 \omega^3 M_Z^2 \sqrt{1-\frac{m_f^2}{M(M-\omega)}}}{36\pi^3 M_H^2\left(\left(4M^2-M_H^2\right)^2+\Gamma_H^2 M_H^2\right)} \times \frac{2(A_f^2+B_f^2)M(M-\omega)+(A_f^2-2B_f^2)m_f^2}{\left(\left(4M(M-\omega)-M_Z^2\right)^2+M_Z^2\Gamma_Z^2\right)}, \tag{6.27}$$

$$\frac{\langle d\sigma v_r\rangle_{\gamma^*}}{d\omega} = \sum_f \frac{N_c \alpha g_{\gamma\gamma}^2 g_s^2 v^2}{36\pi^2 M_H^2\left(\left(4M^2-M_H^2\right)^2+\Gamma_H^2 M_H^2\right)} \times \frac{\omega^3\left(2M(M-\omega)+m_f^2\right)\sqrt{1-\frac{m_f^2}{M(M-\omega)}}}{M^2(M-\omega)^2}. \tag{6.28}$$

There is also an enhancement at the Higgs resonance in these processes and a double-resonant effect in the case of the Z^* intermediate state. The last diagram in Fig. 6.1 involves non-perturbative QCD effects. We calculated these contributions using the Non-Relativistic QCD effective field theory finding them negligible even at the Higgs resonance. There are also contributions with the sequential decays $\bar{D}D \to \gamma*, Z^{0*} \to \gamma H \to \gamma\bar{f}f$ not shown in Fig. 6.1 which are not resonant and are also very small.

Our results for the internal radiation are shown in Fig. 6.6. Sizable contributions to the differential photon flux from $H \to \gamma Z^*$ transition are produced mainly at the Z^0 resonance i.e. for photon energies around $\omega = \frac{M_H}{2}(1-\frac{M_H^2}{M_Z^2}) \approx 30\ GeV$. The $H \to \gamma\gamma^*$ intermediate state contributes only at the upper end of the spectrum.

The most important contributions come from the b channel followed by the c and τ which become competitive at high photon energies. Prompt photon flux from electrons muons and light quarks turn out to be negligible.

6.1.2 Delayed emission: Inverse Compton Scattering contributions

There are at least three different contributions from the delayed photon emission by ICS of propagating fermions produced in the annihilation of TDM.

- **Propagation of electrons produced in $\bar{D}D \to e^+e^-$.** Overall negligible contribution. The Higgs portal part has a small coupling ($g_{Hee} = m_e/v$), and for the spin portal case, since it is proportional to g_t, is heavily constrained from direct detection limits.

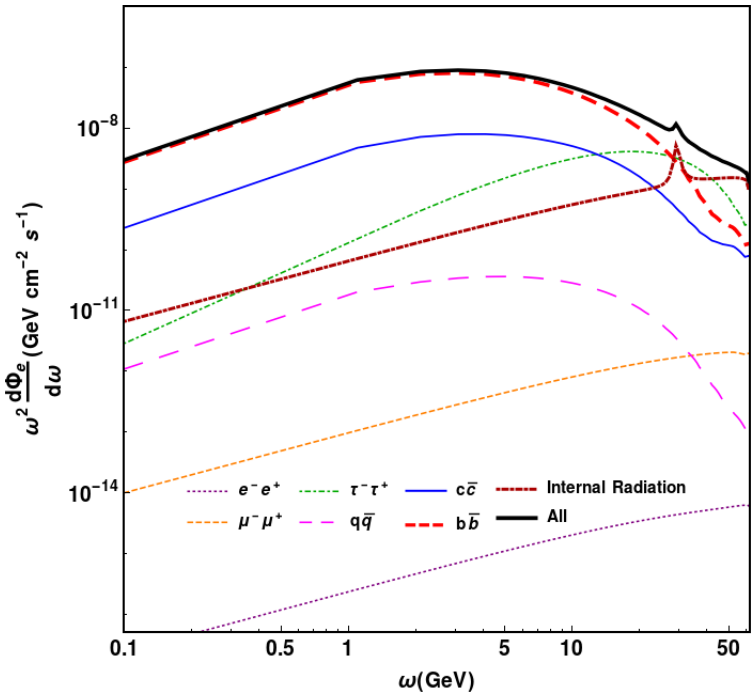

FIGURE 6.6: Differential flux for prompt photons from the annihilation of TDM into fermions for $M = 62.49\ GeV$ and $g_s = 10^{-3}$. We use $M_H = 125.09\ GeV$ in the computation of these contributions.

- **Propagation of muons produced in $\bar{D}D \to \mu^+\mu^-$.** Shown in [124] to yield sizable contributions when the cross section of dark matter annihilation into muons, $\langle \sigma v_r \rangle_\mu$, is of the order of the thermal cross section.
- **Propagation of electrons produced in decay of leptons or hadronization of quarks, produced in $\bar{D}D \to \bar{f}f$ with $f = \mu, \tau, q, c, b$.**

The tabulated electron spectrum and models of propagation provided by the package PPC4DMID [142, 144] allows us to obtain the ICS of photons from the CMB or starlight by electrons produced in decays of heavy leptons and hadronization of quarks. The photon flux from this phenomena is shown in Fig 6.7. It is important to note that these contributions are calculated with the NFW[130] density profile since the PPC4DMID tabulated spectrum is designed only for a number of DM profiles that do not include the gNFW. These contributions, however, are not very sensitive to the density profile, so our results are quite similar using the Moore [145] or Einasto B [131, 142] profiles included in the PPC4DMID setup, profiles that are very similar to the gNFW used in the previously shown computation of prompt photons.

As it was for prompt photons, the b channel is also dominant, with subdominant contributions of the c and τ channels. Light quarks, with electrons and muons yield negligible

contributions. We remark that for both prompt and delayed emission, these contributions increase the further we go into the resonance region, with the results being highly sensible to the specific value of the TDM mass.

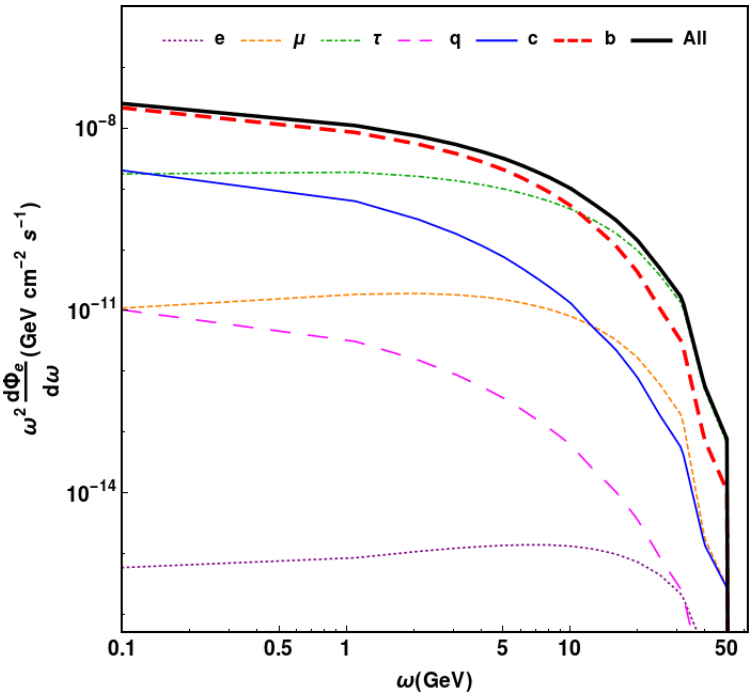

FIGURE 6.7: Differential flux of delayed photons produced in the ICS of electrons off CMB and starlight, for secondary electrons produced in the decay of heavier leptons or hadronization of quarks coming from the annihilation of TDM, for $M = 62.49\ GeV$ and $g_s = 10^{-3}$. We use $M_H = 125.09\ GeV$ in the computation of these contributions.

The contribution from propagation of muons was shown to be important in Ref. [124], however in this case, for the TDM mass window required by the GRE data when including all the contributions, the cross section $\langle \sigma v_r \rangle_\mu$ is about three orders of magnitude below the thermal cross section, thus the corresponding flux turns out to be very small.

6.1.3 Final results for the Gamma-Ray Excess in the Galactic Center

The photon flux from all the contributions mentioned above for tensor dark matter annihilation in the Galactic Center is shown in Fig. 6.8. These results depend on the TDM mass M and the interaction couplings g_s, g_p, g_t, however we have shown that the spin portal (g_t) and pseudoscalar (g_p) couplings yield contributions that are negligible for the photon flux, and only the parity-conserving Higgs-TDM interaction is important for this purpose.

Prompt and delayed photons are of similar importance for the overall photon flux, but prompt photons are dominant for energies bigger than 0.3 GeV. For both cases, the

main source of photons comes from $\bar{D}D \to \bar{b}b$ annihilation, followed by the $\tau^+\tau^-$ and $\bar{c}c$ channels. For prompt photons, the final state radiation dominates the photon production, and internal radiation yields sizable contributions only at the upper end of the spectrum.

The shadowed band shown in Fig.6.8 is a result of the study of the uncertainties of the GRE data obtained in Ref. [112]. Considering these uncertainties, we conclude that for $g_s \in [0.98, 1.01] \times 10^{-3}$ and $M \in [62.470, 62.505]\ GeV$, tensor dark matter annihilation yields a photon flux consistent with GRE data. These is a sharp set of values that provides definite predictions for other observables that we must test against available dark matter constraints. In the following sections we will work out the corresponding observables for other limits from indirect detection experiments.

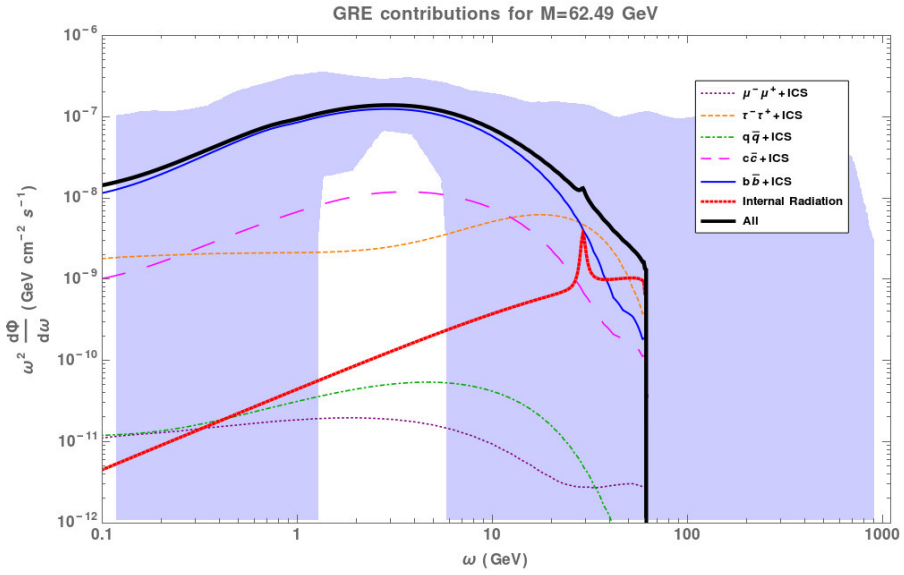

FIGURE 6.8: Differential flux as a function of ω including all the contributions discussed in this paper, for $M = 62.49$ GeV and $g_s = 9.81 \times 10^{-4}$. The shadowed band is a result of the study of the uncertainties of the GRE data obtained in Ref. [112].

6.2 Annihilation into $\mu^+\mu^-$, $\tau^+\tau^-$ and $\bar{b}b$

High precision measurements of the cosmic ray positron fraction from the AMS (Alpha Magnetic Spectrometer) collaboration [140] shows a rise at energies above 10 GeV which cannot be explained with current astronomical models. This data is used in Ref. [139] to put stringent limits on dark matter annihilation into μ pairs. The upper limit of the cross section of this process, for $M = 62.5\ GeV$ is $\langle \sigma v_r \rangle_\mu \leq 8.96 \times 10^{-26} cm^3/seg$, value that remains consistent along the Higgs resonance region. For TDM, the largest values of this cross section compatible with the values consistent with GRE data, found in the

previous section, corresponds to a mass $M = 62.505\ GeV$, for which the measured relic density requires $g_s = 9.81 \times 10^{-4}$ (see Chapter 4). The TDM prediction with these values yields $\langle \sigma v_r \rangle_\mu \leq 8.30 \times 10^{-30} cm^3/seg$, which is well below the experimental upper bound set in [139].

Another important and well-known source of data for indirect detection of dark matter are the dwarf spheroidal satellite galaxies of the Milky Way (dSphs). These are dark matter-dominated objects [146–148] which are believed to be part of a subset of Galactic DM overdensities, called subhalos, predicted by N-body cosmological simulations [149, 150]. Due to their proximity and high content of dark matter, dSphs are exceptional targets for indirect detection experiments. The Fermi-LAT, in collaboration with the Dark Energy Survey (DES), use data from 45 stellar systems, 28 of which are confirmed to be dSphs, to obtain bounds on the cross sections of dark matter annihilation into $\bar{b}b$ and $\tau^+\tau^-$ [52].

For the τ channel the upper limit obtained with this data, for $M = 62.5\ GeV$, is $\langle \sigma v_r \rangle_\tau \leq 1.2 \times 10^{-26} cm^3/seg$, which in our formalism of the largest value compatible with the GRE data yields $\langle \sigma v_r \rangle_\tau = 2.42 \times 10^{-27}\ cm^3/s$, thus perfectly consistent with the experimental upper bound.

However, in the case of the b channel we must perform a closer analysis, since our results are closer to the upper bounds. In Fig. 6.9 we plot the expected limit and the 95% containment region obtained in [52] in comparison to our results for $\frac{1}{2}\langle \sigma v_r \rangle_{\bar{b}b}$ (there is a $\frac{1}{2}$ factor due to the fact that the upper bounds are obtained for self-conjugated dark matter, unlike TDM). In a straight-forward comparison with these limits, TDM annihilation into $\bar{b}b$ is consistent with the 95% containment band for the values of mass compatible with the GRE, and below the median expected limit for a narrower mass interval $M \in [62.470, 62.480]\ GeV$. Regardless, it is important to analyze this compatibility in detail in light of the results of this work, since this mass and cross-section intervals present a promising place to look for signals of TDM. Additionally, it is important to note in this concern that the Higgs has a very narrow resonance ($\Gamma_H/M_H = 3.2 \times 10^{-5}$), its energy resolution is not easy and even in collider experiments it is still a pending task, so a deeper analysis is more than justified.

The upper bounds obtained in Ref. [52] are the result of a combined analysis of the energy flux from 45 stellar objects of which 28 are confirmed dSphs. Only 19 of these have an experimentally derived J-factor, making use of data from stellar-kinematic data in Ref. [151], where they also obtain the uncertainty of the corresponding J-factor taking into account systematic errors due to finite data and uncertainties regarding the shape of the DM density profiles. For the rest of the targets it is estimated from empirical relations between the flux and the inverse square of the distance satisfied by the dSphs.

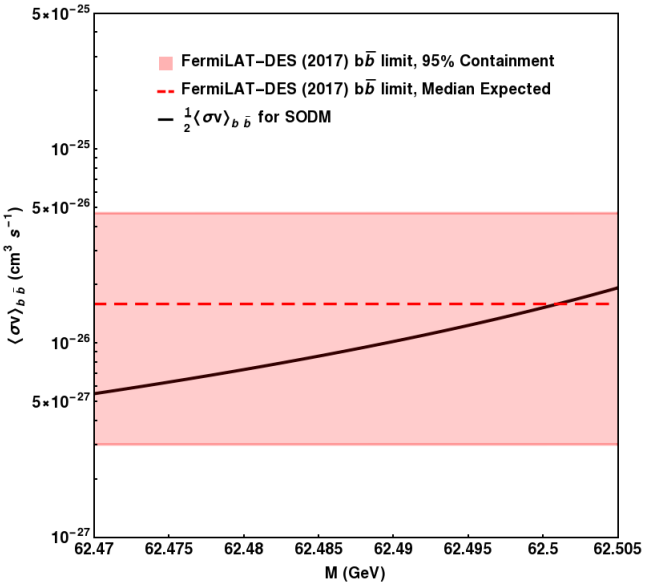

FIGURE 6.9: Cross sections for the annihilation of TDM into $\bar{b}b$ for the mass values compatible with the GRE data (solid line) and $g_s = 9.81 \times 10^{-4}\ GeV$. The dashed line corresponds to the Median Expected limit and the shadowed band to the 95% containment region obtained in [52].

The study done by the FermiLAT-DES collaboration performs a likelihood analysis of the photon energy flux data, considering 24 logarithmically spaced energy bins in the energy interval from 500 MeV to 500 GeV (the likelihood function data is provided in the supplementary material of Ref. [52]). Then, the 95% confidence level upper bounds for the bin-by-bin photon flux excess is calculated employing the formalism described in Ref. [152]. The upper bounds on the photon flux excess for each target can then be used to obtain limits on the dark matter annihilation cross section for the b channel, $\langle\sigma v_r\rangle_{\bar{b}b}$, for a given mass M using the standard model results for the photon spectrum from b quarks. A combined likelihood analysis of these results yields the plot in Fig. 9 in Ref. [52].

Our aim is to make a direct comparison of our result with the experimental data for each target. We first reproduce the bin-by-bin upper bound of the photon flux excess using the likelihood function data at the 95% confidence level provided in the supplementary material of [52], but keeping only the 19 targets with an experimentally determined J-factor. The data from FermiLAT indicates a upper limit on the net flux of each target, and the likelihood function they provide includes the considerations of the background signals. We then make use of the package DarkSUSY [1] [100, 153] to calculate the photon energy flux for b-quarks, produced from TDM annihilation. The package yields the photon spectrum at a given energy from propagation and hadronization of the b-quarks,

[1] J. Edsjö, T. Bringmann, P. Gondolo, P. Ullio, L. Bergström, M. Schelke, E.A. Baltz and G. Duda, http://www.darksusy.org.

and takes as input the values of the mass M, the cross section $\langle \sigma v_r \rangle_{\bar{b}b}$ and the J-factor for the considered target. We extrapolate these points to obtain the photon energy flux as a function of the photon energy. In Fig. 6.10 we show the photon energy flux for $M = 62.505$ and $g_s = 9.81 \times 10^{-4}$, which yields the highest value of $\langle \sigma v_r \rangle_{\bar{b}b}$ that is consistent with GRE, compared with the upper bound including the uncertainties in the measured J-factor (white band) and the likelihood function data (color points) for each of the 19 chosen targets. The photon energy flux from TDM annihilation into b-quark pairs, for each target, turns out to be smaller than the limits obtained using the bin-by-bin likelihood functions provided by FermiLAT-DES in the supplementary material of Ref. [52]. This conclusion remains when considering the rest of the targets.

6.3 Tensor dark matter annihilation into two photons.

The FermiLAT [154] and the High Energy Stereoscopic System (H.E.S.S.) [155] have searched for a monoenergetic spectral line from self-annihilations of DM in the central region of the Milky Way halo in order to derive stringent upper limits on the cross section of DM annihilating into gamma pairs, $\langle \sigma v_r \rangle_{\gamma\gamma}$. For $M \approx M_H/2$, the value of the upper limit is $\langle \sigma v_r \rangle_{\gamma\gamma} \leq 6.75 \times 10^{-29} cm^3/seg$.

The averaged cross section for the annihilation of TDM into two photons is given in Eq.(4.56), which to leading order in v_r^2 yields

$$\langle \sigma v_r \rangle_{\gamma\gamma} = \frac{g_{\gamma\gamma}^2 g_s^2 M^2 v^2}{6\pi M_H^2 \left(\left(4M^2 - M_H^2\right)^2 + M_H^2 \Gamma_H^2 \right)}. \tag{6.29}$$

The upper bounds obtained by FermiLAT [154], including the 95% containment region, are shown in Fig. 6.11 along with our results for the TDM mass values consistent with GRE data. The predictions of the tensor dark matter formalism are consistent with these bounds, but in this channel we are again at the edge of the allowed values of $\langle \sigma v_r \rangle_{\gamma\gamma}$. Lowering this bounds could put a test to the possibility that dark matter could be described as a particle with a $(1,0) \oplus (0,1)$ space-time structure.

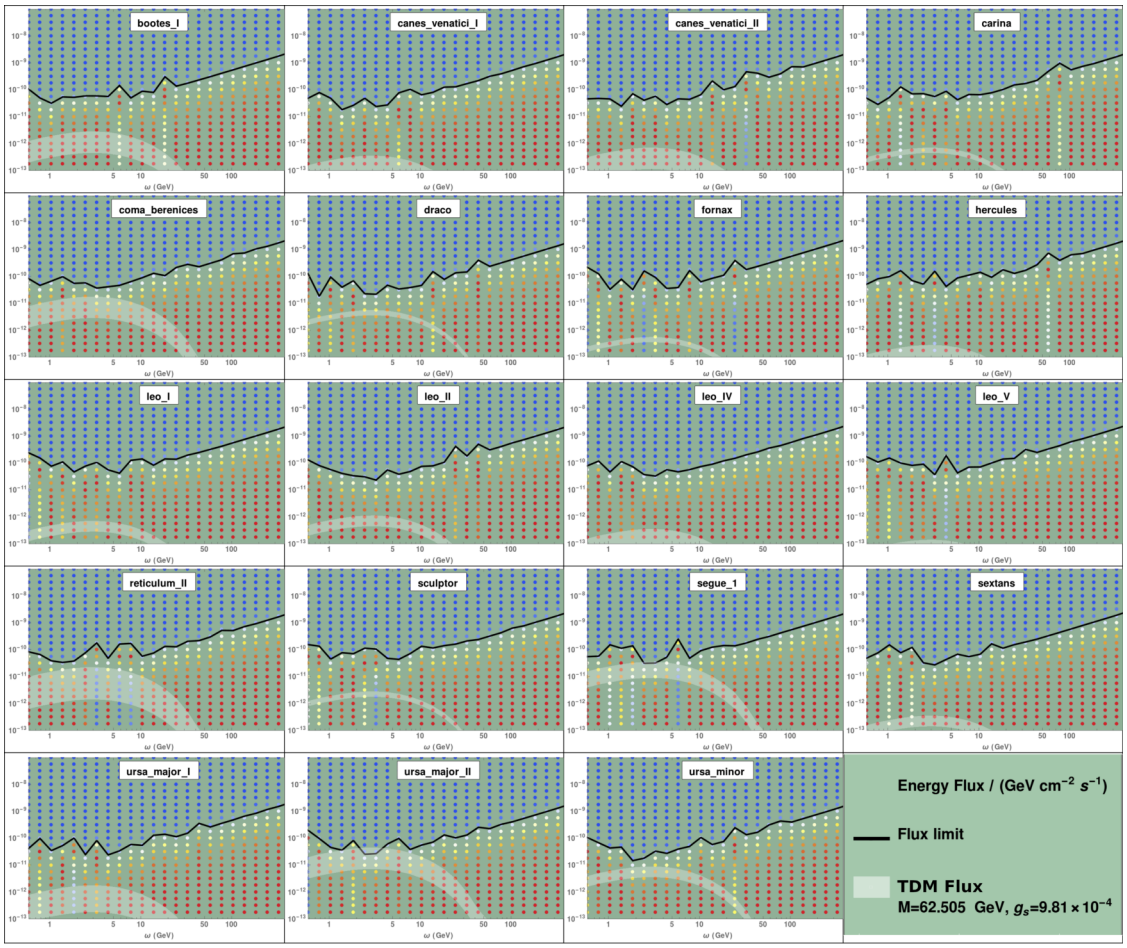

FIGURE 6.10: Energy flux (in units of $GeV\ cm^{-2}\ s^{-1}$) in terms of the photon energy ω, for each of the 19 targets used in [52] with a J-factor derived from stellar kinematics in [151]. The colored dots represent the values of the likelihood function, where red is a higher value and blue is lower. The black solid line is the energy flux upper limit at 95 % confidence level obtained from the bin-by-bin likelihood functions. The shaded white area represents the energy flux for TDM annihilating into b-quark pairs, using the measured J-factor to $1-\sigma$ uncertainty, for $M = 62.505$ GeV and $g_s = 9.81 \times 10^{-4}$.

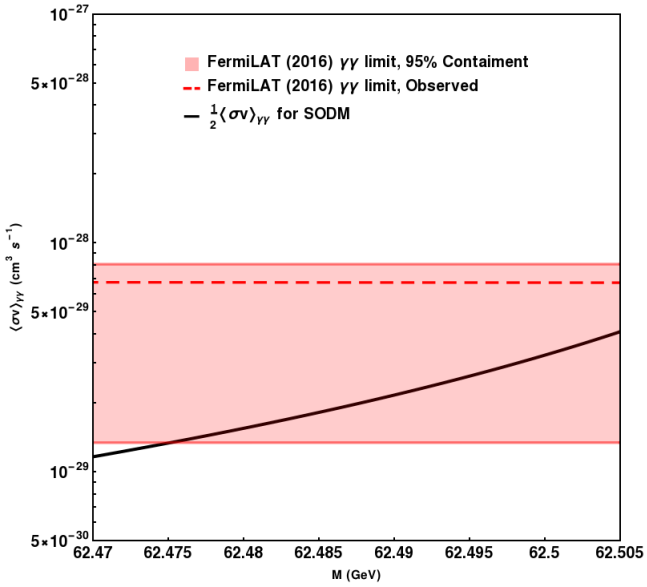

FIGURE 6.11: Annihilation cross section of TDM into two photons for the mass window consistent with GRE data, with $g_s = 9.81 \times 10^{-4}$ (solid line). The dashed line corresponds to the upper limits and the shadow band to the 95% confidence level region obtained in [154].

Chapter 7

Cosmic Ray Antiproton Excess from Tensor Dark Matter

One of the main concerns of particle physics is the absence of antimatter in the observable Universe, and it is a problem that remains unexplained today. Any contribution to the antimatter flux could be generated from exotic sources, so the observation of an excess of antimatter content is a promising mechanism for the detection of these sources, including the prospect of dark matter annihilation. In particular, two instruments have been designed with increased sensitivity to the cosmic antimatter flux: PAMELA [156] and AMS-02 [157, 158], which have measured with good precision the antimatter cosmic-ray spectrum [159–162].

Indeed, during the past decade the AMS-02 Collaboration data has been scrutinized to find an excess of antiprotons in the $\sim 10 - 20\ GeV$ region, with many studies identifying a possible consistency with a contribution from annihilating dark matter [53, 163–170] (see however alternative explanations to this excess regarding secondary cosmic-rays and systematic errors in [171, 172]).

It is an interesting occurrence that most of these studies, scanning independently the values of the dark matter mass and the cross section for its annihilation into standard model particles, find that dark matter with a mass of around $M \sim 60$ GeV and an annihilation cross-section of the order of the thermal relic cross section ($\langle \sigma v_r \rangle \sim 10^{-26} cm^3/seg$) is a possible explanation of this excess. These values fall into the mass and cross section windows for TDM that we have previously shown to be consistent with the gamma ray excess in the Galactic Center and other indirect detection bounds, in Chapter 6. This coincidence is our motivation for looking into the antiproton excess from the AMS-02 data more carefully, in search for a possible consistency with our dark matter proposal.

7.1 Modeling the antiproton and proton cosmic-ray spectrum in the galaxy

The need to uncover the mistery of the observed baryon asymmetry, by collecting data on existing antimatter in the universe, prompted the search and eventual detection of cosmic ray (CR) antiprotons during the 1970's [173, 174]. Several measurements and model proposals for the production of antiparticles in the Galaxy resulted in the conclusion that CR antiprotons are produced after interactions between high-energy nuclei (cosmic ray primaries, i.e. those accelerated by remnants of supernovae) and matter (mostly hydrogen and helium [175]) within the interstellar medium (ISM). These are the so-called secondary antiprotons. Antiprotons could be produced directly (primary antiprotons) in regions consisting of antimatter (not yet observed) [176] or they could also be a product of evaporation of primordial black holes [177]. The spectrum of antiprotons detected at Earth, however, is in agreement with mostly that of secondary origin [178].

The kinematics of the production of secondary antiprotons produce an energy spectrum with a maximum near 2 GeV, which then decreases at energies around tenths of GeV in a steeper form than that of protons [179]. Thus, the antiproton-to-proton ratio is observed to have a steep decrease at these energies. In summary, the antiproton flux is determined by CR propagation and interaction of nuclei with interstellar gas, and since these processes suffer from large uncertainties, one must treat their calculation carefully in order to predict the flux with high precision.

There are different sources for this systematic uncertainty. The first comes from the CR propagation which involves several complicated processes such as diffusion, convection, re-acceleration and loss of energy. The parameters of the model for the CR propagation must be chosen to account for secondary-to-primary nuclei ratios, among which are Boron-to-Carbon (B/C) and other nuclei [180]. The second source of uncertainties is the effect that the solar magnetic field has on the CR spectra, that is, the solar modulation [181]. When CR enter the Solar System, the solar magnetic field modifies their spectra, acting primarily on the low energy part of the spectrum. It is difficult to estimate with precision since it requires the modeling of the solar wind and its effects, which change through time. An overview of the effects of solar modulation of the cosmic rays entering the heliosphere is performed in Ref. [182]. Finally, another important source of uncertainties is the limited characterization of the cross sections for the production, annihilation and scattering of these particles. In this section we will take this into account and will make use of the parameter choice in the first model in Ref. [53] to evaluate the proton and antiproton flux from cosmic rays.

In order to obtain the local flux of the primary and secondary cosmic ray species, we

need to solve the transport equation for this particles. For this purpose, we make use of the publicly available tool GALPROP [1] [183], which solves the transport equation using the appropriate input parameters of a chosen model. We adopt the first model in Table I of [53] and use the input parameters listed in Table 7.1.

Parameter	Value
δ	0.40
z_L (kpc)	5.6
D_0 ($cm^2 s^{-1}$)	4.85×10^{28}
v_A (km/s)	24.0
α_1	1.88
$dv_c/d\|z\|$ (km/s/kpc)	1.0
α_2	2.38
R_{br} (GV*)	11.7

TABLE 7.1: Cosmic-ray injection and propagation model parameters used, adopted from Ref. [53]. *The units GV are giga-volts, or GeV divided by the elementary charge e.

The diffusion coefficient is defined as follows

$$D_{xx}(R) = \beta D_0 (R/4\,\mathrm{GV})^{\delta}, \tag{7.1}$$

where δ is the diffusion index and $\beta \equiv v/c$. The choice for these parameters and the calculation of the injection, diffusion, convection and reacceleration of CR is explained in Ref. [53].

A study of the antiproton production cross section done in Ref. [184] concluded that there is a 10-20% uncertainty coming from the fact that equivalent results are found through very different sets of parameters. To account for this uncertainty, we implement the solution formulated in [185] where the antiproton flux prior to solar modulation is fixed by an scaling factor that is energy dependent, defined as

$$N_{CS}(k_{ISM}) = a + b\left[ln\left(\frac{k_{ISM}}{GeV}\right)\right] + c\left[ln\left(\frac{k_{ISM}}{GeV}\right)\right]^2 + d\left[ln\left(\frac{k_{ISM}}{GeV}\right)\right]^3, \tag{7.2}$$

where k_{ISM} is the kinetic energy of the cosmic ray in the interstellar medium, before entering the Solar System. The fourth term of this scaling function, proportional to $\left[ln\left(\frac{k_{ISM}}{GeV}\right)\right]^3$, can be omitted and an adequate fit can still be reached, as it will be shown later on.

Once we have the antiproton flux, we must apply the effects of solar modulation after the cosmic rays enter the solar system. The differential flux at Earth, $dN^{\oplus}/dE_{kin}$ in terms

[1] https://galprop.stanford.edu/,https://galprop.stanford.edu/webrun/

of k_{ISM}, is obtained as [181]

$$\frac{dN^{\oplus}}{dE_{kin}}(k_{ISM}) = \frac{(k_{ISM} - |Z|e\Phi(R) + m)^2 - m^2}{(k_{ISM} + m)^2 - m^2} \frac{dN^{ISM}}{dk_{ISM}}(k_{ISM}), \tag{7.3}$$

where dN^{ISM}/dk_{ISM} is the differential flux prior solar modulation, E_{kin}, $|Z|e$ and m are the kinetic energy, charge and mass of the cosmic ray. Then, the flux in terms of E_{kin} can be obtained using the equivalence $E_{kin} = k_{ISM} - |Z|e\Phi(R)$. The modulation potential, Φ, is a function that depends on time, the charge of the cosmic ray and its rigidity ($R = \sqrt{k_{ISM}(k_{ISM} + 2m_p)}/e$) prior entering the Solar System, and it is given in units of GV, or GeV divided by the elementary charge e. We follow the analytic expression constructed in Ref. [186],

$$\Phi(R,t,q) = \phi_0\Big(\frac{|B_{tot}(t)|}{4\,\mathrm{nT}}\Big) + \phi_1 N'(q)H(-qA(t))\Big(\frac{|B_{tot}(t)|}{4\,\mathrm{nT}}\Big)\Big(\frac{1+(R/R_0)^2}{\beta(R/R_0)^3}\Big)\Big(\frac{\alpha(t)}{\pi/2}\Big)^4, \tag{7.4}$$

where $R_0 \equiv 0.5$ GV and B_{tot} is the strength of the heliospheric magnetic field (HMF) at Earth, with a polarity $A(t)$, H denotes the Heaviside function and α is the tilt angle of the heliospheric current sheet. $N'(q)$ defines the polarity of the HMF and $N'(q) \neq 1$ when the HMF does not have a well-defined polarity.

We work with the values $\phi_0 \in [0.32, 0.38]$ GV and $\phi_1 \in [0, 16]$ GV in order to stay within the uncertainties for the modulation potential described in Ref. [186]. The averaged values over six-month intervals during the observation period by AMS-02 of B_{tot}, α and $N'(q)H(-qA(t))$ are found in Table II of [185]. We use these values and calculate the potential and flux for each six-month interval, and the final result is the averaged values.

An additional parameter to take into account is the local ISM gas density, taken as an energy-independent normalizing factor, g_{ISM}. In total, there are seven free parameters involved in the fit: ϕ_0, ϕ_1, a, b, c, d and g_{ISM}. The flux ratio is defined as follows.

$$R_{\bar{p}/p} = \frac{\Phi_{\bar{p}}}{\Phi_p} = g_{ISM}\frac{dN^{\oplus}_{\bar{p}}}{dE_{kin}} \Big/ \frac{dN^{\oplus}_{p}}{dE_{kin}}. \tag{7.5}$$

The results for the best fit to the AMS-02 antiproton flux and antiproton-to-proton ratio data [187] are shown in Fig. 7.1. We perform the fit for two cases, $d = 0$ (fit 1) and $d \neq 0$ (fit 2). A summary of the fitting parameters and the corresponding value of χ^2 for each case is given in Table 7.2. The residual between the antiproton-to-proton ratio and the AMS-02 data for each fit is shown in Fig. 7.2. It can be observed that there is indeed an excess in the residual around ∼10-20 GeV and in the higher end of the spectrum.

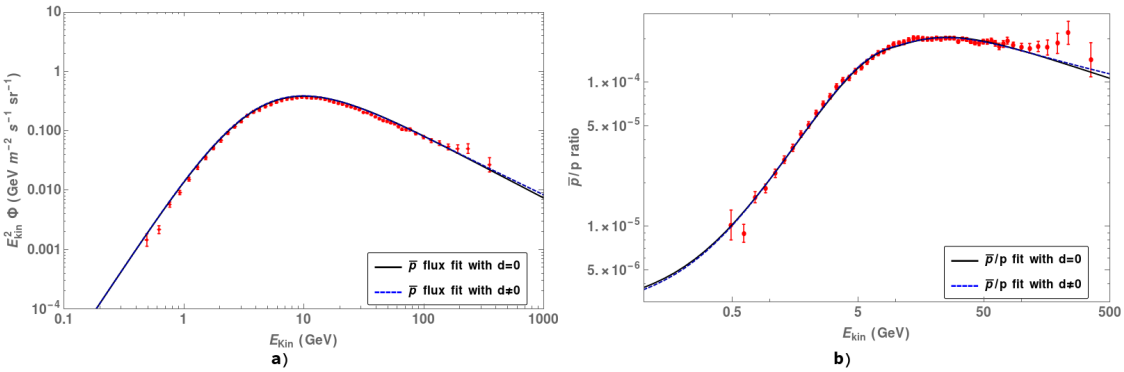

FIGURE 7.1: Best fit to the AMS-02 data on the a) antiproton flux and b) antiproton-to-proton ratio for $d = 0$ (solid line) and $d \neq 0$ (dashed line).

Fit	ϕ_0/GV	ϕ_1/GV	a	b	c	d	g_{ISM}	χ^2
1	0.3257	16	1.1579	-0.1632	0.0216	0	1.1844	1.0561
2	0.32	16	1.1549	-0.1301	0.0038	0.0023	1.1842	0.9243

TABLE 7.2: Best-fit parameters to the AMS-02 antiproton-to-proton ratio data considering secondary antiprotons produced in the ISM, for $d = 0$ (fit 1) and $d \neq 0$ (fit 2).

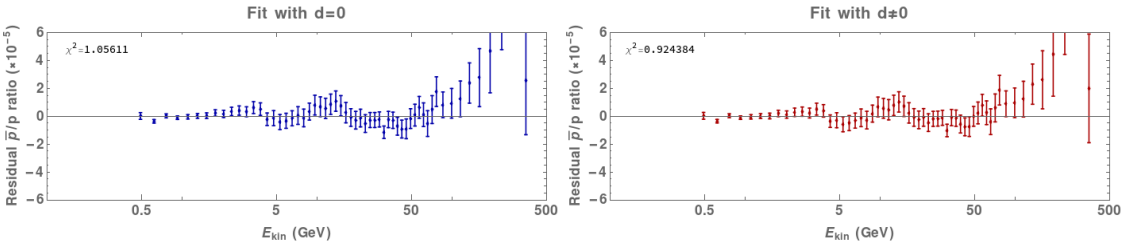

FIGURE 7.2: Antiproton-to-proton ratio residual from the AMS-02 data from Ref. [187].

7.2 Antiproton production from annihilating tensor dark matter

We use the PPC4DMID code [142] to obtain the antiproton flux produced in the hadronization of quarks or the hadronic decay of the τ lepton produced in the annihilation of TDM, and its propagation in the ISM. This code, which uses Monte Carlo simulations to calculate the differential spectra of antiprotons is especially useful since it includes electroweak corrections.

Protons are produced by dark matter annihilation in the same proportion as aniprotons, but their contribution to the overall proton flux is very small compared with the total proton flux in the ISM, and can be neglected. Only the antiproton production is large enough compared to the total antiproton flux in the ISM, so it becomes relevant in the

calculation of the antiproton to proton flux ratio. The relevant channels that contribute to the antiproton-proton ratio are shown in Fig. 7.3. It is easy to see that the most contributing channel, $\bar{b}b$, yields an antiproton flux with a maximum in the energy range of the excess in the AMS-02 data.

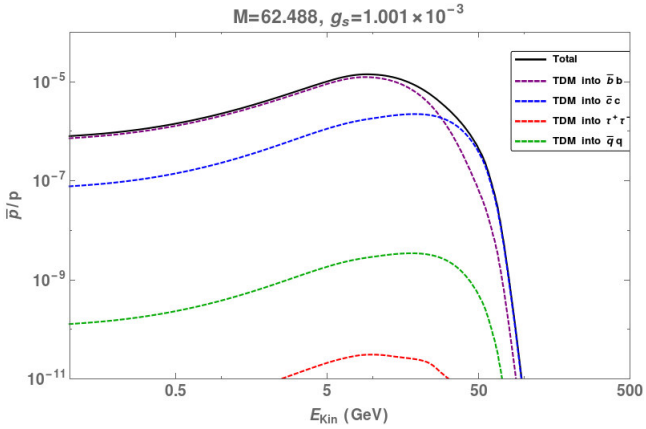

FIGURE 7.3: Antiproton-to-proton flux ratio for antiprotons produced in the annihilation of TDM for $M = 62.488$ GeV and the correlated coupling $g_s(M) = 1.001 \times 10^{-3}$, for the $\bar{b}b$, $\bar{c}c$, $\tau^+\tau^-$ and light quark channels.

The statistical relevance of this contribution can be seen when we perform a fit to the total flux to the AMS-02 data for both cases, $d = 0$ and $d \neq 0$, for fixed value of the mass M and obtain the value of χ^2 for the fit. The results for the whole range $M \in [62.470, 62.505]$ GeV are shown in Fig. 7.4 for the fit including TDM contributions and we compare it to the value for the best fit without the addition of TDM contributions obtained in the previous section for $d = 0$ and $d \neq 0$. We can see that the fit improves for all values of $M \in [62.470, 62.505]$ GeV in both cases. The black point in these plots marks the minimal value of χ^2 for the considered values of M, which correspond to the best fit including TDM contributions in each case. The parameters corresponding to these points are given in Table 7.3.

For $d = 0$, the best fit is obtained for $M = 62.4839$ GeV and the corresponding value of the Higgs portal coupling compatible with the measured relic density is $g_s(M) = 1.0053 \times 10^{-3}$. In the $d \neq 0$ case the best fit corresponds to $M = 62.4877$ GeV and the value of the coupling is $g_s(M) = 1.0009 \times 10^{-3}$.

Fit	M/GeV	ϕ_0/GV	ϕ_1/GV	**a**	**b**	**c**	**d**	g_{ISM}	χ^2
3	62.4839	0.32	16	1.1216	-0.1599	0.0247	0	1.1371	0.8783
4	62.4877	0.32	16	1.1225	-0.1691	0.0290	-0.00043	1.1310	0.8772

TABLE 7.3: Best-fit parameters to the AMS-02 antiproton-to-proton ratio for $d = 0$ (Fit 3) and $d \neq 0$ (Fit 4), including antiprotons from TDM annihilation.

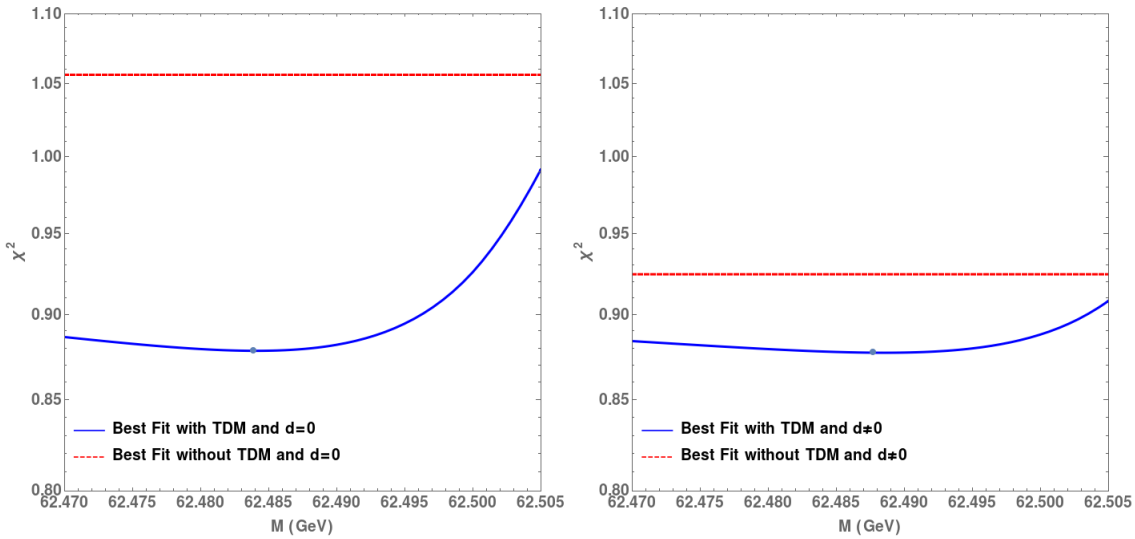

FIGURE 7.4: χ^2 value as a function of M, for $d = 0$ (left) and $d \neq 0$ (right). The dashed lines are the χ^2 values without the TDM annihilation contributions in Section II. The points correspond to the minimal value in each case.

Each contribution of the best-fit results in Table 7.3 are shown in Fig. 7.5, where data points correspond to the AMS-02 data for the antiproton-proton residual ratio and the continuous lines correspond to antiprotons produced in the annihilation of TDM. We can see in these plots that TDM contributions account for the antiprotons excess extracted from the AMS-02 data and this result is not sensitive to the value of d.

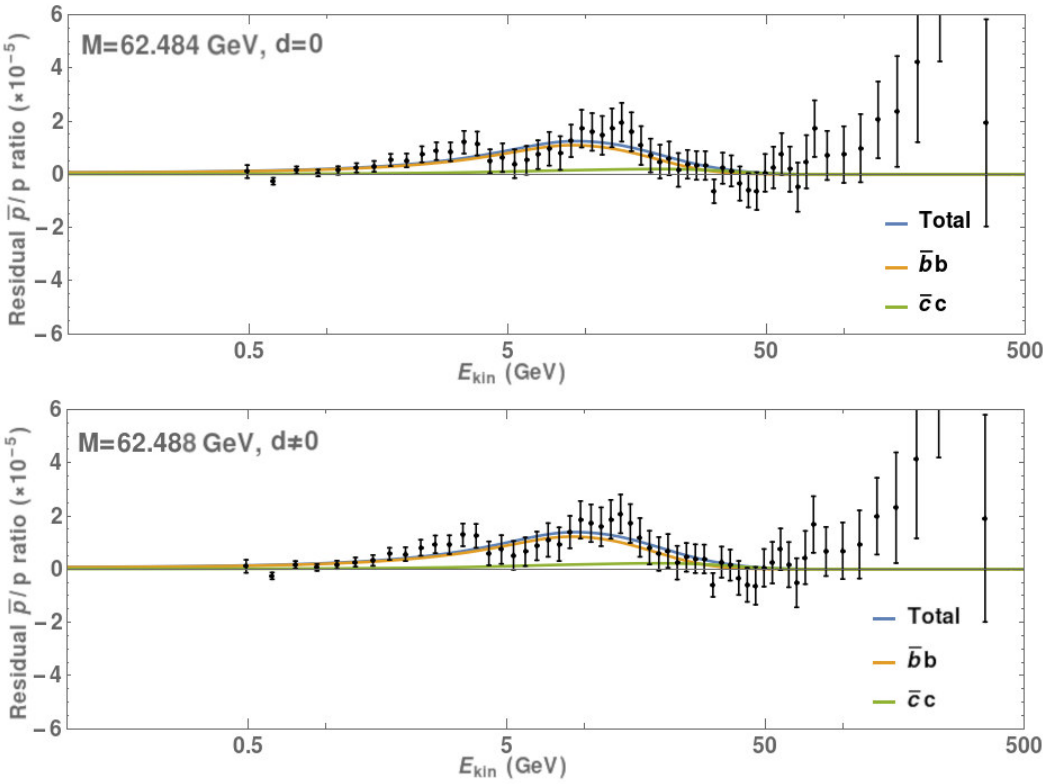

FIGURE 7.5: Antiproton-to-proton ratio pure residual (annihilation contributions not included) from the AMS-02 data [187] for the parameters in the best fit for $d = 0$ (top) and $d \neq 0$ (bottom) in Table 7.3. In both cases we also show the contributions from TDM annihilation into $\bar{b}b$ and $\bar{c}c$ for the corresponding value of M in Table 7.3.

Chapter 8

Simple Gauge Theory for Dark Matter and Collider Constraints

In the past chapters we have described and shown that tensor dark matter, a spinor-like field in the $(1,0)\oplus(0,1)$ space-time structure, is a possible description of dark matter that is consistent with relic density, constraints from Z^0 and H invisible widths, bounds from direct detection experiments such as XENON1T, and indirect detection limits from observations of the photon flux in dwarf spheroidal satellite galaxies (dSphs), the cosmic ray antiproton excess and the Galactic Center gamma ray excess. This consistency is obtained only when the tensor dark matter has a mass $M \approx M_H/2$, specifically within the $[62.470, 62.505]$ GeV window and with a coupling to the scalar Higgs portal $g_s \in [0.98, 1.01] \times 10^{-3}$.

This sharp prediction, along with the fact that the leading terms in the interaction Lagrangian are dimension-four, motivates us to explore a more general construction. In this chapter we will work out the formalism for a Hidden Tensor Dark Matter gauge structure, that is, the inclusion of dark matter fields with a $(1,0)\oplus(0,1)$ space-time structure and the simplest case for an additional dark gauge group $G_d = U(1)_d$, and its spontaneously broken gauge symmetry. In this Hidden TDM scheme, the dark sector does not have SM charges and, viceversa, the SM fields do not have dark sector charges.

Despite both sectors having no charges of the other, there are dark matter interactions coming from the fact that a dark gauge group that includes a factor $U(1)_d$ subgroup mixes kinetically with the $U(1)_Y$ of the standard model. This idea has led to the exploration of new neutral gauge bosons, that are considered the mediators of dark matter gauge interactions and the consequent existence of kinetic mixing of the SM $U(1)_Y$ gauge boson with every abelian dark gauge boson in the dark group G_d [188–212]. We will study the kinetic mixing that occurs in the Hidden TDM scheme in detail.

8.1 Dark gauge group, kinetic mixing and custodial symmetry

The Lagrangian with the addition of a dark $U(1)_D$ gauge group can be written as

$$\mathcal{L} = \mathcal{L}_{SM} + \mathcal{L}_d + \mathcal{L}_{int}, \tag{8.1}$$

with $\mathcal{L}_{SM}$ being the SM Lagrangian, $\mathcal{L}_d$ stands for the $U(1)_d$ gauge theory Lagrangian and $\mathcal{L}_{int}$ includes the interaction terms between SM and the dark sector. The dark sector Lagrangian is given by

$$\mathcal{L}_d = (D^\mu\tilde{)}^\dagger \bar{\psi}\Sigma^{\mu\nu}D_\nu\psi - M^2\bar{\psi}\psi + (D^\mu\Phi)^* D_\mu\Phi - \mu_d^2\Phi^*\Phi - \lambda_d(\Phi^*\Phi)^2 - \frac{1}{4}V^{\mu\nu}V_{\mu\nu}, \tag{8.2}$$

where ψ is the tensor dark matter field and $\Sigma_{\mu\nu} = \frac{1}{2}(g_{\mu\nu} + S_{\mu\nu})$ as it was defined in Chapter 2. We denote the $U(1)_d$ stress tensor as $V^{\mu\nu}$ and the dark Higgs field as Φ. The covariant derivative for this sector is $D_\mu\psi = (\partial_\mu + ig_d\frac{Q_d}{2}V_\mu)\psi$.

The interaction Lagrangian is formed by all dimension four products of operators from the SM and dark sectors, invariant under the complete gauge group $SU(3)_c \otimes SU(2)_L \otimes U(1)_Y \otimes U(1)_d$. Recall that we did the same in Chapter 2, and we found that in the case of the SM, the lowest dimension gauge singlet operators are the $U(1)_Y$ stress tensor $\tilde{B}^{\mu\nu}$ and the Higgs operator $\tilde{\phi}^\dagger\tilde{\phi}$ (from now on we will use a tilde on the SM fields and couplings to distinguish them from the extended theory fields). For the dark sector, we have the $U(1)_d$ stress tensor $V^{\mu\nu}$ and the dark Higgs term $\Phi^\dagger\Phi$ as the lowest dimension gauge singlets. There could be an additional term if we consider new elements for the matter content of the dark sector. For example, if we include a dark neutrino ν^d and its right component is a singlet of $U(1)_d$, we can form a dimension four term $\bar{\tilde{L}}\tilde{\phi}^c\nu_R^d$, but we will focus only in the addition of the dark gauge fields.

Therefore, the interaction Lagrangian is given by

$$\begin{aligned}\mathcal{L}_{int} = &-\bar{\psi}(g_s + ig_p\chi)\psi\hat{\phi}^\dagger\hat{\phi} + g_t\bar{\psi}M_{\mu\nu}\psi\tilde{B}^{\mu\nu} - \bar{\psi}(\tilde{g}_s + i\tilde{g}_p\chi)\psi\Phi^*\Phi \\ &- \frac{sin\chi}{2}\tilde{B}^{\mu\nu}V_{\mu\nu} - 2\kappa\tilde{\phi}^\dagger\tilde{\phi}\Phi^*\Phi + \mathcal{L}_{si}^{\psi},\end{aligned} \tag{8.3}$$

where $\mathcal{L}_{si}^{\Psi}$ stands for the self-interaction Lagrangian of tensor dark matter. Self-interaction terms for fields with this structure are discussed in Ref. [77], but for the purposes of this work we will set them aside for now.

The kinetic terms for all the gauge bosons in the Lagrangian in Eq. (8.1) are

$$\mathcal{L}_{gauge}^K = -\frac{1}{4}(\tilde{W}^{a\mu\nu}\tilde{W}^a_{\mu\nu} + \tilde{B}^{\mu\nu}\tilde{B}_{\mu\nu} + V^{\mu\nu}V_{\mu\nu} + 2\sin\chi V^{\mu\nu}\tilde{B}_{\mu\nu}), \tag{8.4}$$

which contain a kinetic mixing term of the $U(1)_Y$ and $U(1)_d$ gauge bosons. To restore the canonical form of the Lagrangian, we must perform a $GL(2,\mathbb{R})$ transformation on the gauge bosons to obtain properly normalized kinetic terms [213]

$$\tilde{B}_{\mu\nu} = \bar{B}_{\mu\nu} - \tan\chi \bar{V}_{\mu\nu}, \qquad V_{\mu\nu} = \sec\chi \bar{V}_{\mu\nu}. \tag{8.5}$$

Applying this transformation, the Lagrangian recovers the canonical form

$$\mathcal{L}^K_{gauge} = -\frac{1}{4}(\tilde{W}^{a\mu\nu}\tilde{W}^a_{\mu\nu} + \bar{B}^{\mu\nu}\bar{B}_{\mu\nu} + \bar{V}^{\mu\nu}\bar{V}_{\mu\nu}), \tag{8.6}$$

which induces a coupling between the $U(1)_d$ gauge boson and the SM fields. The $SU(2)_L \otimes U(1)_Y \otimes U(1)_d$ covariant derivative now takes the form

$$D^\mu = \partial^\mu + i\tilde{g}T^a\tilde{W}^{a\mu} + i\tilde{g}_Y\frac{Y}{2}\bar{B}^\mu + i(g_d \sec\chi\frac{Q_d}{2} - \tilde{g}_Y\tan\chi\frac{Y}{2})\bar{V}^\mu, \tag{8.7}$$

where $Q_d/2$ is the generator of $U(1)_d$, with g_d being the corresponding coupling constant. Again, the "tilde" notation for the SM electroweak gauge couplings, $\tilde{g}, \tilde{g}_Y$, is to associate them to the extended theory. From the last term of the covariant derivative we notice that the new dark gauge boson acquires a non-vanishing hypercharge due to the kinetic mixing. Effects of this mixing also appear in the mass terms generated by the Higgs mechanism. In order to keep the $U(1)_{em}$ an unbroken symmetry, with the generator $Q = T_3 + Y/2$, we identify that the $\bar{B}_\mu$ boson functions similarly to the non-extended SM hypercharge field $\tilde{B}_\mu$, and both mix with $\tilde{W}^3_\mu$. We can perform a rotation with a weak mixing angle $\tilde{\theta}_\omega$

$$\begin{pmatrix} \bar{B} \\ \tilde{W}_3 \end{pmatrix} = \begin{pmatrix} \cos\tilde{\theta}_w & -\sin\tilde{\theta}_w \\ \sin\tilde{\theta}_w & \cos\tilde{\theta}_w \end{pmatrix} \begin{pmatrix} A \\ \tilde{Z} \end{pmatrix}. \tag{8.8}$$

As a result, we get the relation

$$\tilde{g}T_3\tilde{W}_3 + \tilde{g}_Y\frac{Y}{2}\bar{B} = eQA + \frac{\tilde{g}}{\tilde{c}_w}(T_3 - \tilde{s}^2_w Q)\tilde{Z}, \tag{8.9}$$

with $e = \tilde{g}\tilde{s}_w = \tilde{g}_Y\tilde{c}_w$, and where $\tilde{s}_w = \sin\tilde{\theta}_w$, $\tilde{c}_w = \cos\tilde{\theta}_w$.

The Higgs sector of the $G_{SM} \otimes U(1)_d$ gauge theory has the following Lagrangian

$$\mathcal{L}_{Higgs} = (D^\mu\tilde{\phi})^\dagger D_\mu\tilde{\phi} + (D^\mu\Phi)^* D_\mu\Phi - V(\tilde{\phi},\Phi), \tag{8.10}$$

where the Higgs potential is written as

$$V(\tilde{\phi},\Phi) = \tilde{\mu}^2\tilde{\phi}^\dagger\tilde{\phi} + \tilde{\lambda}(\tilde{\phi}^\dagger\tilde{\phi})^2 + \mu_d^2\Phi^*\Phi + \lambda_d(\Phi^*\Phi)^2 + 2\kappa\Phi^*\Phi\tilde{\phi}^\dagger\tilde{\phi}. \tag{8.11}$$

The minimum conditions are obtained as follows

$$\frac{\partial V}{\partial \tilde{\phi}_i} = 2\tilde{\phi}_i[\tilde{\mu}^2 + 2\tilde{\lambda}(\tilde{\phi}^\dagger\tilde{\phi}) + 2\kappa(\Phi^*\Phi)] = 0, \tag{8.12}$$

$$\frac{\partial V}{\partial \Phi_i} = 2\Phi_i[\tilde{\mu}^2 + 2\tilde{\lambda}(\Phi^*\Phi) + 2\kappa(\tilde{\phi}^\dagger\tilde{\phi})] = 0, \tag{8.13}$$

Using $\langle 0|\tilde{\phi}^\dagger\tilde{\phi}|0\rangle = \tilde{v}^2/2$ and $\langle 0|\Phi^*\Phi|0\rangle = v^2/2$ we obtain the following relations from the minimum conditions

$$\mu^2 + \lambda v^2 + \kappa\tilde{v}^2 = 0, \qquad \tilde{\mu}^2 + \tilde{\lambda}\tilde{v}^2 + \kappa v^2 = 0, \tag{8.14}$$

where $\langle 0|\phi^\dagger\phi|0\rangle = v^2/2$ and $\langle 0|\Phi^*\Phi|0\rangle = \tilde{v}^2/2$.

Here, the spontaneously broken solutions for both Higgs fields in the unitary gauge are

$$\tilde{\phi} = \begin{pmatrix} 0 \\ \frac{\tilde{v}+\tilde{H}}{\sqrt{2}} \end{pmatrix}, \qquad \Phi = \frac{v_d + \bar{S}}{\sqrt{2}}, \tag{8.15}$$

where the expectation values of $\tilde{H}$ and $\bar{S}$ vanish. Spontaneous symmetry breaking generates mass terms for the Tensor Dark Matter field, however, the parity-breaking terms with the coouplings $g_p, \tilde{g}_p$ in Eq. (8.3) generate mass terms with the wrong properties under parity, thus we will discard them. With this into consideration, we have the following Yukawa-like terms

$$\mathcal{L}^D_{yuk} = -g_s\bar{\psi}\psi\hat{\phi}^\dagger\hat{\phi} - \tilde{g}_s\bar{\psi}\psi\hat{\Phi}^*\hat{\Phi}. \tag{8.16}$$

The mass for the TDM field after SSB turns out to be $M^2_\psi = M^2 + \frac{1}{2}(g_s v^2 + \tilde{g}_s\tilde{v}^2)$. From these terms we can also notice a dark matter-Higgs coupling, yielding a Higgs portal interaction similar to what we have studied in the previous chapters of this work, but now there is a additional structure from the dark Higgs producing also a combinated coupling with the SM Higgs.

In this gauge, since $\tilde{\phi}$ is a $U(1)_D$ singlet and Φ is a standard model singlet, Eqs.(8.7,8.10) yield the following gauge boson mass terms

$$\begin{aligned}\mathcal{L}^{gauge}_{mass} = &\frac{\tilde{g}^2\tilde{v}^2}{4}\tilde{W}^{+\mu}\tilde{W}^-_\mu \\ &+ \frac{1}{2}\left[\frac{\tilde{v}^2\tilde{g}^2}{4\tilde{c}^2_w}\tilde{Z}^2 + \frac{\tilde{v}^2\tilde{g}\tilde{g}_Y\tan\chi}{2\tilde{c}_w}\bar{V}^\mu\tilde{Z}_\mu + \left(\frac{\tilde{g}^2_Y\tilde{v}^2\tan^2\chi}{4} + g^2_d\sec^2\chi v^2\right)\bar{V}^2\right].\end{aligned} \tag{8.17}$$

The photon is massless and the $\tilde{W}^{\pm}$ boson maintains the same value of mass as in the SM. We can arrange these terms in the following form

$$\mathcal{L}_{mass}^{gauge} = M_{\tilde{W}}^2 \tilde{W}^{+\mu} \tilde{W}_{\mu}^{-} + \frac{1}{2} \begin{pmatrix} \tilde{Z} & \bar{V} \end{pmatrix} \begin{pmatrix} M_{\tilde{Z}}^2 & \Delta \\ \Delta & M_{\bar{V}}^2 \end{pmatrix} \begin{pmatrix} \tilde{Z} \\ \bar{V} \end{pmatrix}, \tag{8.18}$$

where

$$M_{\tilde{W}}^2 = \frac{\tilde{g}^2 \tilde{v}^2}{4}, \tag{8.19}$$

$$M_{\tilde{Z}}^2 = \frac{M_{\tilde{W}}^2}{\tilde{c}_w^2}, \tag{8.20}$$

$$\Delta = \frac{M_{\tilde{W}}^2}{\tilde{c}_w^2} \tilde{s}_w \tan\chi, \tag{8.21}$$

$$M_{\bar{V}}^2 = M_{\tilde{W}}^2 \tan^2\tilde{\theta}_w \tan^2\chi + g_d^2 v_d^2 \sec^2\chi. \tag{8.22}$$

The SM field $\tilde{Z}$ mantains the expected mass value related to the $\tilde{W}^{\pm}$ mass, $M_{\tilde{W}} = M_{\tilde{Z}} \tilde{c}_w$, which is a consequence of the Higgs sector custodial symmetry. In other words, the Higgs potential has a global $SU(2)_L \otimes SU(2)_R$ symmetry before the breaking of the $SU(2)_L \otimes U(1)_Y$. After the spontaneous symmetry breaking, a $SU(2)_V$ symmetry remains, which is called a custodial symmetry [214–217], and protects the relation between the $\tilde{Z}$ and the $\tilde{W}^{\pm}$ mass.

The neutral gauge boson mass terms can be diagonalized by the following rotation

$$\begin{pmatrix} \tilde{Z} \\ \bar{V} \end{pmatrix} = \begin{pmatrix} \cos\theta_\zeta & -\sin\theta_\zeta \\ \sin\theta_\zeta & \cos\theta_\zeta \end{pmatrix} \begin{pmatrix} Z \\ Z' \end{pmatrix}, \tag{8.23}$$

in which we have the relations

$$M_Z^2 = M_{\tilde{Z}}^2 c_\zeta^2 + M_{\bar{V}}^2 s_\zeta^2 + 2\Delta s_\zeta c_\zeta, \tag{8.24}$$

$$M_{Z'}^2 = M_{\tilde{Z}}^2 s_\zeta^2 + M_{\bar{V}}^2 c_\zeta^2 - 2\Delta s_\zeta c_\zeta, \tag{8.25}$$

$$\tan 2\theta_\zeta = \frac{2\Delta}{M_{\tilde{Z}}^2 - M_{\bar{V}}^2}. \tag{8.26}$$

It is useful to keep the converse relations

$$M_{\tilde{Z}}^2 = M_Z^2 c_\zeta^2 + M_{Z'}^2 s_\zeta^2, \tag{8.27}$$

$$M_{\bar{V}}^2 = M_Z^2 s_\zeta^2 + M_{Z'}^2 c_\zeta^2, \tag{8.28}$$

$$\Delta = \frac{1}{2} \sin 2\theta_\zeta (M_Z^2 - M_{Z'}^2). \tag{8.29}$$

From Eq.(8.27) we can write the mixing angle θ_ζ in terms of the physical Z and Z' masses and the non-diagonal $\tilde{Z}$ mass which in turn can be written in terms of measurable quantities. Explicitly

$$s_\zeta^2 = \frac{M_{\tilde{Z}}^2 - M_Z^2}{M_{Z'}^2 - M_Z^2}. \tag{8.30}$$

After these transformations, we can find the relation between the original gauge fields and the diagonal fields by

$$\begin{pmatrix} \tilde{B} \\ \tilde{W}_3 \\ V \end{pmatrix} = \begin{pmatrix} \tilde{c}_w, & -\tilde{s}_w c_\zeta - \tan\chi s_\zeta, & \tilde{s}_w s_\zeta - \tan\chi c_\zeta \\ \tilde{s}_w & \tilde{c}_w c_\zeta & -\tilde{c}_w s_\zeta \\ 0 & \sec\chi s_\zeta & \sec\chi c_\zeta \end{pmatrix} \begin{pmatrix} A \\ Z \\ Z' \end{pmatrix}. \tag{8.31}$$

Finally, the covariant derivative in terms of the physical fields is

$$\begin{aligned} D_\mu = {} & \partial_\mu + i\frac{\tilde{g}}{\sqrt{2}}(T^+\tilde{W}_\mu^+ + T^-\tilde{W}_\mu^-) + ieQA_\mu \\ & + i\left[\frac{\tilde{g}c_\zeta}{\tilde{c}_w}\left((T_3 - \tilde{s}_w^2 Q) - \tilde{s}_w \tan\theta_\zeta \tan\chi \frac{Y}{2}\right) + g_d s_\zeta \sec\chi \frac{Q_d}{2}\right] Z_\mu \\ & - i\left[\frac{\tilde{g}s_\zeta}{\tilde{c}_w}\left((T_3 - \tilde{s}_w^2 Q) + \frac{\tilde{s}_w \tan\chi}{\tan\theta_\zeta}\frac{Y}{2}\right) - g_d c_\zeta \sec\chi \frac{Q_d}{2}\right] Z'_\mu. \end{aligned} \tag{8.32}$$

The neutral currents arising from this covariant derivative can be compared with experimental data to measure the effects of kinetic mixing. Such comparison would yield bounds to the values of the kinetic mixing parameter χ, the mixing angle θ_ζ or the parameter κ in the Higgs sector in Eq. (8.11). However, the custodial symmetry protects the relation $M_{\tilde{W}} = M_{\tilde{Z}}\tilde{c}_w$ at tree level, so we can attempt to write the matrix elements of Eq. (8.31) in terms of the weak angle, M_W and M_Z which are measured quantities, and the unknown mass of the physical field Z'.

We can test the grounds on new physics by using the fit to the electroweak precision data (EWPD) , but this requires analysis at a loop level.

8.2 Mass Lagrangian at the loop level

The modified minimal subtraction scheme ($\overline{MS}$) is a renormalization scheme that is used, along with radiative corrections, to obtain the precise values of physical constants that are the baseline for particle physics calculations. For instance, the world average for the electromagnetic fine structure constant at low energies, $\alpha^{-1} = 137.035999084(21)$, is extracted from measurements of the electron anomalous magnetic moment, and the Rydberg constant and atomic masses of ^{87}Rb and ^{133}Cs. The Fermi constant G_F =

$1.1663787(6) \times 10^{-5} GeV^{-2}$ is measured from the muon lifetime, and the value $M_Z = 91.1876 \pm 0.021\ GeV$ comes from the Z lineshape at LEP. For details of these measurements, refer to the review *Electroweak Model and Constraints on New Physics* in [3]. These values use the $\overline{MS}$, where the physical Weinberg angle at a scale μ is defined as

$$\sin\hat{\theta}_W(\mu) \equiv \frac{\hat{g}_Y^2(\mu)}{\hat{g}^2(\mu) + \hat{g}_Y^2(\mu)}, \tag{8.33}$$

where the hatted values correspond to those of the $\overline{MS}$ scheme. The masses of the gauge bosons in this scheme are written in terms of other observables, such as

$$M_W^2 = \frac{\pi\alpha}{\sqrt{2}G_F\hat{s}_Z^2(1-\Delta\hat{r}_W)}, \qquad M_Z^2 = \frac{M_W^2}{\hat{\rho}\,\hat{c}_Z^2}, \tag{8.34}$$

where $\hat{s}_Z \equiv \sin\hat{\theta}_W(M_Z)$, $\hat{c}_Z \equiv \cos\hat{\theta}_W(M_Z)$. The factors $\Delta\hat{r}_W$, $\hat{\rho}$ are related to the radiative corrections, which in turn are related with the observables $\alpha, \hat{\alpha}(M_Z), G_F, M_W$ and M_Z. Top quark loops are the dominant contribution to these radiative corrections, quantified in terms of the quadratic mass of the top quark. Including contributions from the b quark, the radiative correction $\hat{\rho}_{tb}$ is [218]

$$\hat{\rho}_{tb} = \frac{3G_F}{8\sqrt{2}\pi^2}\left(m_t^2 + m_b^2 - 2\frac{m_t^2 m_b^2}{m_t^2 - m_b^2}\ln\frac{m_t^2}{m_b^2}\right). \tag{8.35}$$

There is also a subdominant contribution from Higgs loops, $\hat{\rho}_H$, which is

$$\hat{\rho}_H = -\frac{11G_F M_Z^2\hat{s}_Z^2}{24\sqrt{2}\pi^2}\ln\frac{M_H^2}{M_Z^2}. \tag{8.36}$$

Including all bosonic loops, we obtain $\hat{\rho} = 1 + \hat{\rho}_{tb} + \hat{\rho}_H = 1.01019 \pm 0.00009$ [3]. From Eq. (8.34) we get the relation

$$M_Z^2\hat{s}_Z^2\hat{c}_Z^2 = \frac{\pi\alpha}{\sqrt{2}G_F\hat{\rho}(1-\Delta\hat{r}_W)}. \tag{8.37}$$

The global fit to the EWPD measures effects of new physics through the parameter [3]

$$\rho_0 \equiv \frac{M_W^2}{\hat{c}_Z^2 M_Z^2\hat{\rho}}, \tag{8.38}$$

where $\hat{c}_Z \equiv \cos\theta_w(M_Z)$ is the Weinberg angle measured at the Z pole and M_W^2, M_Z^2 stand for the Z and $W^\pm$ masses, respectively. The quantity $\hat{\rho}$ in Eq. (8.38) includes the radiative corrections in the SM. Should there be no new physics contributions, we

will have $\rho_0 = 1$. Deviations from this value would reflect effects from physics beyond the SM. The radiative corrections to $\frac{M_W^2}{\hat{c}_Z^2 M_Z^2}$ from SM particles are mainly ruled by the top quark, while Higgs boson loops contribute to next to leading order effects. In the minimal subtraction ($\overline{MS}$) scheme, we have [3]

$$\hat{\rho} = 1.01019 \pm 0.00009. \tag{8.39}$$

The global fit to electroweak precision data yields [3]

$$\rho_0 = 1.00038 \pm 0.00020. \tag{8.40}$$

That the value of $\rho_0 > 1$ at $1.9\,\sigma$ (94% confidence level) [3], although not enough to be conclusive, could lead to contributions from new physics. We will consider from now on that such effects could be dominated by kinetic mixing effects and we will explore the consequences of this framework, in particular, to the possible values of the mass of Z'.

We must work out the same observables in this framework, including radiative corrections in the $\overline{MS}$ scheme in order to compare with the predictions of the extended theory. In our formalism, the muon lifetime yields a relation similar to the first of Eqs.(8.34),

$$M_{\tilde{W}}^2 = \frac{\pi\alpha}{\sqrt{2}G_F\tilde{s}_Z^2(1-\Delta\tilde{r}_W)}, \tag{8.41}$$

where now $\tilde{s}_Z \equiv \tilde{s}_w(M_Z)$. The value of $\Delta\tilde{r}_W$ accounts for the radiative corrections in the $\overline{MS}$ scheme for our formalism.

The mass Lagrangian for the neutral sector at the loop level is the same as in Eq.(8.18), replacing $M_{\tilde{Z}}^2 \to \hat{M}_{\tilde{Z}}^2$, $\Delta \to \hat{\Delta}$ and $M_{\tilde{V}} \to \hat{M}_{\tilde{V}}$. Again, the hatted terms are measured in the $\overline{MS}$ at the scale $\mu = M_Z$. With these changes, the tree level relation in Eq.(8.20) is

$$\hat{M}_{\tilde{Z}}^2 = \frac{M_{\tilde{W}}^2}{\tilde{\rho}\,\tilde{c}_Z^2}, \tag{8.42}$$

with $\tilde{c}_Z \equiv \tilde{c}_w(M_Z)$. Here, $\tilde{\rho}$ incorporates the radiative corrections in the $\overline{MS}$ scheme. Using this relation with Eq.(8.41), we obtain

$$\hat{M}_{\tilde{Z}}^2\tilde{s}_Z^2\tilde{c}_Z^2 = \frac{\pi\alpha}{\sqrt{2}G_F\tilde{\rho}(1-\Delta\tilde{r}_W)}. \tag{8.43}$$

The extended theory and the measured quantities can be compared from the Eqs.(8.37,8.43), where we find

$$\hat{M}_{\tilde{Z}}^2\tilde{c}_Z^2\tilde{s}_Z^2\tilde{\rho}(1-\Delta\tilde{r}_W) = M_Z^2\hat{s}_Z^2\hat{c}_Z^2\hat{\rho}(1-\Delta\hat{r}_W). \tag{8.44}$$

Then, the observable ρ_0 in Eq.(8.38) can be obtained from Eqs. (8.42,8.44),

$$\rho_0 = \frac{M^2_{\tilde{W}}}{\hat{c}^2_Z M^2_Z \hat{\rho}} = \frac{\hat{M}^2_{\tilde{Z}} \tilde{\rho}\, \tilde{c}^2_Z}{M^2_Z \hat{\rho} \hat{c}^2_Z} = \frac{\hat{s}^2_Z (1 - \Delta\hat{r}_W)}{\tilde{s}^2_Z (1 - \Delta\tilde{r}_W)}. \tag{8.45}$$

The radiative corrections for the extended theory would come from the couplings of the dark particles (Z' and the dark matter fields), which are generated by the kinetic mixing and the Higgs sector mixing in Eq. (8.3). However, these are small enough that we can neglect them in a first approximation, keeping only the radiative corrections from the SM particles. The dominant terms of this correction are the running of α and the top mass, while the Higgs mass contribution is logarithmic and involves the mass of Z, which will introduce only small differences due to the shift in the value of M_Z from kinetic mixing. Thus, we can consider as a good approximation that $\Delta\tilde{r}_W = \Delta\hat{r}_W$, so Eq.(8.45) becomes

$$\rho_0 = \frac{\hat{s}^2_Z}{\tilde{s}^2_Z}. \tag{8.46}$$

The diagonalization for the loop-level mass Lagrangian follows along the lines of the tree-level one, similar to Eq. (8.30),

$$\hat{s}^2_\zeta = \frac{\hat{M}^2_{\tilde{Z}} - M^2_Z}{M^2_{Z'} - M^2_Z}, \tag{8.47}$$

where $\hat{s}_\zeta \equiv \sin\theta_\zeta(M_Z)$ and $\hat{M}^2_{\tilde{Z}}$ in the $\overline{MS}$ scheme at the scale $\mu = M_Z$ is given in Eq.(8.42). From Eq. (8.46) we arrive to the following expression

$$\hat{M}^2_{\tilde{Z}} = \frac{\rho_0^2 \hat{c}^2_Z}{\rho_0 - \hat{s}^2_Z} M^2_Z. \tag{8.48}$$

Employing this relation in Eq.(8.47) yields

$$\hat{s}^2_\zeta = \frac{(\rho_0 - 1)(\rho_0 \hat{c}^2_Z - \hat{s}^2_Z) M^2_Z}{(\rho_0 - \hat{s}^2_Z)(M^2_{Z'} - M^2_Z)}. \tag{8.49}$$

We define a new term

$$\sigma_0 \equiv \frac{M^2_{\tilde{W}}}{\hat{c}^2_Z M^2_{Z'} \hat{\rho}}, \tag{8.50}$$

that we can use to rewrite Eq. (8.49) as

$$\hat{s}^2_\zeta = \frac{\sigma_0 (\rho_0 - 1)(\rho_0 \hat{c}^2_Z - \hat{s}^2_Z)}{(\rho_0 - \hat{s}^2_Z)(\rho_0 - \sigma_0)}. \tag{8.51}$$

In a similar way, from Eqs. (8.21,8.22), the kinetic mixing angle at the same scale, $\hat{\chi} = \chi(M_Z)$, can be written in terms of the same physical quantities as

$$\tan^2\hat{\chi} = \frac{(\rho_0-1)(\rho_0\hat{c}_Z^2-\hat{s}_Z^2)}{\rho_0^2\sigma_0\hat{s}_Z^2\hat{c}_Z^4}[\rho_0(1-\sigma_0\hat{c}_Z^2)-\hat{s}_Z^2]. \tag{8.52}$$

We can use the above relations to write the covariant derivative in Eq. (8.32) in terms of the physical values of the effective couplings depending on α, G_F, M_W, M_Z and $M_{Z'}$ as

$$\begin{aligned} D_\mu = {} & \partial_\mu + i\frac{e\sqrt{\rho_0}}{\sqrt{2}\hat{s}_Z}(T^+W_\mu^+ + T^-W_\mu^-) + ieQA_\mu \\ & + i\left[\frac{e}{\hat{s}_Z\hat{c}_Z}\sqrt{\frac{\rho_0-\hat{s}_Z^2-\rho_0\sigma_0\hat{c}_Z^2}{\hat{c}_Z^2\rho_0(\rho_0-\sigma_0)}}\left(T_3-(1-\rho_0\hat{c}_Z^2)Q\right)+g_d\hat{s}_\zeta\sec\hat{\chi}\frac{Q_d}{2}\right]Z_\mu \\ & - i\left[\frac{e}{\hat{s}_Z\hat{c}_Z}\sqrt{\frac{(\rho_0-1)(\rho_0\hat{c}_Z^2-\hat{s}_Z^2)}{\hat{c}_Z^2\sigma_0(\rho_0-\sigma_0)}}\left(T_3-(1-\sigma_0\hat{c}_Z^2)Q\right)-g_d\hat{c}_\zeta\sec\hat{\chi}\frac{Q_d}{2}\right]Z'_\mu, \end{aligned} \tag{8.53}$$

where

$$\hat{c}_\zeta^2 = \frac{\rho_0(\rho_0-\hat{s}_Z^2-\rho_0\sigma_0\hat{c}_Z^2)}{(\rho_0-\hat{s}_Z^2)(\rho_0-\sigma_0)}, \tag{8.54}$$

$$\hat{s}_\zeta\sec\hat{\chi} = \frac{1}{\rho_0\hat{s}_Z\hat{c}_Z^2}\left[\frac{(\rho_0-1)(\rho_0\hat{c}_Z^2-\hat{s}_Z^2)(\rho_0(\rho_0\hat{c}_Z^2-1)(1-\sigma_0\hat{c}_Z^2)+\hat{s}_Z^2)}{\rho_0-\sigma_0}\right]^{\frac{1}{2}}, \tag{8.55}$$

$$\hat{c}_\zeta\sec\hat{\chi} = \frac{1}{\hat{s}_Z\hat{c}_Z}\left[\frac{\rho_0-\hat{s}_Z^2-\rho_0\sigma_0\hat{c}_Z^2}{\rho_0-\sigma_0}\left(\frac{(\rho_0-1)}{\sigma_0}\frac{(\rho_0(1-\sigma_0)\hat{c}_Z^2-\hat{s}_Z^2)}{\rho_0\hat{c}_Z^2}+\rho_0\hat{s}_Z^2\right)\right]^{\frac{1}{2}}, \tag{8.56}$$

with $\hat{c}_\zeta = c_\zeta(M_Z)$.

With this, we can work out interactions between the physical neutral bosons, Z and Z' in the extended theory, in order to compare with collider data.

8.3 Effective $Z\bar{f}f$ interactions and oblique parameters

Assuming that the SM fermions do not carry $U(1)_d$ charge, the covariant derivative in Eq.(8.53) yields the following $Z\bar{f}f$ Lagrangian at the scale $\mu = M_Z$

$$\mathcal{L}_{Z\bar{f}f} = \frac{e}{2\hat{s}_Z\hat{c}_Z}R\sum_f \bar{f}\gamma^\mu\left[T_{f_L}^3-2(1-\rho_0\hat{c}_Z^2)Q-T_{f_L}^3\gamma^5\right]f\,Z_\mu, \tag{8.57}$$

with

$$R = \sqrt{\frac{\rho_0-\hat{s}_Z^2-\rho_0\sigma_0\hat{c}_Z^2}{\hat{c}_Z^2\rho_0(\rho_0-\sigma_0)}}. \tag{8.58}$$

On the other hand, the corrections to the SM Lagrangian coming from physics beyond the SM can be contained in a set of expressions for electroweak observables that are corrected by a linear combination of three parameters: S, T and U. These are the so-called oblique parameters, and for the effective $Z\bar{f}f$ interaction, we write it as [213, 219–222]

$$\mathcal{L}^{eff}_{Z\bar{f}f} = \frac{e}{2s_W c_W}\left(1+\frac{\alpha T}{2}\right)\sum_f \bar{f}\gamma^\mu\left(T^3_{f_L} - 2s^2_* Q - T^3_{f_L}\gamma^5\right) f Z_\mu, \tag{8.59}$$

where $s_W = \sin\theta_W$, $c_W = \cos\theta_W$ with θ_W being the Weinberg angle and

$$s^2_* = s^2_W + \frac{1}{c^2_W - s^2_W}\left(\frac{\alpha S}{4} - s^2_W c^2_W \alpha T\right). \tag{8.60}$$

Comparing both Lagrangians in Eqs. (8.59,8.57), we can identify

$$\alpha S = 4\hat{c}^2_Z\left[(1-\rho_0)(\hat{c}^2_Z - \hat{s}^2_Z) + 2\hat{s}^2_Z(R-1)\right], \tag{8.61}$$

$$\alpha T = 2(R-1). \tag{8.62}$$

The parameters S and T are functions of the Z' mass, but they are also related by the expression

$$T = \frac{1}{4\hat{s}^2_Z\hat{c}^2_Z}S + (\rho_0 - 1)\frac{\hat{c}^2_Z - \hat{s}^2_Z}{\alpha\hat{s}^2_Z}, \tag{8.63}$$

which holds for all values of $M_{Z'}$. In Ref. [3] the values of the oblique parameters are extracted from the fit to EWPD,

$$S = -0.01 \pm 0.10, \qquad T = 0.03 \pm 0.12, \qquad U = 0.02 \pm 0.11. \tag{8.64}$$

The predicted values of S and T as functions of the Z' mass, for the range of values for ρ_0 extracted from the fit to EWPD in Eq.(8.64), are shown in Fig. (8.1). We also show in these plots the 1σ regions for S and T obtained in the fit. We can see that S and T reach a saturation value for $M_{Z'} \approx 250\ GeV$ and from then on they are not sensitive to the value of $M_{Z'}$. These predicted values are consistent with results from the fit to EWPD for $M_{Z'} > M_Z$. There is a linear relation between T and S, plotted in Fig.(8.2) along with the 1σ bands for the oblique parameters. The values of S and T for which these bands intersect represent predictions of the present formalism in agreement with the fit to EWPD at 1σ level.

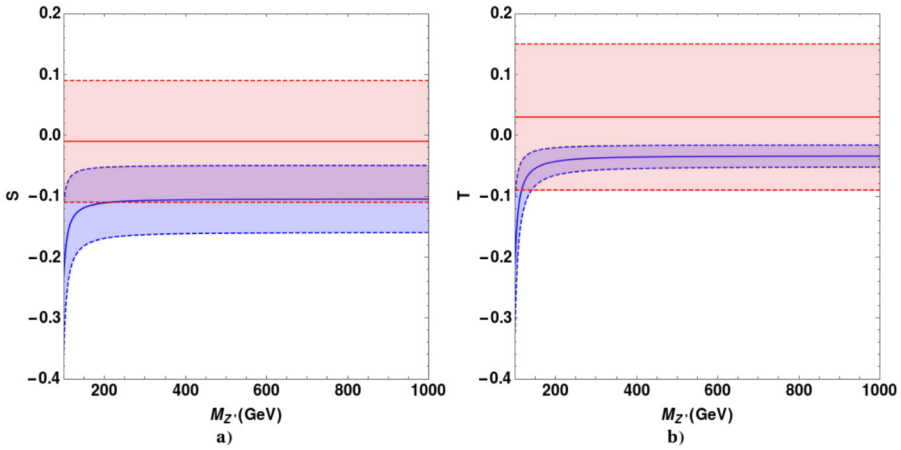

FIGURE 8.1: Oblique parameters S and T as functions of $M_{Z'}$. The solid blue lines are the predictions using the central value of ρ_0, while the shadowed band comes from the 1σ region for ρ_0 in Eq. (8.40). The red bands correspond to the 1σ region for S and T in Eq.(8.64). Solid lines stand for the respective central values.

8.4 Z' contribution to charged lepton pair production at hadron colliders

Searches of charged lepton pair production at Tevatron [223] and the LHC [224, 225] give upper bounds to the Z' cross section into fermion pairs. This cross section in the Z' pole region is

$$\sigma_{\bar{f}f} = \int_{(M_{Z'}-\Delta)^2}^{(M_{Z'}+\Delta)^q 2} \frac{d\sigma}{dM^2}(pp \to Z'X \to \bar{f}fX)dM^2. \tag{8.65}$$

We can simplify this calculation by the narrow width approximation [226]

$$\sigma_{\bar{f}f} \approx \left(\frac{1}{3}\sum_{q=u,d}\frac{dL_{\bar{q}q}}{dM^2_{Z'}}\hat{\sigma}(\bar{q}q \to Z')\right) BR(Z' \to \bar{f}f), \tag{8.66}$$

where $\frac{dL_{\bar{q}q}}{dM^2_{Z'}}$ are the parton luminosities. The branching ratio for the $\bar{f}f$ channel is defined as follows

$$BR(Z' \to \bar{f}f) = \frac{\Gamma(Z' \to \bar{f}f)}{\Gamma_{Z'}}, \tag{8.67}$$

where $\Gamma_{Z'}$ is the total Z' width.

The interaction of the Z' boson with SM fermions can be written as

$$\mathcal{L}_{Z'\bar{f}f} = g' Z'_\mu \sum_f \bar{f}\gamma^\mu \left[g_V^f - g_A^f \gamma^5\right] f. \tag{8.68}$$

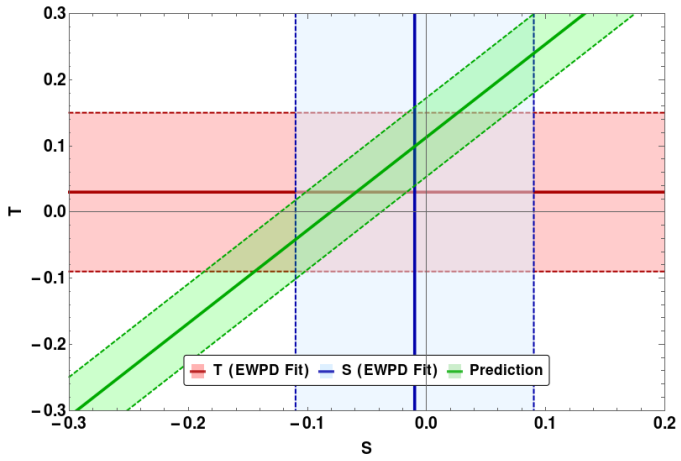

FIGURE 8.2: Oblique parameter S as a function of T. The green band stands for the prediction from the 1σ region of ρ_0 in Eq. (8.40). The red and blue bands are the values of T and S respectively in Eq.(8.64) for the 1σ region. The central values are shown as solid lines.

From here we can obtain the peak cross section

$$\hat{\sigma}(\bar{q}q \to Z') = \frac{\pi g'^2}{12}\left[(g_V^q)^2 + (g_A^q)^2\right], \tag{8.69}$$

while the Z' decay width into a fermion pair yields

$$\Gamma(Z' \to \bar{f}f) = N_c \frac{g'^2 M_{Z'}}{48\pi}\left[(g_V^f)^2 + (g_A^f)^2 + \mathcal{O}\left(\frac{m_f^2}{M_{Z'}^2}\right)\right], \tag{8.70}$$

where $N_c = 3$ for quarks and $N_c = 1$ for leptons. We can omit the terms of the order $\mathcal{O}\left(\frac{m_f^2}{M_{Z'}^2}\right)$, and the total width into fermions will be given by

$$\Gamma_{Z'}^f = \frac{g'^2 M_{Z'}}{48\pi}\left[9\left((g_V^u)^2 + (g_A^u)^2 + (g_V^d)^2 + (g_A^d)^2\right) + 3\left((g_V^\nu)^2 + (g_A^\nu)^2 + (g_V^e)^2 + (g_A^e)^2\right)\right], \tag{8.71}$$

where we assume that the couplings $g_{V/A}^f$ are different for each generation. Since the top quark channel starts at $2m_t = 350\ GeV$, the width is reduced 18% below the $\bar{t}t$ threshold, however for $M_{Z'} = 500\ GeV$ this phase space correction is of the order of 2%, which means we can safely neglect fermion masses.

In hadron colliders, the cross section for the production of charged lepton pairs due to Z' from hadron collisions can be factorized in terms of hadronic structure functions $w_{u/d}$, as [227]

$$\sigma_{l^+l^-} = \frac{\pi}{48s}\left[c_u w_u(s, M_{Z'}^2) + c_d w_d(s, M_{Z'}^2)\right], \tag{8.72}$$

where $w_{u,d}(s, M_{Z'}^2)$ depend only on the invariant Mandelstam variable s of the collision

and on the Z' mass. These functions contain the QCD dependence of the hadrons involved in the collision and are the same for any model with a neutral gauge boson, provided its coupling to quarks is not dependent on the generation. The explicit form of these functions depend on the parton distribution functions of the colliding hadrons, and are specified in Ref. [226]. The coefficients $c_{u,d}$ involve the Z' couplings to fermions,

$$c_u = \frac{g'^2}{2}\left[(g_V^u)^2 + (g_A^u)^2\right] BR(Z' \to l^+ l^-), \tag{8.73}$$

$$c_d = \frac{g'^2}{2}\left[(g_V^d)^2 + (g_A^d)^2\right] BR(Z' \to l^+ l^-). \tag{8.74}$$

From here, experimental data on l^+l^- production in hadron colliders can be used to find upper bounds on the Z' contribution, via exclusion curves in the $c_u - c_d$ plane, for a given $M_{Z'}$. In our case, the couplings of Z' to fermions are fixed by known data. Therefore, the predicted values of $c_{u,d}$ depend only on $M_{Z'}$, and we can compare the results with exclusion curves from collider data.

The $Z'\bar{f}f$ Lagrangian, assuming as before that the SM fermions do not carry the $U(1)_d$ charges, can be obtained using the covariant derivative in Eq.(8.53),

$$\mathcal{L}_{Z'\bar{f}f} = g_{Z'} \sum_f \bar{f}\gamma^\mu \left[T_{f_L}^3 - 2(1-\sigma_0\hat{c}_Z^2)Q - T_{f_L}^3\gamma^5\right] f\, Z'_\mu, \tag{8.75}$$

where

$$g_{Z'} = \frac{e}{2\hat{s}_Z\hat{c}_Z}\sqrt{\frac{(\rho_0-1)(\rho_0\hat{c}_Z^2 - \hat{s}_Z^2)}{\hat{c}_Z^2\sigma_0(\rho_0-\sigma_0)}}. \tag{8.76}$$

This coupling scales as $\sqrt{(\rho_0-1)/\sigma_0}$, being small for Z' masses near the electroweak scale. The factor $\sqrt{1/\sigma_0}$ enhances this value for $M_{Z'} >> M_W$ and at some point, it increases for large values of the Z' mass. The values of the associated fine structure constant, $g_{Z'}^2/4\pi$, in terms of the Z' mass for values within the 1σ level of ρ_0 in Eq. (8.40) are shown in Fig. 8.3. At $M_{Z'} \sim 30\ TeV$ we enter in a non-perturbative regime.

The interacting Lagrangian in Eq. (8.75) can be compared to the general Lagrangian in Eq. (8.68) to conclude that $g' = g_{Z'}$, which depends only on known data and $M_{Z'}$, as seen in Eq. (8.76). The vector and axial factors can be inferred from this comparison as

$$g_V^f = T_f^3 - 2(1-\sigma_0\hat{c}_Z^2)Q_f, \qquad g_A^f = T_f^3. \tag{8.77}$$

With these we can calculate the total Z' decay width into SM fermions

$$\Gamma_{Z'}^f = \frac{\alpha M_{Z'}}{4\hat{s}_Z^2\hat{c}_Z^2}\frac{(\rho_0-1)(\rho_0\hat{c}_Z^2-\hat{s}_Z^2)}{\hat{c}_Z^2\sigma_0(\rho_0-\sigma_0)}\left[1 - 2(1-\sigma_0\hat{c}_Z^2) + \frac{8}{3}(1-\sigma_0\hat{c}_Z^2)^2\right]. \tag{8.78}$$

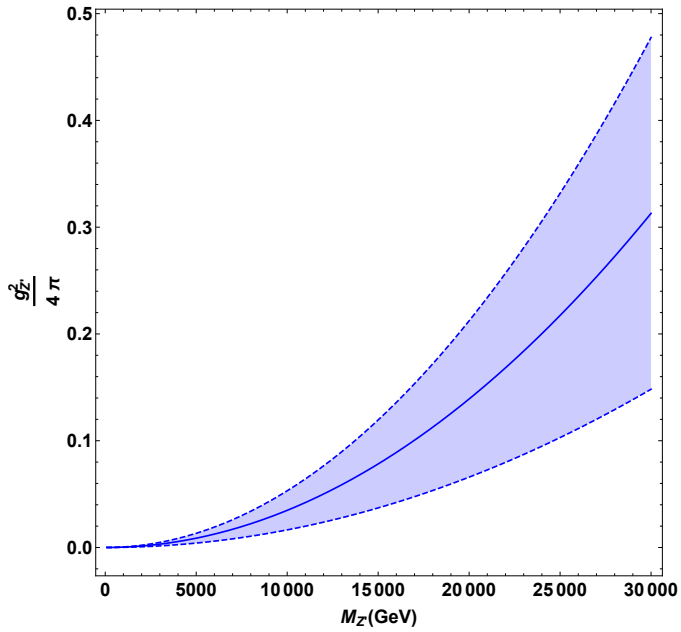

FIGURE 8.3: Fine structure constant for the coupling $g_{Z'}$ induced by kinetic mixing as a function of the Z' mass. The solid line corresponds to the predictions using the central value of ρ_0 and the shadow band to the 1σ region for ρ_0 in Eq.(8.40).

As mentioned before, the production in hadron colliders uses the narrow width approximation [226, 227] so we need to ensure that we are in this regime for the energies at which data is obtained. In a first approximation we will assume that the total width of the Z' is given by its decays to SM fermions only, with possible modifications considered afterwards. Under this assumption, $\Gamma^f_{Z'}$ in Eq.(8.78) is the total width. The ratio $\Gamma^f_{Z'}/M_{Z'}$ as a function of $M_{Z'}$ is shown in Fig. 8.4. We can see that up to masses around 10 TeV, the narrow width approximation is viable, with the ratio at $M_{Z'} = 6\ TeV$ being around $\Gamma^f_{Z'} \approx 0.03$, and reaching 0.1 when $M_{Z'} = 10.6\ TeV$.

The branching ratio for the l^+l^- channel is

$$BR(Z' \to l^+l^-) = \frac{1}{8}\frac{1 - 4(1 - \sigma_0\hat{c}_Z^2) + 8(1 - \sigma_0\hat{c}_Z^2)^2}{3 - 6(1 - \sigma_0\hat{c}_Z^2) + 8(1 - \sigma_0\hat{c}_Z^2)^2}. \tag{8.79}$$

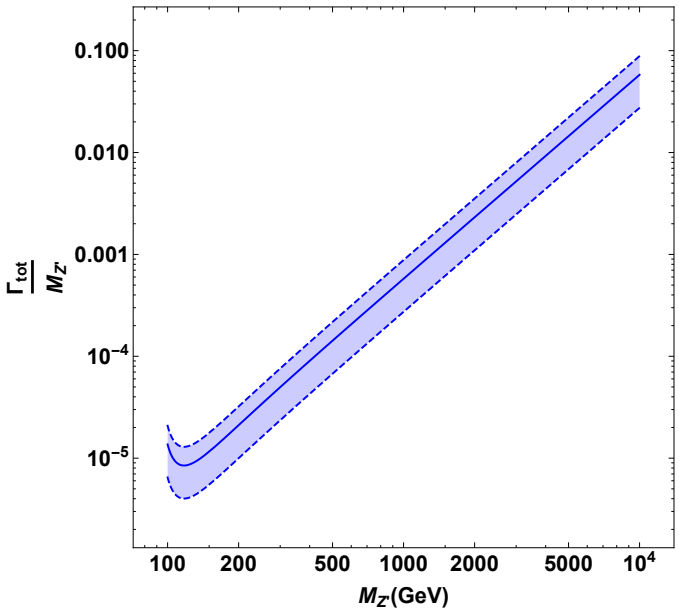

FIGURE 8.4: Width to mass ratio for the Z' boson as a function of the Z' mass. The solid line corresponds to the predictions using the central value of ρ_0 and the shadow band to the 1σ region for $\rho_0 - 1$.

The coefficients $c_{u,d}$ can be obtained from Eqs.(8.73,8.74) with $g' = g_{Z'}$ and the vector and axial factors in Eq. (8.77)

$$c_u = \frac{\pi\alpha}{36\hat{s}_Z^2\hat{c}_Z^2}\frac{(\rho_0-1)(\rho_0\hat{c}_Z^2-\hat{s}_Z^2)}{\hat{c}_Z^2\sigma_0(\rho_0-\sigma_0)}\left[9-24(1-\sigma_0\hat{c}_Z^2)+32(1-\sigma_0\hat{c}_Z^2)^2\right]BR(Z'\to l^+l^-), \tag{8.80}$$

$$c_d = \frac{\pi\alpha}{36\hat{s}_Z^2\hat{c}_Z^2}\frac{(\rho_0-1)(\rho_0\hat{c}_Z^2-\hat{s}_Z^2)}{\hat{c}_Z^2\sigma_0(\rho_0-\sigma_0)}\left[9-12(1-\sigma_0\hat{c}_Z^2)+8(1-\sigma_0\hat{c}_Z^2)^2\right]BR(Z'\to l^+l^-). \tag{8.81}$$

From here we can see that these coefficients are in fact linearly correlated, independently of the value of $BR(Z'\to l^+l^-)$, as

$$c_u = \frac{9-24(1-\sigma_0\hat{c}_Z^2)+32(1-\sigma_0\hat{c}_Z^2)^2}{9-12(1-\sigma_0\hat{c}_Z^2)+8(1-\sigma_0\hat{c}_Z^2)^2}c_d. \tag{8.82}$$

This relation depends on $M_{Z'}^2$, but for large values of the Z' mass, it reaches an asymptotic constant value,

$$c_u = \frac{17}{5}c_d. \tag{8.83}$$

At this point, the branching ratio in Eq.(8.79) reaches a saturation value $BR(l^+l^-) = 1/8$ and the values of the $c_{u,d}$ are proportional to $M^2_{Z'}$

$$c_u \approx \frac{17}{8}\frac{\pi\alpha}{36\hat{s}^2_Z\hat{c}^2_Z}\frac{(\rho_0\hat{c}^2_Z - \hat{s}^2_Z)}{\rho_0}\frac{(\rho_0 - 1)}{\hat{c}^2_Z\sigma_0} = 1.67\times 10^{-6}\frac{M^2_{Z'}}{M^2_W}, \tag{8.84}$$

$$c_d \approx \frac{5}{8}\frac{\pi\alpha}{36\hat{s}^2_Z\hat{c}^2_Z}\frac{(\rho_0\hat{c}^2_Z - \hat{s}^2_Z)}{\rho_0}\frac{(\rho_0 - 1)}{\hat{c}^2_Z\sigma_0} = 0.49\times 10^{-6}\frac{M^2_{Z'}}{M^2_W}. \tag{8.85}$$

Note that in this context, a large Z' mass means $\sigma_0 << 1$, satisfied for $M_{Z'} \gtrsim 500\ GeV$.

The experimental data on the upper bounds for Z' production at the LHC comes in the form of $c_d - c_u$ exclusion curves for given values of $M_{Z'}$. We plot the exclusion curves from Ref. [225] in Fig. 8.5 (solid lines) and we include the values for $(c_d(M_{Z'}), c_u(M_{Z'}))$ from Eqs. (8.80,8.81) as dots for each corresponding value of $M_{Z'}$, taking the central value of ρ_0 in Eq.(8.40) and adding the 1σ region as error bars. For $M_{Z'} < 5200\ GeV$ the predicted values for c_u, c_d, including the 1σ uncertainties of ρ_0, are above the exclusion curves, thus inconsistent with the data.

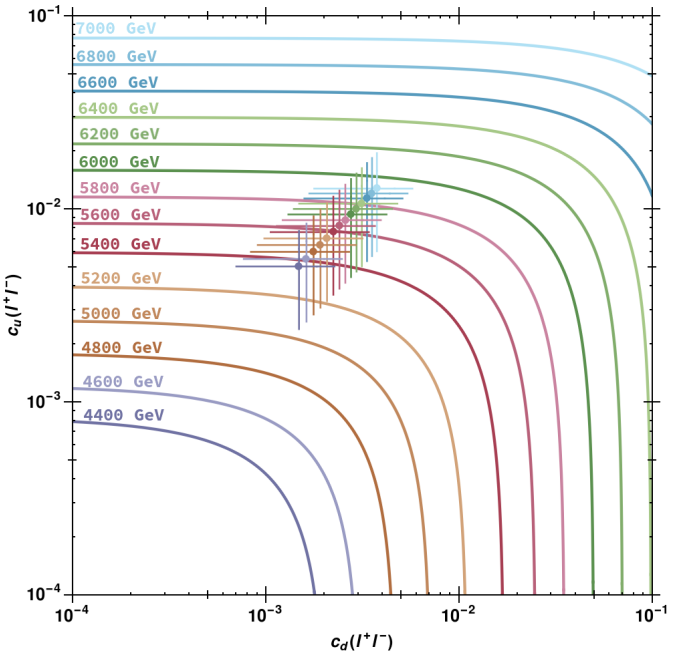

FIGURE 8.5: Exclusion curves for the c_u, c_d couplings extracted from Ref. [225] and the corresponding predictions in theories for physics BSM containing an extra spontaneously broken $U(1)_d$ and respecting custodial symmetry. Each dot corresponds to the predicted value for a given Z' boson mass from Eqs. (8.80,8.81) and is marked in the same color as the corresponding exclusion curve. Uncertainties correspond to the 1σ region for ρ_0 in Eq. (8.40).

There are uncertainties in c_u, c_d due to changes in $BR(Z' \to l^+l^-)$ coming from contributions of other decay channels to the total decay width, which need to be included for a more precise calculation.

For instance, mixing with the SM fields generates couplings of the Z' to ZZ, W^+W^- and ZH, proportional to single mixing factors s_z. The corresponding decay widths are proportional to $\rho_0 - 1$, which turns to be small compared to the decay widths to fermions, which as mentioned before, are enhanced by the $1/\sigma_0$ factor, and end up being proportional to $(\rho_0 - 1)M_{Z'}^2/M_W^2$.

Additionally, decay to non-SM particles in the ultraviolet completing theory may yield more important contributions since, from Eqs. (8.53,8.56), we can see that the corresponding coupling has the same enhancement factor as the fermion case, so we need at least a rough estimate of the decay width to these non-SM particles. Thus, it is important to work out the possibility that dark matter couple to SM fields via kinetic mixing, in which case, it is natural to expect dark matter particles with masses of the order of the electroweak scale.

We can estimate the effect of including the tensor dark matter field ψ with $U(1)_d$ charge $Q_d^\psi = 2$, which from Eq. (8.2) involves a coupling g_d with the V_μ field. This in turn creates a coupling with the Z' field, from the covariant derivative in Eq. (8.53) we can see that the Lagrangian of such interaction is

$$\mathcal{L}_{Z'\bar{\psi}\psi} = -ig_d\hat{c}_\zeta sec\hat{\chi}\Big[\bar{\psi}\Sigma^{\mu\nu}(\partial_\nu\psi) - (\partial_\nu\bar{\psi})\Sigma^{\mu\nu}\psi\Big]Z'_\mu. \tag{8.86}$$

This yields the following squared invariant amplitude

$$\begin{aligned}\sum_{\lambda,\lambda_1,\lambda_2}|M_{Z'\to\bar{\psi}\psi}|^2 = \frac{1}{3}\frac{g_d^2 c_\zeta^2 sec^2\hat{\chi}}{4M^4}\Big(-g^{\mu\alpha} + \frac{k^\mu k^\alpha}{M_{Z'}^2}\Big) \\ \times Tr\Big[\Big(S(p_2) + M_\psi^2\Big)\Sigma^{\mu\omega}(p_1 - p_2)_\omega\Big(S(p_1) + M_\psi^2\Big)\Sigma^{\nu\eta}(p_1 - p_2)_\eta\Big].\end{aligned} \tag{8.87}$$

We obtain the following decay width

$$\Gamma(Z' \to \bar{\psi}\psi) = \frac{\alpha_d\hat{c}_\zeta^2 sec^2\hat{\chi}M_{Z'}^2}{96M^4}(M_{Z'}^2 - 4M_\psi^2)^{3/2}\Big[1 - 6\Big(\frac{M_\psi}{M_{Z'}}\Big)^2 + 24\Big(\frac{M_\psi}{M_{Z'}}\Big)^4\Big], \tag{8.88}$$

where $\alpha_d = g_d^2/4\pi$ is the $U(1)_d$ fine structure constant.

This decay width depends on α_d, M_ψ and $M_{Z'}$, which are unknown, so it is not possible to find bounds with certainty. We can estimate the results by considering $M_\psi \sim 62.5\ GeV$, but the choice of the coupling must be done with care. For the results obtained

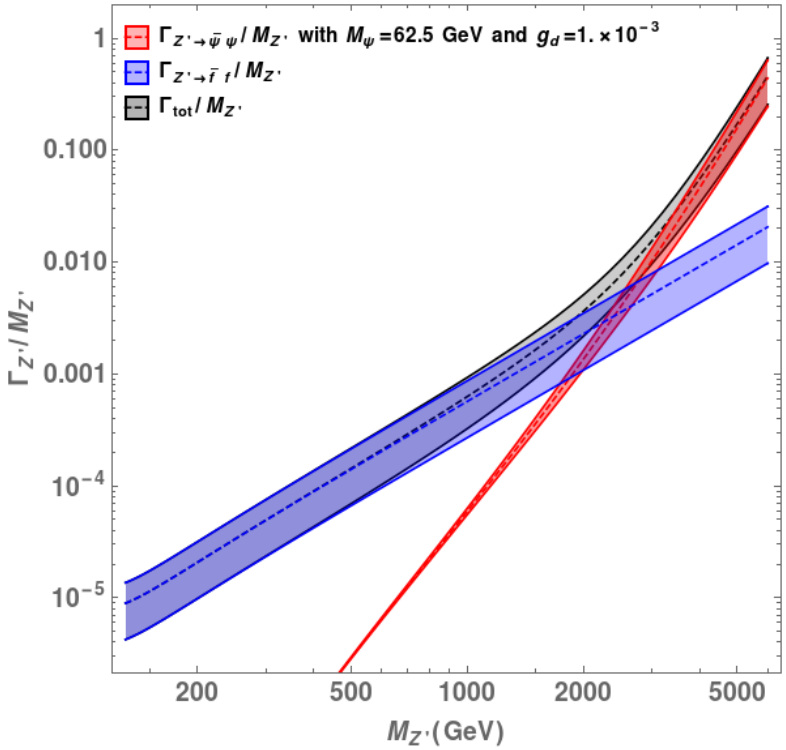

FIGURE 8.6: Width to mass ratio for the Z' boson as a function of the Z' mass with the inclusion of decay into tensor dark matter. The solid line corresponds to the predictions using the central value of ρ_0 and the shadow band to the 1σ region for $\rho_0 - 1$. We show the contribution of Z' decay into TDM (red) for $M_\psi = 62.5\ GeV$ and $g_d = 10^{-3}$, the contribution from SM fermions (blue) and the total width (black).

only with SM fermions to remain more or less unchanged, that is, for the narrow width approximation to remain valid, the Z' decay width into tensor dark matter must be of the order of the decay into fermions. For that to happen, we need the $U(1)_d$ coupling to be of around $g_d = 10^{-3}$, or equivalently, $\alpha_d = 10^{-5}\alpha$. We plot the results with these considerations in Fig. 8.6, where we can see that the narrow width approximation for this case remains valid up to masses of 6 TeV, being around 46% at this value of $M_{Z'}$. To illustrate how sensitive is this result for different values of M_ψ, we show the contributions for $M_\psi = 20, 60$ and 100 GeV in Fig. 8.7. The narrow width approximation is valid only until masses of $1 - 2$ TeV for $M_\psi = 20$ GeV and overpowers the contribution from SM fermions.

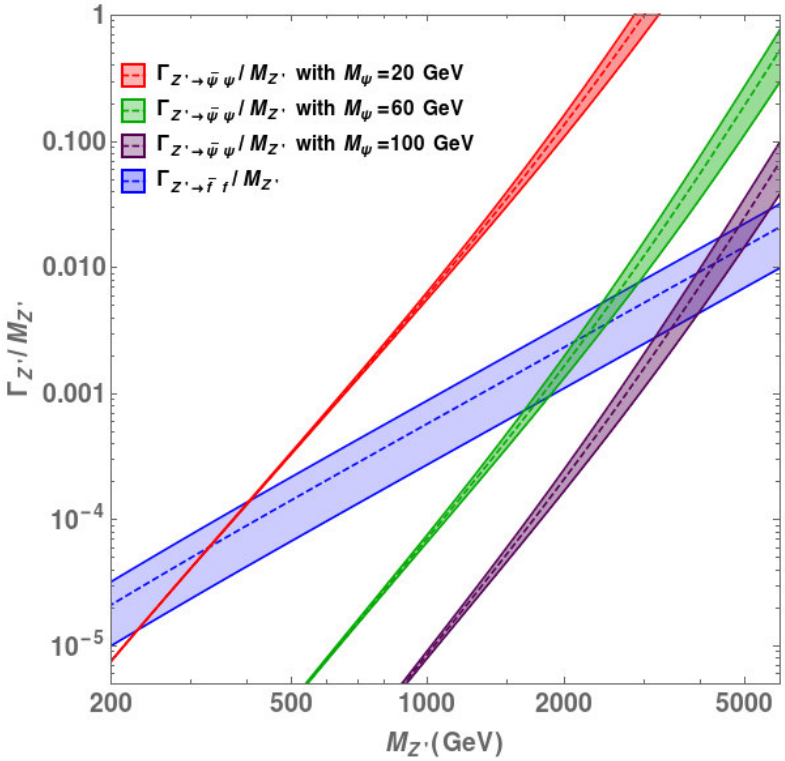

FIGURE 8.7: Width to mass ratio for the Z' boson decay into tensor dark matter as a function of the Z' mass. The solid line corresponds to the predictions using the central value of ρ_0 and the shadow band to the 1σ region for $\rho_0 - 1$. We show the contribution of Z' decay into TDM for $M_\psi = 20\ GeV$ (red), $60\ GeV$ (green) and $100\ GeV$ (purple), with $g_d = 10^{-3}$. For comparison, we show the contribution from SM fermions (blue).

Chapter 9

Conclusions and perspectives

The Standard Model, as a quantum field theory, has a history of extraordinary success at explaining several phenomenological observations. Its construction culminated with the discovery of the Higgs boson in 2012, with a measured mass $M_H = 125.25\ GeV$ [3]. After the great achievements of the Standard Model, there are still many questions yet to decipher. Some attempts to solve these questions fall into extensions or modifications of the theory, in what is called physics beyond the standard model.

One of the great mysteries yet to be solved by any theory is the nature of dark matter. There has been an extensive effort in the spawn of more than five decades to try and propose a description of this phenomenon, and yet there has been no success at finding excruciating evidence that could point out as to what exactly is dark matter. However, these efforts have at least produced a recipe that contains criteria that we must obey in order to propose a candidate that could explain this unknown content of our universe.

The standard model uses only a few of the irreps of the Homogeneous Lorentz Group: the $(1/2, 0) \oplus (0, 1/2)$ for quarks and leptons, the $(1/2, 1/2)$ for gauge bosons and the $(0, 0)$ for the Higgs boson; and proposals for physics beyond the standard model mentioned above use the very same representations. In this work we proposed a different alternative, a $(1, 0) \oplus (0, 1)$ space-time structure to describe a dark matter particle, which we call tensor dark matter. We employ the covariant basis for the single spin $(j, 0) \oplus (0, j)$ representation worked out in Ref. [73]. A field transforming in this representation is conventionally described using an equivalent antisymmetric tensor with two indices, and the quantum field theory for the $j = 1$ case was developed in Ref. [77]. We described and employed this formalism to obtain the interactions that such particle would have with standard model particles and performed the calculation of numerous processes. We compared our results with current experimental data.

As a starting point, we obtained the limits on Z and H boson decay from the measured invisible decay widths of these particles, and concluded that for tensor dark matter, masses below 42 GeV are ruled out.

Next, we calculated the relic density for tensor dark matter, and comparing our results with the measured relic abundance from the CMB data. We arrived at a relation between the TDM mass and the coupling constants of the model.

From here, we went forward to the comparison of experimental bounds from a number of observations. Firstly, from the direct detection front, we obtained the dark matter - nucleon cross section and compared this result with the experimental limits from the XENON1T experiment, finding that the spin portal coupling is heavily constrained, but the scalar Higgs coupling to tensor dark matter falls into values of the order of $\mathcal{O}(10^{-3})$ for masses around 100 GeV. Secondly, we looked into limits from indirect dark matter searches. Tensor dark matter turns out to be a consistent candidate for the explanation of the gamma ray excess in the Galactic Center, for values of the scalar coupling to the Higgs of $g_s \in [0.98, 1.01] \times 10^{-3}$ and $M \in [62.470, 62.505]$ GeV. We showed that for this mass and coupling window, other experimental observations are successfully explained, such as annihilation into $\mu^+\mu^-$, $\tau^+\tau^-$ and $\bar{b}b$ from the measurements of gamma flux of 19 dwarf spheroidal satellite galaxies. Additionally, such parameters are also consistent with dark matter annihilation into $\gamma\gamma$ from measurements of monoenergetic spectral lines from self-annihilations of DM in the central region of the Milky Way halo.

We also worked out the possibility of explaining the cosmic ray antiproton excess observed in data from the AMS-02 collaboration, and show that with the inclusion of tensor dark matter annihilating into fermions, a fit to this excess is improved for the mass window consistent with the aforementioned indirect detection limits.

In summary, we showed that tensor dark matter, a spinor-like field in the $(1,0) \oplus (0,1)$ space-time structure, is a possible description of dark matter that is consistent with relic density, constraints from Z^0 and H invisible widths, bounds from direct detection experiments such as XENON1T, and indirect detection limits from observations of the photon flux in dwarf spheroidal satellite galaxies (dSphs), the cosmic ray antiproton excess, and the Galactic Center gamma ray excess. This consistency is obtained only when the tensor dark matter has a mass $M \approx M_H/2$, specifically within the $[62.470, 62.505]$ GeV window and with a coupling to the scalar Higgs portal $g_s \in [0.98, 1.01] \times 10^{-3}$.

Such sharp prediction, along with the fact that the leading terms in the interaction Lagrangian are dimension-four, motivated us to explore a more general construction. We introduced the possibility of dark matter interactions coming from a dark gauge structure, a dark gauge group that includes a factor $U(1)_d$ subgroup that mixes kinetically with the $U(1)_Y$ of the standard model, and worked out the the formalism derived from this inclusion, in what is known as a Hidden Dark Matter gauge structure.

We showed that for an extension of the standard model with a spontaneously broken $U(1)_d$ factor dark gauge group and kinetic mixing, when the Higgs sector of such theory respects custodial symmetry, small couplings between the SM and dark sectors appear, and new mixing terms exist in the neutral gauge sector. In this hidden dark matter scenario, custodial symmetry still relates the W_μ^3 mass term to the SM Z_μ mass term. There is a tree-level mixing $\tilde{Z} - \bar{V}$ mixing which modifies the custodial symmetry relation in the extended theory, resulting in the EWPD parameter $\rho_0 \neq 1$. We calculate ρ_0 in the extended theory and use it to rewrite the Z and Z' couplings in terms of ρ_0 and the analogous ratio $\sigma_0 = M_W^2/\hat{c}_Z^2 M_{Z'}^2 \hat{\rho}$, which depend on measured observables and the mass of Z'. We studied the intermediate Z' contributions to the production of a charged lepton pair at the LHC, where the corresponding cross section can be written in terms of two parameters, c_u and c_d. These parameters carry all the information of the Z' couplings to SM fermions, and we calculated them in our formalism considering only the Z' couplings to SM fermions generated by the kinetic mixing. We compared the results of our calculation using the range of values of ρ_0 extracted from the global fit to the EWPD at the 1σ level with the exclusion curves in the $c_u - c_d$ plane for Z' masses in the range $3.8 - 7.0\ TeV$ obtained by the CMS Collaboration. Consistency of our calculation with the CMS data requires $M_{Z'} \geq 5.2\ TeV$.

There is still much work to be done in regards to this proposal. We focused mainly on observables that were prominent in the particle physics community, but there are many observables that we are yet to explore and will be important to study to continue testing our dark matter model. One aspect that was not mentioned about this framework, and unlike scalar DM models, a spin-1 DM field will have interactions with the electromagnetic multipoles, meaning that such DM particle would add E and B modes to the CMB that should be consistent with the observations. Other cosmological observations are of great importance, particularly the observed Lyman-α power spectrum and the Tully-Fisher relation.

While the ΛCDM scheme works for large-scale structures of the Universe (for distances larger than 1 Mpc), there are observations at small scales where structure formation is nonlinear and cannot be successfully described by this framework. Among these problems are the missing satellites problem (cosmological simulations of DM haloes predict large numbers of satellite galaxies while such amount is not observed in our galaxy), the cusp-core problem (many low-mass galaxies' density profiles are not in agreement with the mass density profiles of DM haloes predicted by ΛCDM simulations) and the too-big-to-fail problem (fewer galaxies with large central densities are found than what is predicted from the ΛCDM scheme). There are some proposed solutions to these problems that do not require a change in the DM framework, but there are proposals that involve modifications to the nature of the DM particle (for example, warm dark

matter). More interestingly, from the perspective of our work, dark matter with self-interactions could alleviate some of these inconsistencies. We have yet to work out the self-interactions of our model, which is an important step if we want to compare with the cosmological observations mentioned.

In the short-term, the positron excess should also be looked into. The results of this work are also on the edge of current bounds, so future observations of greater precision could discard the model. Of course, as a result of this work, we plan to continue studying the non-Abelian structure as an extension of the standard model in a more fundamental approach and the possible answers it may have for the dark matter mystery that concerns the physics community today.

Bibliography

[1] P.A.M. Dirac, *Quantum theory of emission and absorption of radiation*, *Proc. Roy. Soc. Lond. A* **114** (1927) 243.

[2] C.D. Anderson, *The positive electron*, *Phys. Rev.* **43** (1933) 491.

[3] PARTICLE DATA GROUP collaboration, *Review of Particle Physics*, *PTEP* **2020** (2020) 083C01.

[4] MUON G-2 collaboration, *Measurement of the Positive Muon Anomalous Magnetic Moment to 0.46 ppm*, *Phys. Rev. Lett.* **126** (2021) 141801 [2104.03281].

[5] L. Canetti, M. Drewes and M. Shaposhnikov, *Matter and antimatter in the universe*, *New Journal of Physics* **14** (2012) 095012.

[6] J. Schechter and J.W.F. Valle, *Neutrino masses in su(2) $\otimes$ u(1) theories*, *Phys. Rev. D* **22** (1980) 2227.

[7] PLANCK collaboration, *Planck 2018 results. VI. Cosmological parameters*, *Astron. Astrophys.* **641** (2020) A6 [1807.06209].

[8] J.G. de Swart, G. Bertone and J. van Dongen, *How dark matter came to matter*, March, 2017.

[9] G. Bertone, D. Hooper and J. Silk, *Particle dark matter: evidence, candidates and constraints*, *Physics Reports* **405** (2005) 279.

[10] F. Zwicky, *Republication of: The redshift of extragalactic nebulae*, *General Relativity and Gravitation* **41** (2009) 207.

[11] H. Poincare, *The Milky Way and the Theory of Gases*, *Popular Astronomy* **14** (1906) 475.

[12] G. Bertone and D. Hooper, *History of dark matter*, *Rev. Mod. Phys.* **90** (2018) 045002 [1605.04909].

[13] V.C. Rubin and J. Ford, W. Kent, *Rotation of the Andromeda Nebula from a Spectroscopic Survey of Emission Regions*, *Astrophysical Journal* **159** (1970) 379.

[14] D.H. Rogstad and G.S. Shostak, *Gross Properties of Five Scd Galaxies as Determined from 21-CENTIMETER Observations*, *Astrophysical Journal* **176** (1972) 315.

[15] J. Einasto, A. Kaasik and E. Saar, *Dynamic evidence on massive coronas of galaxies*, *Nature* **250** (1974) 309.

[16] J.P. Ostriker, P.J.E. Peebles and A. Yahil, *The Size and Mass of Galaxies, and the Mass of the Universe*, *Astrophysical Journal* **193** (1974) L1.

[17] A. Doroshkevich, V. Lukash and E. Mikheeva, *A solution to the problems of cusps and rotation curves in dark matter halos in the cosmological standard model*, *Physics-uspekhi - PHYS-USP* **55** (2012) .

[18] B. Paczynski, *Gravitational Microlensing by the Galactic Halo*, *Astrophysical Journal* **304** (1986) 1.

[19] MACHO collaboration, *The MACHO project: Microlensing results from 5.7 years of LMC observations*, *Astrophys. J.* **542** (2000) 281 [astro-ph/0001272].

[20] EROS collaboration, *Not enough stellar mass machos in the galactic halo*, *Astron. Astrophys.* **355** (2000) L39 [astro-ph/0002253].

[21] EROS-2 collaboration, *Limits on the Macho Content of the Galactic Halo from the EROS-2 Survey of the Magellanic Clouds*, *Astron. Astrophys.* **469** (2007) 387 [astro-ph/0607207].

[22] R.A. Alpher and R. Herman, *Evolution of the Universe*, *Nature* **162** (1948) 774.

[23] C.L. Bennett, D. Larson, J.L. Weiland, N. Jarosik, G. Hinshaw, N. Odegard et al., *Nine-year Wilkinson Microwave Anisotropy Probe (WMAP) Observations: Final Maps and Results*, *The Astrophysical Journal Supplement* **208** (2013) 20 [1212.5225].

[24] A. Friedmann, *Über die Krümmung des Raumes*, *Zeitschrift fur Physik* **10** (1922) 377.

[25] G. Lemaître, *Un Univers homogène de masse constante et de rayon croissant rendant compte de la vitesse radiale des nébuleuses extra-galactiques*, *Annales de la Société Scientifique de Bruxelles* **47** (1927) 49.

[26] E. Hubble, *A Relation between Distance and Radial Velocity among Extra-Galactic Nebulae*, *Proceedings of the National Academy of Science* **15** (1929) 168.

[27] S. Dodelson, *Modern Cosmology*, Academic Press, Amsterdam (2003).

[28] J. Bernstein, *KINETIC THEORY IN THE EXPANDING UNIVERSE*, Cambridge Monographs on Mathematical Physics, Cambridge University Press, Cambridge, U.K. (1988), 10.1017/CBO9780511564185.

[29] A.G. Riess, S. Casertano, W. Yuan, J.B. Bowers, L. Macri, J.C. Zinn et al., *Cosmic distances calibrated to 1% precision with gaia EDR3 parallaxes and hubble space telescope photometry of 75 milky way cepheids confirm tension with λCDM*, *The Astrophysical Journal Letters* **908** (2021) L6.

[30] E. Kolb and M. Turner, *The Early Universe*, Frontiers in physics, Addison-Wesley (1990).

[31] A. Lewis, A. Challinor and A. Lasenby, *Efficient computation of cosmic microwave background anisotropies in closed friedmann-robertson-walker models*, *Astrophysical Journal - ASTROPHYS J* **538** (2000) 473.

[32] D. Blas, J. Lesgourgues and T. Tram, *The cosmic linear anisotropy solving system (class). part ii: Approximation schemes*, *Journal of Cosmology and Astroparticle Physics* **2011** (2011) 034.

[33] D.J. Fixsen, *The Temperature of the Cosmic Microwave Background*, *The Astrophysical Journal* **707** (2009) 916 [0911.1955].

[34] M. Milgrom, *A modification of the Newtonian dynamics as a possible alternative to the hidden mass hypothesis.*, *Astrophysical Journal* **270** (1983) 365.

[35] M. Milgrom, *On the Use of Galaxy Rotation Curves to Test the Modified Dynamics*, *Astrophysical Journal* **333** (1988) 689.

[36] S.M. Kent, *Dark Matter in Spiral Galaxies. II. Galaxies with H I Rotation Curves*, *Astrophysical Journal* **93** (1987) 816.

[37] S.S. McGaugh, *The baryonic tully–fisher relation of gas-rich galaxies as a test of λcdm and mond*, *The Astronomical Journal* **143** (2012) 40.

[38] F. Lelli, S.S. McGaugh, J.M. Schombert, H. Desmond and H. Katz, *The baryonic Tully–Fisher relation for different velocity definitions and implications for galaxy angular momentum*, *Mon. Not. Roy. Astron. Soc.* **484** (2019) 3267 [1901.05966].

[39] S.S. McGaugh, *A tale of two paradigms: the mutual incommensurability of ΛCDM and MOND*, *Can. J. Phys.* **93** (2015) 250 [1404.7525].

[40] C. Skordis, D.F. Mota, P.G. Ferreira and C. Boehm, *Large Scale Structure in Bekenstein's theory of relativistic Modified Newtonian Dynamics*, *Phys. Rev. Lett.* **96** (2006) 011301 [astro-ph/0505519].

[41] S.D.M. White, C.S. Frenk and M. Davis, *Clustering in a neutrino-dominated universe*, *Astrophysical Journal* **274** (1983) L1.

[42] J. Hisano, K. Kohri and M.M. Nojiri, *Neutralino warm dark matter*, *Phys. Lett. B* **505** (2001) 169 [hep-ph/0011216].

[43] W.B. Lin, D.H. Huang, X. Zhang and R.H. Brandenberger, *Nonthermal production of WIMPs and the subgalactic structure of the universe*, *Phys. Rev. Lett.* **86** (2001) 954 [astro-ph/0009003].

[44] G. Gelmini and C.E. Yaguna, *Constraints on Minimal SUSY models with warm dark matter neutralinos*, *Phys. Lett. B* **643** (2006) 241 [hep-ph/0607012].

[45] R.N. Mohapatra and S. Nussinov, *Possible manifestation of heavy stable colored particles in cosmology and cosmic rays*, *Phys. Rev. D* **57** (1998) 1940.

[46] M. Taoso, G. Bertone and A. Masiero, *Dark Matter Candidates: A Ten-Point Test*, *JCAP* **03** (2008) 022 [0711.4996].

[47] R.B. Tully and J.R. Fisher, *A New method of determining distances to galaxies*, *Astron. Astrophys.* **54** (1977) 661.

[48] S.S. McGaugh, J.M. Schombert, G.D. Bothun and W.J.G. de Blok, *The baryonic tully-fisher relation*, *The Astrophysical Journal* **533** (2000) L99.

[49] H.L. Bray and A.S. Goetz, *Wave Dark Matter and the Tully-Fisher Relation*, 1409.7347.

[50] S.S. McGaugh, *The Baryonic Tully-Fisher relation of galaxies with extended rotation curves and the stellar mass of rotating galaxies*, *Astrophys. J.* **632** (2005) 859 [astro-ph/0506750].

[51] XENON collaboration, *First Dark Matter Search Results from the XENON1T Experiment*, *Phys. Rev. Lett.* **119** (2017) 181301 [1705.06655].

[52] FERMI-LAT, DES collaboration, *Searching for Dark Matter Annihilation in Recently Discovered Milky Way Satellites with Fermi-LAT*, *Astrophys. J.* **834** (2017) 110 [1611.03184].

[53] I. Cholis, T. Linden and D. Hooper, *A Robust Excess in the Cosmic-Ray Antiproton Spectrum: Implications for Annihilating Dark Matter*, *Phys. Rev. D* **99** (2019) 103026 [1903.02549].

[54] P.J. Fox, R. Harnik, J. Kopp and Y. Tsai, *LEP Shines Light on Dark Matter*, *Phys. Rev. D* **84** (2011) 014028 [1103.0240].

[55] O. Buchmueller, C. Doglioni and L.T. Wang, *Search for dark matter at colliders*, *Nature Phys.* **13** (2017) 217 [1912.12739].

[56] S. Dodelson and L.M. Widrow, *Sterile-neutrinos as dark matter*, *Phys. Rev. Lett.* **72** (1994) 17 [hep-ph/9303287].

[57] S. Gariazzo, *Light steriles with pseudoscalar interaction Cosmology*, *PoS* **NOW2016** (2017) 083 [1610.01330].

[58] M. Archidiacono, S. Gariazzo, C. Giunti, S. Hannestad, R. Hansen, M. Laveder et al., *Pseudoscalar—sterile neutrino interactions: reconciling the cosmos with neutrino oscillations*, *JCAP* **08** (2016) 067 [1606.07673].

[59] R.D. Peccei, *The Strong CP problem and axions*, *Lect. Notes Phys.* **741** (2008) 3 [hep-ph/0607268].

[60]

[61] L. Hui, J.P. Ostriker, S. Tremaine and E. Witten, *Ultralight scalars as cosmological dark matter*, *Phys. Rev. D* **95** (2017) 043541 [1610.08297].

[62] J. Ellis and K.A. Olive, *Supersymmetric Dark Matter Candidates*, 1001.3651.

[63] G. Arcadi, M. Dutra, P. Ghosh, M. Lindner, Y. Mambrini, M. Pierre et al., *The waning of the WIMP? A review of models, searches, and constraints*, *Eur. Phys. J.* **C78** (2018) 203 [1703.07364].

[64] T. Pilling, *Symmetry of massive Rarita-Schwinger fields*, *Int. J. Mod. Phys. A* **20** (2005) 2715 [hep-th/0404131].

[65] A.J. Amsel and G. Compere, *Supergravity at the boundary of AdS supergravity*, *Phys. Rev. D* **79** (2009) 085006 [0901.3609].

[66] K. Johnson and E. Sudarshan, *Inconsistency of the local field theory of charged spin32 particles*, *Annals of Physics* **13** (1961) 126.

[67] G. Velo and D. Zwanzinger, *Noncausality and other defects of interaction lagrangians for particles with spin one and higher*, *Phys. Rev.* **188** (1969) 2218.

[68] G. Velo and D. Zwanziger, *Propagation and quantization of rarita-schwinger waves in an external electromagnetic potential*, *Phys. Rev.* **186** (1969) 1337.

[69] G. Velo, *Anomalous behaviour of a massive spin two charged particle in an external electromagnetic field*, *Nuclear Physics B* **43** (1972) 389.

[70] A.Z. Capri and A. Shamaly, *On the connection between acausal propagation and the non-local structure of higher spin fields*, *Canadian Journal of Physics* **54** (1976) 1089 [https://doi.org/10.1139/p76-131].

[71] S. Deser and A. Waldron, *Acausality of massive charged spin-2 fields*, hep-th/0304050.

[72] M. Porrati and R. Rahman, *Intrinsic cutoff and acausality for massive spin 2 fields coupled to electromagnetism*, *Nuclear Physics B* **801** (2008) 174.

[73] S. Gómez-Ávila and M. Napsuciale, *Covariant basis induced by parity for the $(j,0)\bigoplus(0,j)$ representation*, *Phys. Rev. D* **88** (2013) 096012 [1307.4711].

[74] S. Weinberg, *The Quantum Theory of Fields*, vol. 1, Cambridge University Press (1995), 10.1017/CBO9781139644167.

[75] S. Weinberg, *Feynman rules for any spin*, *Phys. Rev.* **133** (1964) B1318.

[76] E. Delgado-Acosta, M. Kirchbach, M. Napsuciale and S. Rodriguez, *Electromagnetic multipole moments of elementary spin-1/2, 1, and 3/2 particles*, *Phys.Rev.* **D85** (2012) 116006 [1204.5337].

[77] M. Napsuciale, S. Rodríguez, R. Ferro-Hernández and S. Gómez-Ávila, *Spin one matter fields*, *Phys. Rev.* **D93** (2016) 076003 [1509.07938].

[78] P.A.M. Dirac, *Lectures on quantum mechanics*, New York : Belfer Graduate School of Science, Yeshiva University (1964).

[79] H. Hernández-Arellano, M. Napsuciale and S. Rodríguez, *Spin portal to dark matter*, *Phys. Rev.* **D98** (2018) 015001 [1801.09853].

[80] H. Hernández-Arellano, M. Napsuciale and S. Rodríguez, *Spin-one dark matter and gamma ray signals from the galactic center*, *JHEP* **08** (2020) 106 [1911.01604].

[81] MuLan collaboration, *Measurement of the Positive Muon Lifetime and Determination of the Fermi Constant to Part-per-Million Precision*, *Phys. Rev. Lett.* **106** (2011) 041803 [1010.0991].

[82] Particle Data Group collaboration, *Review of Particle Physics*, *Chin. Phys.* **C40** (2016 and 2017 update) 100001.

[83] CMS collaboration, *Searches for invisible decays of the Higgs boson in pp collisions at sqrt(s) = 7, 8, and 13 TeV*, *JHEP* **02** (2017) 135 [1610.09218].

[84] M. Cannoni, *Lorentz invariant relative velocity and relativistic binary collisions*, *International Journal of Modern Physics A* **32** (2016) .

[85] Planck collaboration, *Planck 2015 results. XIII. Cosmological parameters*, *Astron. Astrophys.* **594** (2016) A13 [1502.01589].

[86] P. Gondolo and G. Gelmini, *Cosmic abundances of stable particles: Improved analysis*, *Nucl. Phys.* **B360** (1991) 145.

[87] M. Cannoni, *Lorentz invariant relative velocity and relativistic binary collisions*, *Int. J. Mod. Phys.* **A32** (2017) 1730002 [1605.00569].

[88] K. Griest and D. Seckel, *Three exceptions in the calculation of relic abundances*, *Phys. Rev.* **D43** (1991) 3191.

[89] L. Bergstrom and G. Hulth, *Induced Higgs Couplings to Neutral Bosons in e^+e^- Collisions*, *Nucl. Phys.* **B259** (1985) 137.

[90] A. Barroso, J. Pulido and J.C. Romao, *HIGGS PRODUCTION AT e+ e- COLLIDERS*, *Nucl. Phys.* **B267** (1986) 509.

[91] R. Bonciani, V. Del Duca, H. Frellesvig, J.M. Henn, F. Moriello and V.A. Smirnov, *Next-to-leading order QCD corrections to the decay width $H \to Z\gamma$*, *JHEP* **08** (2015) 108 [1505.00567].

[92] PARTICLE DATA GROUP collaboration, *Review of Particle Physics*, *Phys. Rev.* **D98** (2018) 030001.

[93] G. Bertone, *Particle Dark Matter : Observations, Models and Searches*, Cambridge University Press (2010), 10.1017/CBO9780511770739.

[94] M.W. Goodman and E. Witten, *Detectability of certain dark-matter candidates*, *Phys. Rev. D* **31** (1985) 3059.

[95] T. Marrodan Undagoitia and L. Rauch, *Dark matter direct-detection experiments*, *J. Phys.* **G43** (2016) 013001 [1509.08767].

[96] J.I. Read, *The Local Dark Matter Density*, *J. Phys. G* **41** (2014) 063101 [1404.1938].

[97] G. Jungman, M. Kamionkowski and K. Griest, *Supersymmetric dark matter*, *Phys. Rept.* **267** (1996) 195 [hep-ph/9506380].

[98] XENON100 collaboration, *XENON100 Dark Matter Results from a Combination of 477 Live Days*, *Phys. Rev.* **D94** (2016) 122001 [1609.06154].

[99] M. Cirelli, E. Del Nobile and P. Panci, *Tools for model-independent bounds in direct dark matter searches*, *JCAP* **1310** (2013) 019 [1307.5955].

[100] P. Gondolo, J. Edsjo, P. Ullio, L. Bergstrom, M. Schelke and E.A. Baltz, *DarkSUSY: Computing supersymmetric dark matter properties numerically*, *JCAP* **07** (2004) 008 [astro-ph/0406204].

[101] D. Hooper and L. Goodenough, *Dark Matter Annihilation in The Galactic Center As Seen by the Fermi Gamma Ray Space Telescope*, *Phys. Lett.* **B697** (2011) 412 [1010.2752].

[102] A. Boyarsky, D. Malyshev and O. Ruchayskiy, *A comment on the emission from the Galactic Center as seen by the Fermi telescope*, *Phys. Lett.* **B705** (2011) 165 [1012.5839].

[103] D. Hooper and T. Linden, *On The Origin Of The Gamma Rays From The Galactic Center*, *Phys. Rev.* **D84** (2011) 123005 [1110.0006].

[104] K.N. Abazajian and M. Kaplinghat, *Detection of a Gamma-Ray Source in the Galactic Center Consistent with Extended Emission from Dark Matter Annihilation and Concentrated Astrophysical Emission*, *Phys. Rev.* **D86** (2012) 083511 [1207.6047].

[105] O. Macias and C. Gordon, *Contribution of cosmic rays interacting with molecular clouds to the Galactic Center gamma-ray excess*, *Phys. Rev.* **D89** (2014) 063515 [1312.6671].

[106] C. Gordon and O. Macias, *Dark Matter and Pulsar Model Constraints from Galactic Center Fermi-LAT Gamma Ray Observations*, *Phys. Rev.* **D88** (2013) 083521 [1306.5725].

[107] K.N. Abazajian, N. Canac, S. Horiuchi and M. Kaplinghat, *Astrophysical and Dark Matter Interpretations of Extended Gamma-Ray Emission from the Galactic Center*, *Phys. Rev.* **D90** (2014) 023526 [1402.4090].

[108] T. Daylan, D.P. Finkbeiner, D. Hooper, T. Linden, S.K.N. Portillo, N.L. Rodd et al., *The characterization of the gamma-ray signal from the central Milky Way: A case for annihilating dark matter*, *Phys. Dark Univ.* **12** (2016) 1 [1402.6703].

[109] F. Calore, I. Cholis and C. Weniger, *Background Model Systematics for the Fermi GeV Excess*, *JCAP* **1503** (2015) 038 [1409.0042].

[110] B. Zhou, Y.-F. Liang, X. Huang, X. Li, Y.-Z. Fan, L. Feng et al., *GeV excess in the Milky Way: The role of diffuse galactic gamma-ray emission templates*, *Phys. Rev.* **D91** (2015) 123010 [1406.6948].

[111] FERMI-LAT collaboration, *Fermi-LAT Observations of High-Energy γ-Ray Emission Toward the Galactic Center*, *Astrophys. J.* **819** (2016) 44 [1511.02938].

[112] FERMI-LAT collaboration, *The Fermi Galactic Center GeV Excess and Implications for Dark Matter*, *Astrophys. J.* **840** (2017) 43 [1704.03910].

[113] F. Yusef-Zadeh et al., *Interacting Cosmic Rays with Molecular Clouds: A Bremsstrahlung Origin of Diffuse High Energy Emission from the Inner 2deg by 1deg of the Galactic Center*, *Astrophys. J.* **762** (2013) 33 [1206.6882].

[114] T. Linden, E. Lovegrove and S. Profumo, *The Morphology of Hadronic Emission Models for the Gamma-Ray Source at the Galactic Center*, *Astrophys. J.* **753** (2012) 41 [1203.3539].

[115] E. Carlson and S. Profumo, *Cosmic Ray Protons in the Inner Galaxy and the Galactic Center Gamma-Ray Excess*, *Phys. Rev.* **D90** (2014) 023015 [1405.7685].

[116] J. Petrovic, P.D. Serpico and G. Zaharijas, *Galactic Center gamma-ray "excess" from an active past of the Galactic Centre?*, *JCAP* **1410** (2014) 052 [1405.7928].

[117] I. Cholis, D. Hooper and T. Linden, *Challenges in Explaining the Galactic Center Gamma-Ray Excess with Millisecond Pulsars*, *JCAP* **1506** (2015) 043 [1407.5625].

[118] M. Carena, J. Osborne, N.R. Shah and C.E.M. Wagner, *Return of the WIMP: Missing energy signals and the Galactic Center excess*, *Phys. Rev.* **D100** (2019) 055002 [1905.03768].

[119] J.M. Cline, K. Kainulainen, P. Scott and C. Weniger, *Update on scalar singlet dark matter*, *Phys. Rev.* **D88** (2013) 055025 [1306.4710].

[120] N. Okada and O. Seto, *Gamma ray emission in Fermi bubbles and Higgs portal dark matter*, *Phys. Rev.* **D89** (2014) 043525 [1310.5991].

[121] T. Mondal and T. Basak, *Class of Higgs-portal Dark Matter models in the light of gamma-ray excess from Galactic center*, *Phys. Lett.* **B744** (2015) 208 [1405.4877].

[122] P. Agrawal, B. Batell, P.J. Fox and R. Harnik, *WIMPs at the Galactic Center*, *JCAP* **1505** (2015) 011 [1411.2592].

[123] T. Lacroix, C. Boehm and J. Silk, *Fitting the Fermi-LAT GeV excess: On the importance of including the propagation of electrons from dark matter*, *Phys. Rev.* **D90** (2014) 043508 [1403.1987].

[124] F. Calore, I. Cholis, C. McCabe and C. Weniger, *A Tale of Tails: Dark Matter Interpretations of the Fermi GeV Excess in Light of Background Model Systematics*, *Phys. Rev.* **D91** (2015) 063003 [1411.4647].

[125] M. Duerr, P. Fileviez Perez and J. Smirnov, *Gamma-Ray Excess and the Minimal Dark Matter Model*, *JHEP* **06** (2016) 008 [1510.07562].

[126] A. Cuoco, B. Eiteneuer, J. Heisig and M. Kramer, *A global fit of the γ-ray galactic center excess within the scalar singlet Higgs portal model*, *JCAP* **1606** (2016) 050 [1603.08228].

[127] F.S. Sage and R. Dick, *Gamma ray signals of the annihilation of Higgs-portal singlet dark matter*, 1604.04589.

[128] T.R. Slatyer, *Indirect Detection of Dark Matter*, in *Theoretical Advanced Study Institute in Elementary Particle Physics: Anticipating the Next Discoveries in Particle Physics*, pp. 297–353, 2018, DOI [1710.05137].

[129] S. Gillessen, F. Eisenhauer, S. Trippe, T. Alexander, R. Genzel, F. Martins et al., *Monitoring stellar orbits around the Massive Black Hole in the Galactic Center*, *Astrophys. J.* **692** (2009) 1075 [0810.4674].

[130] J.F. Navarro, C.S. Frenk and S.D.M. White, *The Structure of cold dark matter halos*, *Astrophys. J.* **462** (1996) 563 [astro-ph/9508025].

[131] A.W. Graham, D. Merritt, B. Moore, J. Diemand and B. Terzic, *Empirical models for Dark Matter Halos. I. Nonparametric Construction of Density Profiles and Comparison with Parametric Models*, *Astron. J.* **132** (2006) 2685 [astro-ph/0509417].

[132] E. Retana-Montenegro, E. Van Hese, G. Gentile, M. Baes and F. Frutos-Alfaro, *Analytical properties of einasto dark matter haloes*, *Astronomy & Astrophysics* **540** (2012) A70.

[133] J.F. Navarro, A. Ludlow, V. Springel, J. Wang, M. Vogelsberger, S.D.M. White et al., *The diversity and similarity of simulated cold dark matter haloes*, *Monthly Notices of the Royal Astronomical Society* **402** (2010) 21 [https://academic.oup.com/mnras/article-pdf/402/1/21/18573804/mnras0402-0021.pdf].

[134] A. Burkert, *The Structure of dark matter halos in dwarf galaxies*, *Astrophys. J. Lett.* **447** (1995) L25 [astro-ph/9504041].

[135] K.G. Begeman, A.H. Broeils and R.H. Sanders, *Extended rotation curves of spiral galaxies: dark haloes and modified dynamics*, *Monthly Notices of the Royal Astronomical Society* **249** (1991) 523 [https://academic.oup.com/mnras/article-pdf/249/3/523/18160929/mnras249-0523.pdf].

[136] M. Cirelli, G. Corcella, A. Hektor, G. Hutsi, M. Kadastik, P. Panci et al., *PPPC 4 DM ID: A Poor Particle Physicist Cookbook for Dark Matter Indirect Detection*, *JCAP* **03** (2011) 051 [1012.4515].

[137] H. Zhao, *Analytical models for galactic nuclei*, *Mon. Not. Roy. Astron. Soc.* **278** (1996) 488 [astro-ph/9509122].

[138] S. Ghigna, B. Moore, F. Governato, G. Lake, T.R. Quinn and J. Stadel, *Density profiles and substructure of dark matter halos. Converging results at ultra-high numerical resolution*, *Astrophys. J.* **544** (2000) 616 [astro-ph/9910166].

[139] L. Bergstrom, T. Bringmann, I. Cholis, D. Hooper and C. Weniger, *New Limits on Dark Matter Annihilation from AMS Cosmic Ray Positron Data*, *Phys. Rev. Lett.* **111** (2013) 171101 [1306.3983].

[140] AMS collaboration, *First Result from the Alpha Magnetic Spectrometer on the International Space Station: Precision Measurement of the Positron Fraction in Primary Cosmic Rays of* $0.5 - 350$ *GeV*, *Phys. Rev. Lett.* **110** (2013) 141102.

[141] J.L. Lucio Martinez and M. Napsuciale, *Loop effects in phi –> pi+ pi- gamma*, *Phys. Lett.* **B331** (1994) 418.

[142] M. Cirelli, G. Corcella, A. Hektor, G. Hütsi, M. Kadastik, P. Panci et al., *PPPC 4 DM ID: a poor particle physicist cookbook for dark matter indirect detection*, *Journal of Cosmology and Astroparticle Physics* **2011** (2011) 051.

[143] P. Ciafaloni, M. Cirelli, D. Comelli, A. De Simone, A. Riotto and A. Urbano, *On the Importance of Electroweak Corrections for Majorana Dark Matter Indirect Detection*, *JCAP* **06** (2011) 018 [1104.2996].

[144] J. Buch, M. Cirelli, G. Giesen and M. Taoso, *PPPC 4 DM secondary: A Poor Particle Physicist Cookbook for secondary radiation from Dark Matter*, *JCAP* **09** (2015) 037 [1505.01049].

[145] J. Diemand, B. Moore and J. Stadel, *Convergence and scatter of cluster density profiles*, *Mon. Not. Roy. Astron. Soc.* **353** (2004) 624 [astro-ph/0402267].

[146] J.D. Simon and M. Geha, *The Kinematics of the Ultra-Faint Milky Way Satellites: Solving the Missing Satellite Problem*, *Astrophys. J.* **670** (2007) 313 [0706.0516].

[147] SDSS collaboration, *Cats and Dogs, Hair and A Hero: A Quintet of New Milky Way Companions*, *Astrophys. J.* **654** (2007) 897 [astro-ph/0608448].

[148] L.E. Strigari, S.M. Koushiappas, J.S. Bullock, M. Kaplinghat, J.D. Simon, M. Geha et al., *The Most Dark Matter Dominated Galaxies: Predicted Gamma-ray Signals from the Faintest Milky Way Dwarfs*, *Astrophys. J.* **678** (2008) 614 [0709.1510].

[149] J. Diemand, M. Kuhlen, P. Madau, M. Zemp, B. Moore, D. Potter et al., *Clumps and streams in the local dark matter distribution*, *Nature* **454** (2008) 735 [0805.1244].

[150] V. Springel, J. Wang, M. Vogelsberger, A. Ludlow, A. Jenkins, A. Helmi et al., *The Aquarius Project: the subhalos of galactic halos*, *Mon. Not. Roy. Astron. Soc.* **391** (2008) 1685 [0809.0898].

[151] A. Geringer-Sameth, S.M. Koushiappas and M. Walker, *Dwarf galaxy annihilation and decay emission profiles for dark matter experiments*, *Astrophys. J.* **801** (2015) 74 [1408.0002].

[152] FERMI-LAT collaboration, *Dark Matter Constraints from Observations of 25 Milky Way Satellite Galaxies with the Fermi Large Area Telescope*, *Phys. Rev. D* **89** (2014) 042001 [1310.0828].

[153] T. Bringmann, J. Edsjö, P. Gondolo, P. Ullio and L. Bergström, *DarkSUSY 6 : An Advanced Tool to Compute Dark Matter Properties Numerically*, *JCAP* **07** (2018) 033 [1802.03399].

[154] FERMI-LAT collaboration, *Updated search for spectral lines from Galactic dark matter interactions with pass 8 data from the Fermi Large Area Telescope*, *Phys. Rev.* **D91** (2015) 122002 [1506.00013].

[155] HESS collaboration, *Search for γ-Ray Line Signals from Dark Matter Annihilations in the Inner Galactic Halo from 10 Years of Observations with H.E.S.S.*, *Phys. Rev. Lett.* **120** (2018) 201101 [1805.05741].

[156] O. Adriani and B. Alpat, *The magnetic spectrometer PAMELA for the study of cosmic antimatter in space*, .

[157] S. Ahlen et al., *An Antimatter spectrometer in space*, *Nucl. Instrum. Meth. A* **350** (1994) 351.

[158] R. Battiston, *The antimatter spectrometer (AMS-02): A particle physics detector in space*, *Nuclear Instruments and Methods in Physics Research A* **588** (2008) 227.

[159] PAMELA collaboration, *PAMELA Measurements of Cosmic-ray Proton and Helium Spectra*, *Science* **332** (2011) 69 [1103.4055].

[160] AMS COLLABORATION collaboration, *Precision measurement of the proton flux in primary cosmic rays from rigidity 1 gv to 1.8 tv with the alpha magnetic spectrometer on the international space station*, *Phys. Rev. Lett.* **114** (2015) 171103.

[161] AMS COLLABORATION collaboration, *Precision measurement of the helium flux in primary cosmic rays of rigidities 1.9 gv to 3 tv with the alpha magnetic spectrometer on the international space station*, *Phys. Rev. Lett.* **115** (2015) 211101.

[162] AMS COLLABORATION collaboration, *Precision measurement of the boron to carbon flux ratio in cosmic rays from 1.9 gv to 2.6 tv with the alpha magnetic spectrometer on the international space station*, *Phys. Rev. Lett.* **117** (2016) 231102.

[163] T. Bringmann, M. Vollmann and C. Weniger, *Updated cosmic-ray and radio constraints on light dark matter: Implications for the GeV gamma-ray excess at the Galactic center*, *Phys. Rev. D* **90** (2014) 123001 [1406.6027].

[164] M. Cirelli, D. Gaggero, G. Giesen, M. Taoso and A. Urbano, *Antiproton constraints on the GeV gamma-ray excess: a comprehensive analysis*, *JCAP* **12** (2014) 045 [1407.2173].

[165] D. Hooper, T. Linden and P. Mertsch, *What Does The PAMELA Antiproton Spectrum Tell Us About Dark Matter?*, *JCAP* **03** (2015) 021 [1410.1527].

[166] M.-Y. Cui, Q. Yuan, Y.-L.S. Tsai and Y.-Z. Fan, *Possible dark matter annihilation signal in the AMS-02 antiproton data*, *Phys. Rev. Lett.* **118** (2017) 191101 [1610.03840].

[167] A. Cuoco, J. Heisig, M. Korsmeier and M. Krämer, *Probing dark matter annihilation in the Galaxy with antiprotons and gamma rays*, *JCAP* **10** (2017) 053 [1704.08258].

[168] A. Cuoco, M. Krämer and M. Korsmeier, *Novel dark matter constraints from antiprotons in light of ams-02*, *Phys. Rev. Lett.* **118** (2017) 191102.

[169] S.-J. Lin, X.-J. Bi, J. Feng, P.-F. Yin and Z.-H. Yu, *Systematic study on the cosmic ray antiproton flux*, *Phys. Rev. D* **96** (2017) 123010.

[170] S.J. Clark, B. Dutta and L.E. Strigari, *Dark matter annihilation into four-body final states and implications for the ams antiproton excess*, *Phys. Rev. D* **97** (2018) 023003.

[171] J. Heisig, M. Korsmeier and M.W. Winkler, *Dark matter or correlated errors: Systematics of the AMS-02 antiproton excess*, *Phys. Rev. Res.* **2** (2020) 043017 [2005.04237].

[172] M. Boudaud, Y. Génolini, L. Derome, J. Lavalle, D. Maurin, P. Salati et al., *AMS-02 antiprotons' consistency with a secondary astrophysical origin*, *Phys. Rev. Res.* **2** (2020) 023022 [1906.07119].

[173] R.L. Golden, S. Horan, B.G. Mauger, G.D. Badhwar, J.L. Lacy, S.A. Stephens et al., *EVIDENCE FOR THE EXISTENCE OF COSMIC RAY ANTI-PROTONS*, *Phys. Rev. Lett.* **43** (1979) 1196.

[174] E.A. Bogomolov, N.D. Lubyanaya, V.A. Romanov, S.V. Stepanov and M.S. Shulakova, *a Stratospheric Magnetic Spectrometer Investigation of the Singly Charged Component Spectra and Composition of the Primary and Secondary Cosmic Radiation*, in *International Cosmic Ray Conference*, International Cosmic Ray Conference, (Kyoto, Japan), ICRC, 1979.

[175] K.M. Ferriere, *The interstellar environment of our galaxy*, *Rev. Mod. Phys.* **73** (2001) 1031 [astro-ph/0106359].

[176] C.S. Shen and G.B. Berkey, *Antiprotons and positrons in cosmic rays*, *Phys. Rev.* **171** (1968) 1344.

[177] A. Barrau, G. Boudoul, F. Donato, D. Maurin, P. Salati and R. Taillet, *Anti-protons from primordial black holes*, *Astron. Astrophys.* **388** (2002) 676 [astro-ph/0112486].

[178] A.S. Beach, J.J. Beatty, A. Bhattacharyya, C. Bower, S. Coutu, M.A. DuVernois et al., *Measurement of the cosmic-ray antiproton-to-proton abundance ratio between 4 and 50 gev*, *Phys. Rev. Lett.* **87** (2001) 271101.

[179] I.V. Moskalenko, A.W. Strong, J.F. Ormes and M.S. Potgieter, *Secondary anti-protons and propagation of cosmic rays in the galaxy and heliosphere*, *Astrophys. J.* **565** (2002) 280 [astro-ph/0106567].

[180] A.W. Strong and I.V. Moskalenko, *Propagation of cosmic-ray nucleons in the galaxy*, *The Astrophysical Journal* **509** (1998) 212.

[181] L.J. Gleeson and W.I. Axford, *Solar Modulation of Galactic Cosmic Rays*, *Astrophysical Journal* **154** (1968) 1011.

[182] M. Potgieter, *Solar modulation of cosmic rays*, *Living Reviews in Solar Physics* **10** (2013) .

[183] I. Moskalenko, A. Strong, J. Ormes and S. Mashnik, *Propagation of secondary antiprotons and cosmic rays in the Galaxy*, *Advances in Space Research* **35** (2005) 156.

[184] M. di Mauro, F. Donato, A. Goudelis and P.D. Serpico, *New evaluation of the antiproton production cross section for cosmic ray studies*, *Phys. Rev. D* **90** (2014) 085017 [1408.0288].

[185] I. Cholis, D. Hooper and T. Linden, *Possible evidence for the stochastic acceleration of secondary antiprotons by supernova remnants*, *Phys. Rev. D* **95** (2017) 123007.

[186] I. Cholis, D. Hooper and T. Linden, *A predictive analytic model for the solar modulation of cosmic rays*, *Phys. Rev. D* **93** (2016) 043016.

[187] AMS COLLABORATION collaboration, *Antiproton flux, antiproton-to-proton flux ratio, and properties of elementary particle fluxes in primary cosmic rays measured with the alpha magnetic spectrometer on the international space station*, *Phys. Rev. Lett.* **117** (2016) 091103.

[188] N. Arkani-Hamed, D.P. Finkbeiner, T.R. Slatyer and N. Weiner, *A Theory of Dark Matter*, *Phys. Rev. D* **79** (2009) 015014 [0810.0713].

[189] M. Baumgart, C. Cheung, J.T. Ruderman, L.-T. Wang and I. Yavin, *Non-Abelian Dark Sectors and Their Collider Signatures*, *JHEP* **04** (2009) 014 [0901.0283].

[190] C. Cheung, J.T. Ruderman, L.-T. Wang and I. Yavin, *Kinetic Mixing as the Origin of Light Dark Scales*, *Phys. Rev. D* **80** (2009) 035008 [0902.3246].

[191] A. Ibarra, A. Ringwald, D. Tran and C. Weniger, *Cosmic Rays from Leptophilic Dark Matter Decay via Kinetic Mixing*, *JCAP* **08** (2009) 017 [0903.3625].

[192] A. Hook, E. Izaguirre and J.G. Wacker, *Model Independent Bounds on Kinetic Mixing*, *Adv. High Energy Phys.* **2011** (2011) 859762 [1006.0973].

[193] E.J. Chun, J.-C. Park and S. Scopel, *Dark matter and a new gauge boson through kinetic mixing*, *JHEP* **02** (2011) 100 [1011.3300].

[194] Y. Mambrini, *The Kinetic dark-mixing in the light of CoGENT and XENON100*, *JCAP* **09** (2010) 022 [1006.3318].

[195] Y. Mambrini, *The ZZ′ kinetic mixing in the light of the recent direct and indirect dark matter searches*, *JCAP* **07** (2011) 009 [1104.4799].

[196] B. Brahmachari and A. Raychaudhuri, *Kinetic mixing and symmetry breaking dependent interactions of the dark photon*, *Nucl. Phys. B* **887** (2014) 441 [1409.2082].

[197] C.A. Arguelles, X.-G. He, G. Ovanesyan, T. Peng and M.J. Ramsey-Musolf, *Dark Gauge Bosons: LHC Signatures of Non-Abelian Kinetic Mixing*, *Phys. Lett. B* **770** (2017) 101 [1604.00044].

[198] G. Belanger, J. Da Silva and H.M. Tran, *Dark matter in U(1) extensions of the MSSM with gauge kinetic mixing*, *Phys. Rev. D* **95** (2017) 115017 [1703.03275].

[199] G. Arcadi, T. Hugle and F.S. Queiroz, *The Dark $L_\mu - L_\tau$ Rises via Kinetic Mixing*, *Phys. Lett. B* **784** (2018) 151 [1803.05723].

[200] R. Foot, *Implications of mirror dark matter kinetic mixing for CMB anisotropies*, *Phys. Lett. B* **718** (2013) 745 [1208.6022].

[201] A. Kamada, M. Yamada and T.T. Yanagida, *Self-interacting dark matter with a vector mediator: kinetic mixing with the* $\mathrm{U}(1)_{(B-L)_3}$ *gauge boson*, *JHEP* **03** (2019) 021 [1811.02567].

[202] T.G. Rizzo, *Kinetic mixing, dark photons and an extra dimension. Part I*, *JHEP* **07** (2018) 118 [1801.08525].

[203] T.G. Rizzo, *Kinetic mixing, dark photons and extra dimensions. Part II: fermionic dark matter*, *JHEP* **10** (2018) 069 [1805.08150].

[204] T.G. Rizzo, *Kinetic Mixing and Portal Matter Phenomenology*, *Phys. Rev. D* **99** (2019) 115024 [1810.07531].

[205] A. Banerjee, G. Bhattacharyya, D. Chowdhury and Y. Mambrini, *Dark matter seeping through dynamic gauge kinetic mixing*, *JCAP* **12** (2019) 009 [1905.11407].

[206] T.D. Rueter and T.G. Rizzo, *Towards A UV-Model of Kinetic Mixing and Portal Matter*, *Phys. Rev. D* **101** (2020) 015014 [1909.09160].

[207] LUX collaboration, *First direct detection constraint on mirror dark matter kinetic mixing using LUX 2013 data*, *Phys. Rev. D* **101** (2020) 012003 [1908.03479].

[208] J. Lao, C. Cai, Z.-H. Yu, Y.-P. Zeng and H.-H. Zhang, *Fermionic and scalar dark matter with hidden* $\mathrm{U}(1)$ *gauge interaction and kinetic mixing*, *Phys. Rev. D* **101** (2020) 095031 [2003.02516].

[209] J. Gehrlein and M. Pierre, *A testable hidden-sector model for Dark Matter and neutrino masses*, *JHEP* **02** (2020) 068 [1912.06661].

[210] G.D. Kribs, D. McKeen and N. Raj, *Breaking up the Proton: An Affair with Dark Forces*, *Phys. Rev. Lett.* **126** (2021) 011801 [2007.15655].

[211] D. Binh, V. Binh and H. Long, *Bounds on Dipole Moments of hidden Dark Matter through kinetic mixing*, 2006.09020.

[212] P. Barnes, Z. Johnson, A. Pierce and B. Shakya, *Simple Hidden Sector Dark Matter*, *Phys. Rev. D* **102** (2020) 075019 [2003.13744].

[213] K. Babu, C.F. Kolda and J. March-Russell, *Implications of generalized Z - Z-prime mixing*, *Phys. Rev. D* **57** (1998) 6788 [hep-ph/9710441].

[214] S. Weinberg, *Implications of Dynamical Symmetry Breaking*, *Phys. Rev. D* **13** (1976) 974.

[215] L. Susskind, *Dynamics of Spontaneous Symmetry Breaking in the Weinberg-Salam Theory*, *Phys. Rev. D* **20** (1979) 2619.

[216] P. Sikivie, L. Susskind, M.B. Voloshin and V.I. Zakharov, *Isospin Breaking in Technicolor Models*, *Nucl. Phys. B* **173** (1980) 189.

[217] R.A. Diaz and R. Martinez, *The Custodial symmetry*, *Rev. Mex. Fis.* **47** (2001) 489 [hep-ph/0302058].

[218] M.J.G. Veltman, *Diagrammatica: The Path to Feynman rules*, vol. 4, Cambridge University Press (5, 2012).

[219] B. Holdom, *Oblique electroweak corrections and an extra gauge boson*, *Phys. Lett. B* **259** (1991) 329.

[220] M. Golden and L. Randall, *Radiative Corrections to Electroweak Parameters in Technicolor Theories*, *Nucl. Phys. B* **361** (1991) 3.

[221] G. Altarelli and R. Barbieri, *Vacuum polarization effects of new physics on electroweak processes*, *Phys. Lett. B* **253** (1991) 161.

[222] C. Burgess, S. Godfrey, H. Konig, D. London and I. Maksymyk, *A Global fit to extended oblique parameters*, *Phys. Lett. B* **326** (1994) 276 [hep-ph/9307337].

[223] V. Abazov, B. Abbott, M. Abolins, B. Acharya, M. Adams, T. Adams et al., *Search for a heavy neutral gauge boson in the dielectron channel with* 5.4 fb^{-1} *of* $p\bar{p}$ *collisions at* $s = 1.96$ *tev*, *Physics Letters B* **695** (2011) 88.

[224] CMS collaboration, *Search for high-mass resonances in dilepton final states in proton-proton collisions at* $\sqrt{s} = 13$ *TeV*, *JHEP* **06** (2018) 120 [1803.06292].

[225] CMS collaboration, *Search for resonant and nonresonant new phenomena in high-mass dilepton final states at* $\sqrt{s} = 13$ *TeV*, *JHEP* **07** (2021) 208 [2103.02708].

[226] M. Carena, A. Daleo, B.A. Dobrescu and T.M. Tait, *Z' gauge bosons at the Tevatron*, *Phys. Rev. D* **70** (2004) 093009 [hep-ph/0408098].

[227] E. Accomando, A. Belyaev, L. Fedeli, S.F. King and C. Shepherd-Themistocleous, *Z' physics with early LHC data*, *Phys. Rev. D* **83** (2011) 075012 [1010.6058].

Appendices

Appendix A

Traceology of the $(1,0) \oplus (0,1)$ representation

The covariant basis is orthogonal with respect to the scalar product defined as $\langle A|B\rangle = Tr(AB)$, thus these matrices satisfy the following relations

$$Tr\left(\chi\right) = Tr\left(S\right) = Tr\left(M\right) = Tr\left(\chi S\right) = Tr\left(C\right) = 0,$$
$$Tr\left(\chi M\right) = Tr\left(\chi C\right) = Tr\left(MS\right) = Tr\left(M\chi S\right) = Tr\left(MC\right) = Tr\left(S\chi S\right) = Tr\left(SC\right) = Tr\left(\chi SC\right) = 0, \tag{A.1}$$

where we suppressed the Lorentz indices.

Calculations in this work requires traces of products of the $S^{\mu\nu}$ tensor and other elements in the covariant basis. Let us consider first

$$Tr\left(SMM\right) = Tr\left(\chi^2 SMM\right) = -Tr\left(\chi S\chi MM\right) = -Tr\left(\chi SMM\chi\right) = -Tr\left(SMM\right) \Rightarrow Tr\left(SMM\right) = 0, \tag{A.2}$$

where we used Eqs. (2.33) and (2.34) and the cyclic property of a trace. Since χ commutes also with C, this procedure can be used to show that in general if we have a term with an odd numbers of S tensors the trace of this term will vanish

$$Tr(\text{term with an odd \# of } S\text{'s}) = 0. \tag{A.3}$$

The trace of terms with an even number of S factors can always be reduced to a linear combination of terms with the trace of the product of two S or two M factors using the

following (anti)commutation relations

$$[M^{\mu\nu},M^{\alpha\beta}]=-i\left(g^{\mu\alpha}M^{\nu\beta}-g^{\nu\alpha}M^{\mu\beta}-g^{\mu\beta}M^{\nu\alpha}+g^{\nu\beta}M^{\mu\alpha}\right), \tag{A.4}$$

$$\{M^{\mu\nu},M^{\alpha\beta}\}=\frac{4}{3}(g^{\mu\alpha}g^{\nu\beta}-g^{\mu\beta}g^{\nu\alpha})-\frac{4}{3}i\varepsilon^{\mu\nu\alpha\beta}\chi+\frac{1}{6}C^{\mu\nu\alpha\beta}, \tag{A.5}$$

$$[M^{\mu\nu},S^{\alpha\beta}]=-i\left(g^{\mu\alpha}S^{\nu\beta}-g^{\nu\alpha}S^{\mu\beta}+g^{\mu\beta}S^{\nu\alpha}-g^{\nu\beta}S^{\mu\alpha}\right), \tag{A.6}$$

$$\left\{M^{\mu\nu},S^{\alpha\beta}\right\}=\varepsilon^{\mu\nu\sigma\beta}\chi S^{\alpha}{}_{\sigma}+\varepsilon^{\mu\nu\sigma\alpha}\chi S^{\beta}{}_{\sigma}, \tag{A.7}$$

$$[S^{\mu\nu},S^{\alpha\beta}]=-i\left(g^{\mu\alpha}M^{\nu\beta}+g^{\nu\alpha}M^{\mu\beta}+g^{\nu\beta}M^{\mu\alpha}+g^{\mu\beta}M^{\nu\alpha}\right), \tag{A.8}$$

$$\left\{S^{\mu\nu},S^{\alpha\beta}\right\}=\frac{4}{3}\left(g^{\mu\alpha}g^{\nu\beta}+g^{\nu\alpha}g^{\mu\beta}-\frac{1}{2}g^{\mu\nu}g^{\alpha\beta}\right)-\frac{1}{6}\left(C^{\mu\alpha\nu\beta}+C^{\mu\beta\nu\alpha}\right). \tag{A.9}$$

The simplest case appears in the calculation of $H\to\bar{D}D$

$$Tr\left(S^{\mu\nu}S^{\alpha\beta}\right)=Tr\left(\frac{1}{2}[S^{\mu\nu},S^{\alpha\beta}]+\frac{1}{2}\{S^{\mu\nu},S^{\alpha\beta}\}\right)=4\left(g^{\mu\alpha}g^{\nu\beta}+g^{\mu\beta}g^{\nu\alpha}-\frac{1}{2}g^{\mu\nu}g^{\alpha\beta}\right)\equiv 4T^{\mu\nu\alpha\beta}. \tag{A.10}$$

Similarly, the calculation of $Z^0\to\bar{D}D$ requieres

$$Tr\left(M^{\mu\nu}M^{\alpha\beta}\right)=Tr\left(\frac{1}{2}[M^{\mu\nu},M^{\alpha\beta}]+\frac{1}{2}\{M^{\mu\nu},M^{\alpha\beta}\}\right)=4(g^{\mu\alpha}g^{\nu\beta}-g^{\mu\beta}g^{\nu\alpha})\equiv 4G^{\mu\nu\alpha\beta}. \tag{A.11}$$

The first example of the reduction mentioned above is faced in the calculation of $Z^0\to\bar{D}D$ which also requires to calculate

$$\begin{aligned}Tr\left(S^{\mu\nu}S^{\alpha\beta}M^{\rho\sigma}\right)&=Tr\left(\frac{1}{2}\left\{S^{\mu\nu},S^{\alpha\beta}\right\}M^{\rho\sigma}+\frac{1}{2}\left[S^{\mu\nu},S^{\alpha\beta}\right]M^{\rho\sigma}\right)\\&=\frac{-i}{2}Tr\left(\left(g^{\mu\alpha}M^{\nu\beta}+g^{\nu\alpha}M^{\mu\beta}+g^{\nu\beta}M^{\mu\alpha}+g^{\mu\beta}M^{\nu\alpha}\right)M^{\rho\sigma}\right)\\&=-2i\left(g^{\mu\alpha}G^{\nu\beta\rho\sigma}+g^{\nu\alpha}G^{\mu\beta\rho\sigma}+g^{\nu\beta}G^{\mu\alpha\rho\sigma}+g^{\mu\beta}G^{\nu\alpha\rho\sigma}\right),\end{aligned} \tag{A.12}$$

and

$$
\begin{aligned}
Tr\left(S^{\alpha\beta}M^{\mu\nu}S^{\rho\sigma}M^{\gamma\delta}\right) &= Tr\left(\left(\frac{1}{2}[S^{\alpha\beta},M^{\mu\nu}]+\frac{1}{2}\{S^{\alpha\beta},M^{\mu\nu}\}\right)\left(\frac{1}{2}[S^{\rho\sigma},M^{\gamma\delta}]+\frac{1}{2}\{S^{\rho\sigma},M^{\gamma\delta}\}\right)\right)\\
&= Tr\left(\left(\frac{i}{2}(g^{\mu\alpha}S^{\nu\beta}-g^{\nu\alpha}S^{\mu\beta}+g^{\mu\beta}S^{\nu\alpha}-g^{\nu\beta}S^{\mu\alpha})-\varepsilon^{\mu\nu\tau\beta}\chi S^{\alpha}{}_{\tau}-\varepsilon^{\mu\nu\tau\alpha}\chi S^{\beta}{}_{\tau}\right)\right.\\
&\left.\left(\frac{i}{2}(g^{\gamma\rho}S^{\delta\sigma}-g^{\delta\rho}S^{\gamma\sigma}+g^{\gamma\sigma}S^{\delta\rho}-g^{\delta\sigma}S^{\gamma\rho})-\varepsilon^{\gamma\delta\lambda\sigma}\chi S^{\rho}{}_{\lambda}-\varepsilon^{\gamma\delta\lambda\rho}\chi S^{\sigma}{}_{\lambda}\right)\right)\\
&= -g^{\mu\alpha}g^{\gamma\rho}T^{\nu\beta\delta\sigma}+g^{\mu\alpha}g^{\delta\rho}T^{\nu\beta\gamma\sigma}-g^{\mu\alpha}g^{\gamma\sigma}T^{\nu\beta\delta\rho}+g^{\mu\alpha}g^{\delta\sigma}T^{\nu\beta\gamma\rho}\\
&+g^{\nu\alpha}g^{\gamma\rho}T^{\mu\beta\delta\sigma}-g^{\nu\alpha}g^{\delta\rho}T^{\mu\beta\gamma\sigma}+g^{\nu\alpha}g^{\gamma\sigma}T^{\mu\beta\delta\rho}-g^{\nu\alpha}g^{\delta\sigma}T^{\mu\beta\gamma\rho}\\
&-g^{\mu\beta}g^{\gamma\rho}T^{\nu\alpha\delta\sigma}+g^{\mu\beta}g^{\delta\rho}T^{\nu\alpha\gamma\sigma}-g^{\mu\beta}g^{\gamma\sigma}T^{\nu\alpha\delta\rho}+g^{\mu\beta}g^{\delta\sigma}T^{\nu\alpha\gamma\rho}\\
&+g^{\nu\beta}g^{\gamma\rho}T^{\mu\alpha\delta\sigma}-g^{\nu\beta}g^{\delta\rho}T^{\mu\alpha\gamma\sigma}+g^{\nu\beta}g^{\gamma\sigma}T^{\mu\alpha\delta\rho}-g^{\nu\beta}g^{\delta\sigma}T^{\mu\alpha\gamma\rho}\\
&-4\left(\varepsilon^{\mu\nu\tau\beta}\varepsilon^{\gamma\delta\lambda\sigma}T^{\alpha}{}_{\tau}{}^{\rho}{}_{\lambda}+\varepsilon^{\mu\nu\tau\beta}\varepsilon^{\gamma\delta\lambda\rho}T^{\alpha}{}_{\tau}{}^{\sigma}{}_{\lambda}\right.\\
&\left.+\varepsilon^{\mu\nu\tau\alpha}\varepsilon^{\gamma\delta\lambda\sigma}T^{\beta}{}_{\tau}{}^{\rho}{}_{\lambda}+\varepsilon^{\mu\nu\tau\alpha}\varepsilon^{\gamma\delta\lambda\rho}T^{\beta}{}_{\tau}{}^{\sigma}{}_{\lambda}\right). \qquad \text{(A.13)}
\end{aligned}
$$

Similarly it can be shown that

$$Tr\left(M^{\mu\nu}M^{\alpha\beta}M^{\rho\sigma}\right) = -2i\left(g^{\mu\alpha}G^{\nu\beta\rho\sigma}-g^{\nu\alpha}G^{\mu\beta\rho\sigma}-g^{\mu\beta}G^{\nu\alpha\rho\sigma}+g^{\nu\beta}G^{\mu\alpha\rho\sigma}\right), \qquad \text{(A.14)}$$

$$Tr\left(\chi S^{\gamma\delta}S^{\alpha\beta}M^{\mu\nu}\right) = -2\left(\varepsilon^{\mu\nu\sigma\beta}T^{\gamma\delta\alpha}{}_{\sigma}+\varepsilon^{\mu\nu\sigma\alpha}T^{\gamma\delta\beta}{}_{\sigma}\right), \qquad \text{(A.15)}$$

$$Tr\left(\chi M^{\mu\nu}M^{\alpha\beta}\right) = -4i\varepsilon^{\mu\nu\alpha\beta}. \qquad \text{(A.16)}$$

The calculation of the trace of terms involving six or eight S or M factors (with an even number of S factors) needed in this paper are reduced in a similar way.

There is a simpler way to obtain these results however, which is specially useful for terms with six or more factors. Since the result rests only on the algebraic properties in Eqs. (A.4, A.5,A.6,A.7,A.8,A.9) we can use any representation of these operators for the calculation of the trace. In this concern the use of the representation where the internal matrix indices transform as Lorentz indices is convenient, since in this case the calculation of the trace reduces to contractions of Lorentz indices which can be easily done using conventional algebraic manipulation codes like FeynCalc. In this representation, each internal matrix index a is replaced by a pair of antisymmetric Lorentz indices $\alpha\beta$ [76]. The explicit form of the operators in the covariant basis is given by

$$(\mathbf{1})_{\alpha\beta\gamma\delta} = \frac{1}{2}(g_{\alpha\gamma}g_{\beta\delta} - g_{\alpha\delta}g_{\beta\gamma}), \tag{A.17}$$

$$(\chi)_{\alpha\beta\gamma\delta} = \frac{i}{2}\varepsilon_{\alpha\beta\gamma\delta}, \tag{A.18}$$

$$\left(M_{\mu\nu}\right)_{\alpha\beta\gamma\delta} = -i\left(g_{\mu\gamma}\mathbf{1}_{\alpha\beta\nu\delta} + g_{\mu\delta}\mathbf{1}_{\alpha\beta\gamma\nu} - g_{\gamma\nu}\mathbf{1}_{\alpha\beta\mu\delta} - g_{\delta\nu}\mathbf{1}_{\alpha\beta\gamma\mu}\right), \tag{A.19}$$

$$\left(S_{\mu\nu}\right)_{\alpha\beta\gamma\delta} = g_{\mu\nu}\mathbf{1}_{\alpha\beta\gamma\delta} - g_{\mu\gamma}\mathbf{1}_{\alpha\beta\nu\delta} - g_{\mu\delta}\mathbf{1}_{\alpha\beta\gamma\nu} - g_{\gamma\nu}\mathbf{1}_{\alpha\beta\mu\delta} - g_{\delta\nu}\mathbf{1}_{\alpha\beta\gamma\mu}. \tag{A.20}$$

The explicit form of $C^{\mu\nu\alpha\beta}$ can be constructed from Eq. (2.38) and the above relations.

CARTAS DE AUTORIZACIÓN

Sinodales

Dra. Myriam Mondragón Ceballos (IF-UNAM).

Dr. Justiniano Lorenzo Díaz Cruz (FCFM-BUAP).

Dr. Erick Vázquez Jáuregui (IF-UNAM).

Dr. Gustavo Niz Quevedo (DCI-UG-CL)

Dra. Alma Xóchitl González Morales (DCI-UG-CL).

Dr. Mauro Napsuciale Mendívil (DCI-UG-CL, sinodal suplente).

INSTITUTO DE FISICA
Departamento de Física Teórica
Apartado Postal 20-364, 01000 México D.F., México

— Dra. Myriam Mondragón Ceballos —

CD MX, a 28 de marzo de 2022.

Dr. David Delepine
División de Ciencias e Ingenierías
Universidad de Guanajuato
Presente

Estimado Dr. Delepine:

La presente es para informarle que he leido y revisado la tesis titulada *Tensor dark matter*, presentada por la M.F. Haydée Hernández Arellano para obtener el grado de Doctor en Física. En mi opinión la tesis reúne los requisitos de calidad y originalidad para el nivel de doctorado y se puede proceder a la defensa de la tesis.

Sin más por el momento, aprovecho la ocasión para mandarle un saludo cordial.

Atentamente,

Dra. Myriam Mondragón C.

Sria.: +(52 55) 5622-5020 Fax: +(52 55) 5622-5015, 5616-1535 Tel.: +(52 55) 5622-5167

Facultad de Ciencias Físico-Matemáticas,
BUAP

Puebla, Pue., Marzo 25, 2022

Dr. David Delepine
División de Ciencias e Ingenierías Universidad de Guanajuato

Presente

Por medio de la presente me permito informarle que he leído la tesis titulada *"**Tensor dark matter**",* que se presenta para obtener el grado de Doctor en Física por la M. F. Haydee Hernández Arellano. Las observaciones que formulé, han sido incorporadas a la versión final de la tesis, la cual cumple con altos estándares de calidad y forma para el grado correspondiente y por lo tanto estoy de acuerdo en que se realice la correspondiente defensa de tesis.

Sin otro particular, reciba un cordial saludo de mi parte,

Atentamente

Dr. J. Lorenzo Díaz-Cruz
Profesor Titular C.- FCFM-BUAP (México)

26 de marzo de 2022

Dr. David Delepine
División de Ciencias e Ingenierías
Universidad de Guanajuato
Presente

Estimado Dr. Delepine:

Por este conducto le informo que he leído la tesis titulada "Tensor dark matter" que para obtener el grado de Doctor en Física ha formulado la M. F. Haydee Hernández Arellano. Las observaciones de parte de su servidor han sido incorporadas a la versión final del documento que, en mi opinión, reúne las características de calidad y forma para el grado al que se aspira; por lo cual, no tengo inconveniente en que se realice la correspondiente defensa de tesis.

Sin otro particular, reciba un cordial saludo.

Atentamente,

Eric Vázquez Jáuregui
Investigador Titular "A"
Instituto de Física, UNAM

Gustavo Niz Quevedo
Departamento de Física
División de Ciencias e Ingenierías

León, Gto., 23 de Marzo de 2022.

Dr. David Yves Ghislain Delepine
Director de la División de Ciencias e Ingenierías
Universidad de Guanajuato

Estimado Dr. David Yves Ghislain Delepine

Por medio de la presente le informo que he recibido, leído y revisado la tesis de Doctorado titulada "Tensor Dark Matter" de la alumna Haydee Hernández Arellano, bajo la supervisión de los Drs. Mauro Napsuciale y Simón Rodríguez.

Después de la atención a ciertas correcciones menores, creo que el trabajo cumple con los estándares requeridos para la obtención del grado, y apoyo la defensa del mismo en la fecha convenida.

Me pongo a su disposición para cualquier duda sobre la revisión de dicho trabajo de tesis.

Atentamente,

Gustavo Niz

Universidad de Guanajuato

CAMPUS LEÓN
DIVISIÓN DE CIENCIAS E INGENIERÍAS
DEPARTAMENTO DE FISICA

30 de Marzo de 2021

DR. DAVID Y. G. DELEPINE
DIRECTOR DE LA DIVISIÓN DE CIENCIAS E INGENIERÍAS
PRESENTE

Por este medio le comunico que he revisado la tesis titulada **Tensor Dark Matter** , escrita por la estudiante Haydee Hernández Arellano, para efecto de presentarla y obtener el grado de Doctorado en Física. El texto de la tesis se encuentra completo y se presentan resultados interesantes sobre la viabilidad de que la materia oscura del universo sea descrita por el modelo denominado “Tensor Dark Matter”.

En mi opinión, la tesis cumple con los elementos necesarios para ser defendida ante el comité sinodal designado en fecha próxima que sea acordada de manera conjunta.

Agradeciendo su amable atención, aprovecho la ocasión para enviarle un cordial saludo.

Alma X. González Morales
Cátedra CONACYT
Departamento de Física
División de Ciencias e Ingenierías
Universidad de Guanajuato

León, Guanajuato, 25 de Marzo de 2022

Dr. David Delepine
División de Ciencias e Ingenierías
Universidad de Guanajuato
Presente

Por este conducto le informo que he leído la tesis titulada *"**Tensor dark matter**"* que para obtener el grado de Doctor en Física ha formulado la M. F. Haydee Hernández Arellano. Las observaciones de parte de su servidor han sido incorporadas a la versión final del documento que, en mi opinión, reúne las características de calidad y forma para el grado al que se aspira; por lo cual, no tengo inconveniente en que se realice la correspondiente defensa de tesis.

Sin otro particular, reciba un cordial saludo.

Atentamente

Dr. Mauro Napsuciale Mendivil

Profesor Titular C

Sinodal

c.c.p. archivo

DEPARTAMENTO DE FISICA, DIVISION DE CIENCIAS E INGENIERÍAS, CAMPUS LEÓN
Loma del Bosque 103, Fracc. Lomas del Campestre C.P. 37150 León, Gto., Ap. Postal E-143 C.P. 37000 Tel. (477) 788-5100, Fax: (477) 788-5100 ext. 8410, http://www.fisica.ugto.mx